New Methods to Control Melt Elasticity for Long-Chain Branched Polyethylene

MONCHAI SIRIPRUMPOONTHUM

Japan Advanced Institute of Science and Technology

New Methods to Control Melt Elasticity for Long-Chain Branched Polyethylene

by

MONCHAI SIRIPRUMPOONTHUM

Submitted to
Japan Advanced Institute of Science and Technology
in partial fulfillment of the requirements
for the degree of
Doctor of philosophy

Supervisor: **Prof. Dr. Masayuki Yamaguchi**

School of Materials Science
Japan Advanced Institute of Science and Technology

September 2014

Referee-in-chief : **Professor Dr. Masayuki Yamaguchi**
Japan Advanced Institute of Science and Technology

Referees : **Associate Professor Dr. Kazuaki Matsumura**
Japan Advanced Institute of Science and Technology

Associate Professor Dr. Tatsuo Kaneko
Japan Advanced Institute of Science and Technology

Associate Professor Dr. Toshiaki Taniike
Japan Advanced Institute of Science and Technology

Professor Dr. Shuichi Tanoue
University of *Fukui*

Preface

Polyethylene is one of common plastics which are extensively used in many products. The statistics report that more than 60 million ton of polyethylene is produced in every year. During the production, a large amount of waste caused by production loss is emitted. Therefore, the processability is very important to fully utilize a raw material and minimize the emission of waste. In order to improve the processability, control of rheological properties is very important. Therefore, many techniques have been proposed to modify the rheological properties of polyethylene.

In this thesis, the rheological modification of polyethylene by thermal history is studied using various types of polyethylene including blends. I hope the study would provide useful information to improve the processability.

Monchai Siriprumpoonthum

Contents

Chapter 1

General Introduction

1.1 Introduction

Rheological properties in the molten state play an important role at polymer processing, which are decided by molecular architecture such as chemical structures, molecular weight and its distribution, and long/short chain branches. Information on rheological properties is crucial to predict the processability, morphology development, and mechanical properties in the solid state.

Because of topological interactions of polymer chains, known as entanglement couplings, pronounced elastic properties are expected even in the molten state of a polymer. This specific interaction provides complicated rheological responses of a molten polymer, which, in turn, enables various processing operations.

For some processes operations, such as thermoforming, foaming, extrusion coating, and blow-molding, high melt elasticity is required. Therefore, various types of polymers with high melt elasticity, such as polymers with long-chain branches and/or broad molecular weight distribution, are produced on a commercial scale in the industry. These polymers have a wide range of fabricating ability to produce desired products.

Among conventional polymers, polyethylene (PE) has the widest variety of molecular structure with short- and long-chain branches and molecular weight distribution

(MWD), which greatly affect its rheological behavior in the molten state. It is known that the rheological properties of a branched polymer are changed by "processing history" such as shear history or thermal history.[1,2] Furthermore, several techniques have been proposed for rheological modification, such as addition of linear low-density polyethylene (LLDPE) having high molecular weight[3-6] and cross-linking with and without peroxide addition.[7-10] The modification techniques have a strong impact on the elongational viscosity which is one of the most important rheological properties at polymer processing.

In this chapter, the following topics are reviewed; (1) PE and polymerization, (2) linear and non-linear vicoelastic properties, (3) tube model, (4) processing operations such as extrusion coating, thermal forming and blown film, and (5) several techniques to control and modify the melt elasticity for PE. Finally, the objectives of this research will be explained

1.2 Polyethylene

PE is one of commodity plastics and the versatile applications penetrate deeply in society to support our daily life. The structure of PE is represented as a simple alkane formula C_nH_{2n+2} consists of covalently linked carbon atoms with pendant hydrogen atoms. However, PE provides a wide range of mechanical properties due to variations in polymer chain structure. PE is generally classified by the density, although the catalyst and polymerization conditions also affect the properties. Table l-l shows the types of PE and the definition of high-density polyethylene (HDPE), medium-density polyethylene (MDPE), and low-density polyethylene (LDPE) in accordance with JIS K 6922-1, Plastics-Polyethylene (PE) molding and extrusion materials-Part 1; Designation system and basis

for specifications, and ASTM D 1248, standard specification for polyethylene plastics extrusion materials for wire and cable.[11]

Table l-l. Classification of PE

	Density (kg/m^3)	
	JIS K 6922	ASTM D 1248
HDPE	942.0-960.0	941.0-959.0
MDPE	930.0-941.0	926.0-940.0
LDPE	910.0-929.0	910.0-925.0

In addition, copolymers of ethylene and α-olefin are generally regarded as PE, as well as linear low-density polyethylene (LLDPE) or very low-density polyethylene (VLDPE) when the density range is within LDPE or lower than LDPE, respectively. Further, copolymers of ethylene and non-olefin monomer, in which the functional group consists of carbon, oxygen and hydrogen, are involved in PE.[12] PE can also be classified differently by the applied pressure at polymerization, which is closely related with the catalyst used.

1.2.1 Polymerization of linear PE

HDPE, having low degree of branching, is produced by low pressure polymerization. The conversion is highly exothermic, in which the process releases a lot of heat. The polymerization due to Ziegler-Natta catalyst was developed by Karl Ziegler in Max Planck in 1955.[13] Medium pressure polymerization is also made it possible to produce HDPE with Standard catalyst by Standard Oil in USA or Phillips catalyst

developed by Phillips Petroleum in USA. The combination of the name of catalyst and polymerization conditions is shown in Table 1-2.[11]

Table 1-2. PE catalyst and polymerization conditions

Catalyst	Structure	Polymerization conditions
Ziegler-Natta catalyst	$TiCl_4$-$Al(C_2H_5)_3$	ambient to 100 ^oC, atmospheric to 1 MPa
Phillips catalyst	CrO_3/SiO_2	125 to 175 °C, 2 to 3 MPa
Standard catalyst	$MoCVAl_2O_3$-Na	150 to 250 °C, 3.5 to 10 MPa

The Ziegler-Natta catalyst is also employed to produce LLDPE. However, the advent of metallocene catalyst is more amazing to polyolefins production. The catalyst was discovered by Kaminsky in 1980s.[14] The metallocene catalyst generally consists of metallocene compound and methylaluminoxane, and the polymerization takes place under various conditions. It is particularly applied to produce ethylene-α-olefin copolymers. As the metallocene catalyst contains only one type of active site, the catalyst gives narrow MWD than the Ziegler-Natta catalyst, in which the distribution of molecular weight, indicated by M_w/M_n, is around 2.0. Nowadays the metallocene catalyst has mostly superseded the Ziegler-Natta catalyst in commercial production of LLDPE. It enhances mechanical strength and heat-seal strength as well as less stacking. Moreover, heat seal initiation temperature is low due to the homogeneous composition of short-chain branches.

1.2.2 Polymerization of LDPE

LDPE was the first PE developed in 1933 and then commercialized in 1939. It is produced exclusively by polymerization under high pressure and temperature conditions with a free radical initiator. The polymerization process consists of initiation, chain propagation, chain branching, chain transfer, and termination reactions.[15]

<Initiation>

The typical initiators are generated by decomposition of organic peroxides and/or azo compounds.

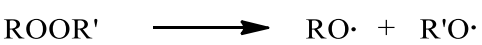

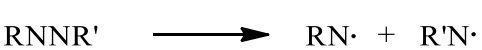

where R and R' stand for alkyl or aryl group.

The free radical attaches to an ethylene molecule, and then the new small molecule with a radical at the end of a molecule is generated.

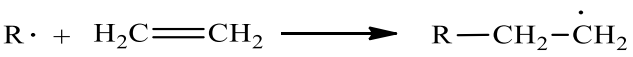

<Chain propagation>

A free radical initiates the polymerization by abstracting a hydrogen atom from an ethylene monomer to create a new small polymer chain. The free radical on the end reacts with another ethylene molecule. The incoming ethylene is bonded by C-C covalent bond, and then the radical transfers to the end of new chain. Thus, the growth of PE chain proceeds by the repeated addition of ethylene monomers to the end of extending chain.

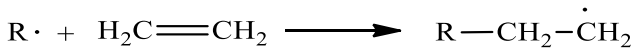

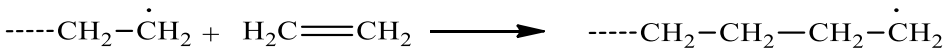

<Chain branching>

During the polymerization, however, the terminal radical can abstract a hydrogen atom from its own polymer chain. Then, the chain growth at the end of original chain is terminated, instead, the newly created radical site in the chain is capable to react with an ethylene monomer or another chain nearby. In this way, the branching structure is formed. The difference in LCB and short-chain branches (SCB) is that the LCB is formed by intermolecular transfer of radicals. The possibility of the intermolecular hydrogen abstraction from a given molecule is proportional to the molecular length.

To create LCB, the radical transfer occurs in adjacent chains when a terminal radical attack another polymer chain. Then chain propagation is initiated in an existing polymer chain.

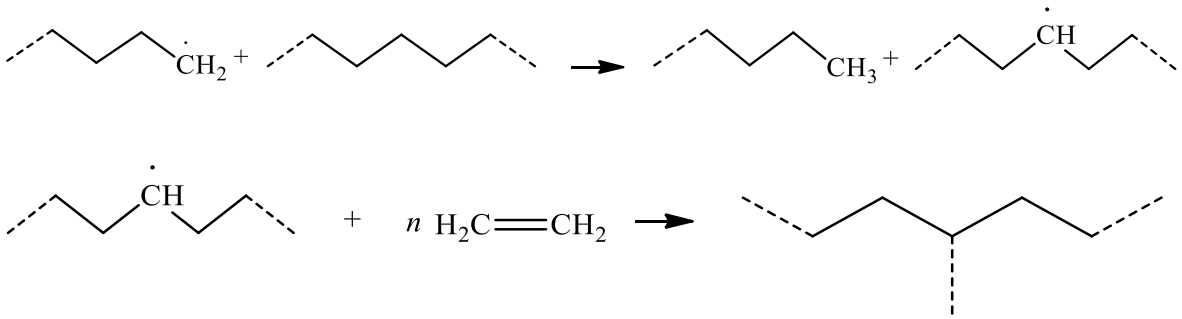

On the other hand, the creation of SCB occurs when the end of a chain turns back on itself, which is called “backbiting”, and then the terminal radical abstracts a hydrogen

atom from the backbone structure. After that, the chain propagation continues from the new radical site as the starting point.

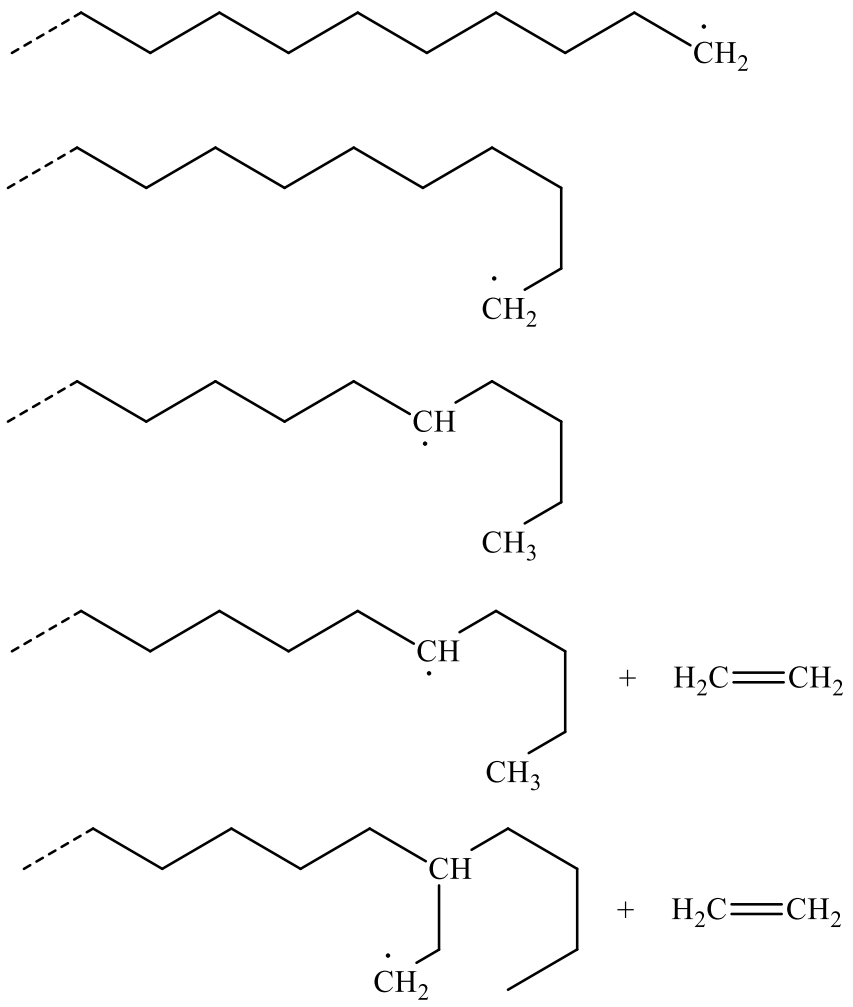

This reaction generates a butyl branch as follows;

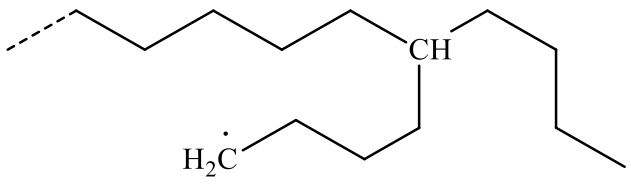

Or the new radical abstracts a hydrogen atom from the backbone.

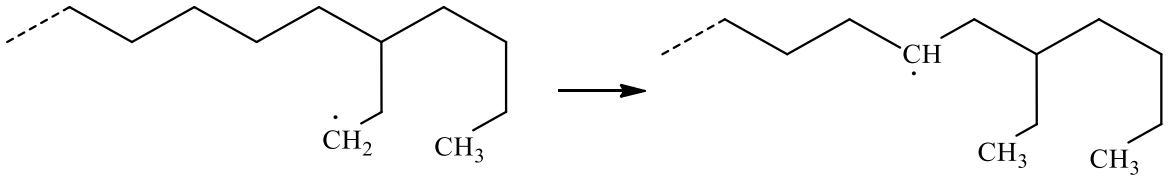

The polymer terminal is left as 2-methyl hexyl branch by the growth from the new radical site.

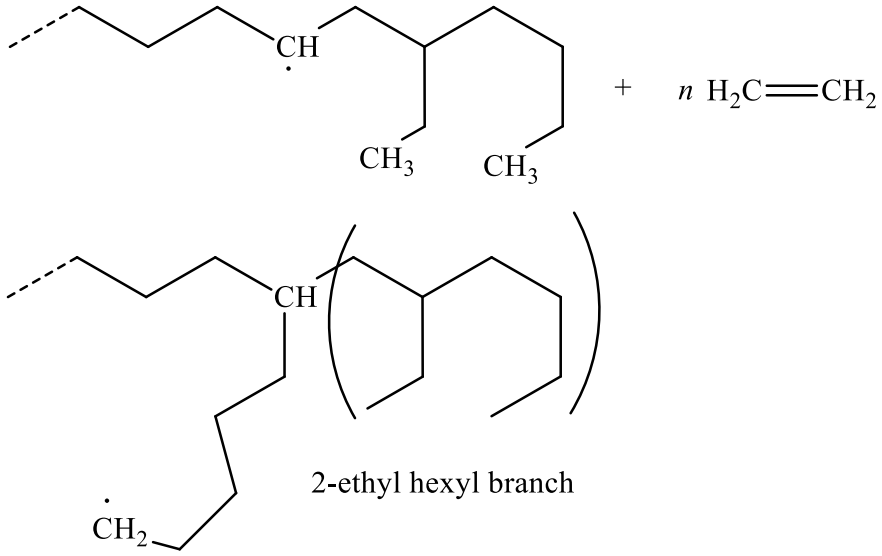

<Chain transfer>

The growth of a chain can be terminated by transfer of a chain end radical to an ethylene monomer, thus overall number of radicals is preserved through the chain transfer. The following reactions can occur.

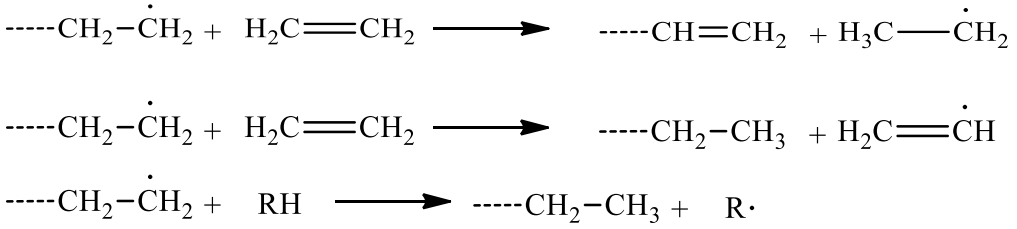

<Termination>

The growth of PE chain is terminated by the radical transfer to another molecule. The termination of chain growth occurs by the encounter of two radicals. A new bond is formed by the association of each radical of in two molecules. The chain transfer controls molecular weight, which is achieved by altering reaction conditions.[16] There are two different reactions; coupling and disproportionation. When two chain ends meet, the two chains are coupled to be one chain, or create disproportionate to leave two chains having different chain end from each other. Some possible reactions are as follow:

When two radicals meet, they react to form a covalent bond.

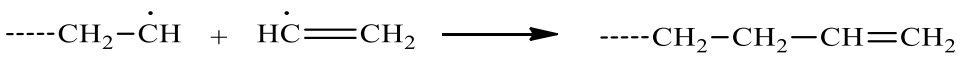

The reaction couples two polymer chains.

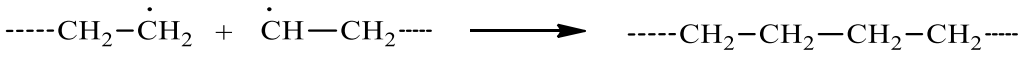

A following disproportionation reaction can also occur.

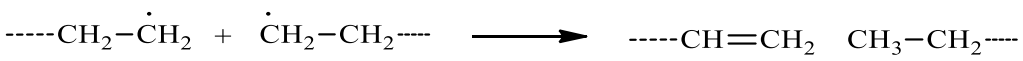

1.2.3 HDPE

HDPE is a linear polymer with a high degree of crystallinity. Basically, it consists of unbranched molecules, and thus the crystallization is not hindered severely. However, a very small concentration of 1-alkene is sometimes copolymerized in order to control the crystallinity. The illustration is shown in Figure l-1(a). Ziegler-Natta catalyst, consists of

triethyl aluminum and titanium tetrachloride, was first developed to produce HDPE. The MWD, *i.e.*, M_w/M_n, is usually between 5 to 15 for HDPE, whereas it is around 20 for LDPE. In contrast to the high pressure method for LDPE, HDPE is produced under a low or medium pressure with a suitable catalyst for the polymerization. Not only Ziegler-Natta catalyst, Phillips catalyst also gives HDPE. In the case of HDPE produced by Phillips catalyst, a small amount of long-chain branching (LCB) exists especially in a large molecular weight fraction.[17] According to Yoshikawa et al., one long-chain branch per 10,000 carbon atoms exists.[18,19] It means that the LCB content in HDPE is about one to two orders lower than that in LDPE.[20,21] The LCB with broad MWD in HDPE produced by Phillips catalyst is responsible for the elastic properties in the molten state and thus the good processability for various processing operations.

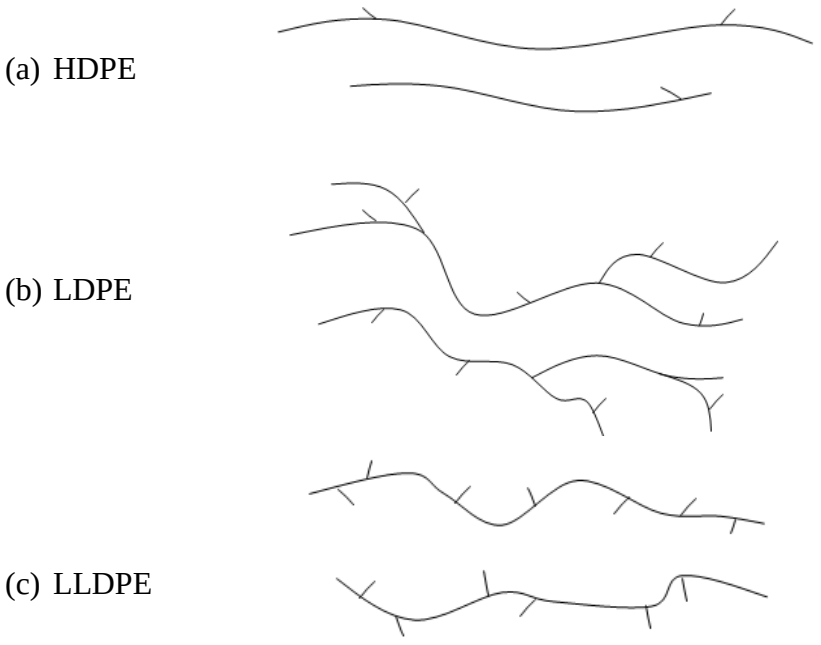

Figure 1-1. Illustrations of various PE structures; (a) HDPE, (b) LDPE and (c) LLDPE

1.2.4 LDPE

LDPE is a branched PE, obtained by radical polymerization under high pressure and high temperature. It contains LCB as well as SCB. These days, two standard polymerization methods are available in industry; one is produced in a batch-type autoclave reactor, known as the vessel or autoclave process, and the other is obtained using a continuous tube-type reactor, and is known as the tubular process. It has been believed that autoclave LDPE has more and/or longer LCB than tubular LDPE.[22] The polymer features substantial number of SCB, which consists of ethyl, butyl and 2-ethyl hexyl branches, and LCB created at random intervals along the length of the main chain.[17] The SCB prevents the crystallization by disrupting chain packing, resulting in relatively low density compared to HDPE.

1.2.5 LLDPE

LLDPE is a copolymer of ethylene and α-olefin obtained through low-pressure process, where a 1-alkene is used as a comonomer. The polymer consists of linear main chain with pendant alkyl groups that are recognized as SCB. The comonomers of 1-butene, 1-hexene or 1-octene are commonly used and generate ethyl, butyl, or hexyl branches, respectively with average 10 to 40 branches per 1,000 carbon atoms at random intervals.[15] The impediment of crystallization by SCB results in low-density of a polymer, although methyl branch is believed to be involved into the crystalline lattice.[23] The illustration is shown in Figure l-l(c). The probability of LCB existing in LLDPE is considered to be almost zero. Although, the degree of LCB in LLDPE is reported to be fewer than 3/10,000 carbon atoms.[24] However, this is the lower limit of detection in the use of light scattering.[25]

Recently, new technologies developed by Dow Chemical Company and Exxon Mobil in single-site metallocene catalysis have leaded to advances in LLDPE synthesis. Catalysts designed for the incorporation of α-olefins lead to Dow's constrained geometry catalysts (CGC) which is responsible for the homogeneous distribution of the comonomer.[26] LLDPE produced by CGC contains LCBs and thus it shows several processing advantages.[27]

1.3 Rheological control of PE

1.3.1 Linear viscoelastic property

Linear viscoelastic properties provide basic characterization of a polymer. Some rheometers such as cone-and-plate rheometer and parallel-plate rheometer are used to measure the linear viscoelastic properties under shear. The common method used to measure the linear viscoelasticity is the small-amplitude oscillatory shear measurement. In oscillatory shear measurements, both shear stress σ and strain γ are measured as a function of angular frequency ω. (Equations 1-1 and 1-2)

$$\gamma(t) = \gamma_0 \sin(\omega t) \tag{1-1}$$

$$\sigma(t) = \sigma_0 \sin(\omega t + \delta) \tag{1-2}$$

where $\gamma(t)$ the sinusoidal strain, γ_0 the strain amplitude, ω the angular frequency of oscillation, $\sigma(t)$ the sinusoidal stress, σ_0 the stress amplitude and δ is the phase angle. The shear storage modulus $G'(\omega)$ and loss modulus $G''(\omega)$ are given as follows; (Equations 1-3 and 1-4)

$$G'(\omega) = \frac{\sigma_0}{\gamma_0}\cos\delta \tag{1-3}$$

$$G''(\omega) = \frac{\sigma_0}{\gamma_0}\sin\delta \tag{1-4}$$

At low frequencies, it is possible to obtain the zero-shear viscosity η_0 from the loss modulus.

$$\eta_0 = \lim_{\omega \to 0} \frac{G''(\omega)}{\omega} \tag{1-5}$$

For typical polymers, the relationships between η_0 and M_w have already been reported.[28,29] Therefore, M_w can be predicted from the zero-shear viscosity. In case of linear PE, the following relationships have been proposed based on experimental results.[30,31]

$$\eta_0 = 9.0 \times 10^{-15} M_w^{\,3.6} \qquad \text{(at 150 °C)} \tag{1-6}$$

$$\eta_0 = 4.743 \times 10^{-10} \left(\frac{M_w}{m_b} \right)^{3.33} \qquad \text{(at 190 °C)} \tag{1-7}$$

where m_b is the molecular weight per backbone repeating unit.[28]

Further, the steady-state compliance J_e^0 and the weight-average relaxation time τ_w can be calculated by Equations 1-8 to 1-9.

$$J_e^0 = \lim_{\omega \to 0} \frac{G'(\omega)}{G''(\omega)^2} \tag{1-8}$$

$$\tau_w = \eta_0 J_e^0 \tag{1-9}$$

The relaxation spectra $H(\tau)$ can be calculated from *G'* and *G''* using Tschoegl equation.[32] (Equations 1-10 and 1-11)

$$H(\tau) = \frac{dG'}{d\ln(\omega)} - \frac{1}{2}\frac{d^2G''}{2(d\ln\omega)^2}\Bigg|_{1/\omega=\tau/\sqrt{2}} \tag{1-10}$$

and

$$H(\tau) = \frac{2}{\pi}\left[G'' - \frac{4}{3}\frac{dG'}{d\ln(\omega)} + \frac{1}{3}\frac{d^2G''}{(d\ln\omega)^2}\right]\Bigg|_{1/\omega=\tau/\sqrt{5}} \tag{1-11}$$

In case the sample has only one relaxation time. The longest relaxation time is given by the inverse of the angular frequency at the crossover of *G'* and *G''*. Further, the molecular weight between entanglement couplings, M_e, can be evaluated when the plateau modulus is identified, using Equation 1-12.[28,33] However, it is very difficult for PE to find a plateau modulus because of the crystallinity.

$$M_e = \frac{\rho RT}{G_N^0} \tag{1-12}$$

where G_N^0 the rubbery plateau modulus, ρ the density, R the universal gas constant (8.314 J mol^{-1} K^{-1}) and T the absolute temperature.

The value of G_N^0 can be determined using Equation 1-13

$$G_N^0 = \frac{2}{\pi}\int_{-\infty}^{a} G'' d\ln\omega \qquad (1\text{-}13)$$

where *a* is the upper limit before the transition zone is entered.

1.3.2 Rheological response under shear flow in non-linear region

The major property to be considered at processing operation is melt viscosity. In industry, the information on melt viscosity of a polymer is given as melt flow index (MFI) or melt flow rate (MFR), which is the weight of a polymer melt per 10 min [g/10min], through an orifice die under a specific load and temperature, as determined by ASTM D 1238.[34] In case of PE, the temperature is 190 ^{o}C and the load is 2.16 kg. Therefore, a polymer with high molecular weight has a low melt flow rate and vice versa. In general, extrusion blow-molding process usually requires a polymer whose melt index is below 2 [g/10 min]. In contrast, high-melt-index polymers between 6 to 60 [g/10 min] are necessary in extrusion coating, injection-molding, and injection blow-molding.[35] However, the value can represent the viscosity data only at a specific shear rate. Therefore, non-Newtonian behavior should be checked to obtain exact information by other techniques.

Steady-state shear flow is an important method to determine the non-Newtonian behavior of a polymer melt. It can be evaluated using a cone-and-plate rheometer or a capillary rheometer. A capillary rheometer is the best method to obtain the viscosity at higher shear rate. It also gives information on the Barus effect and flow instability. To express the Barus effect quantitatively, the extrudate swell (or die swell), defined as the ratio of the area of cross section for the extruded strand to that of the die section, is

employed.[36] This phenomenon closely relates to the primary normal stress difference. Polymer melts with high melt elasticity always show high value of extrudate swell. Further, molten strands always show flow instability at high extrusion shear rate, although extrudate strands exhibit smooth surfaces at low shear rate.[37-39]

1.3.3 Rheological response under elongational flow

1.3.3.1 Elongational viscosity

Uniaxial elongational viscosity is the most appropriate method to evaluate strain-hardening characteristics during uniaxial stretching of a polymer melt. The growth curve of elongational viscosity is calculated from Equation 1-14.[40]

$$\eta_E^+(t) = \frac{\sigma_E^+}{\dot{\varepsilon}} \tag{1-14}$$

where $\sigma_E^+(t)$ *is* the elongational stress as a function of time and $\dot{\varepsilon}$ is the elongational strain rate.

Trouton[41] and some researchers found that the elongation viscosity $\eta_E^+(t)$ is three times of the shear viscosity $\eta^+(t)$ at low strain rates.[42] Therefore, the transient shear viscosity at a low strain rate asymptote $\eta^+(t)$ can be estimated from oscillatory shear moduli using an approximate equation shown in Equation 1-15, which was proposed by Osaki et al.[43]

$$\eta^+(t) = t\left[G''(\omega) + 1.12G'(\omega/2) - 0.2G'(\omega)\right]_{\omega=1/t} \tag{1-15}$$

1.3.3.2 Strain-hardening in elongational viscosity

Besides molecular weight and its distribution, long-chain branches play a major role in rheological properties, especially elastic properties in the terminal zone.[44] It is well known that chain stretching in LDPE leads to strain-hardening in the transient elongational viscosity, as demonstrated by advanced molecular models such as the MSF theory[45] and the Pom-pom model[46] based on the tube model proposed by Doi and Edward.[44] According to the tube model, the branch point is assumed to be fixed and the repation is prohibited. Consequently, conformation changes in long-chain branches have to occur via contour length fluctuation, *i.e.*, chain retraction to the branch point within the tube. This retraction process leads the polymer chain to a low enthalpy state, since the conformation around the branch point will be distorted. Consequently, the reptation time, a time required to escape from the original tube, increases exponentially with the length of branches. Moreover, the "chain contraction process", which occurs prior to the reptation motion, has to be seriously considered. When there are more than two branch points in a backbone chain, chain contraction between the branch points is prohibited owing to the topological interaction with neighbor chains as illustrated in Figure 1-2. Because of the entropy loss due to the chain stretching between the branch points, a high level of stress is generated. This mechanism is responsible for the strain-hardening behavior, *i.e.*, rapid stress increase with strain, in the transient elongational viscosity for long-chain branched polymers as exemplified in Figure 1-3.

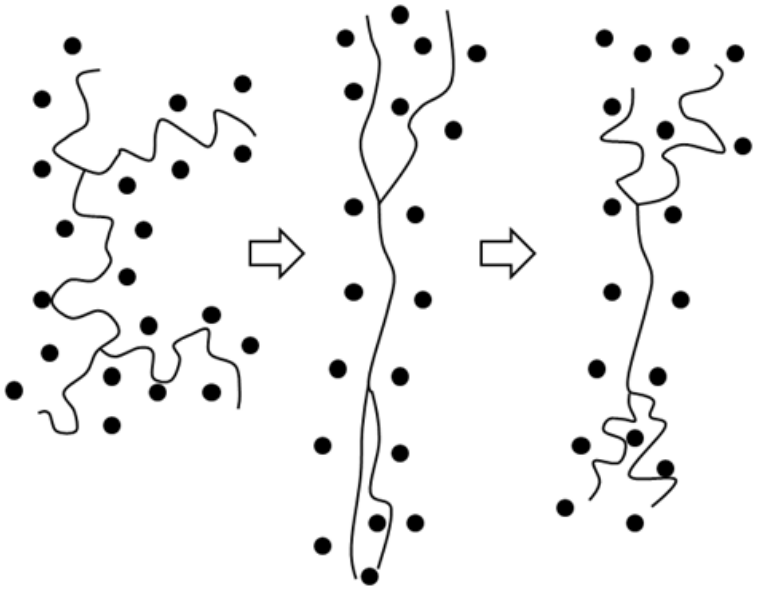

Figure 1-2. Chain stretching and contraction process for a branched polymer; (left) equilibrium state, (center) polymer chain is stretched by the applied strain, and (right) a part of a chain between branch points cannot be shrunk and thus provides a large stress because of the low entropy state.[22]

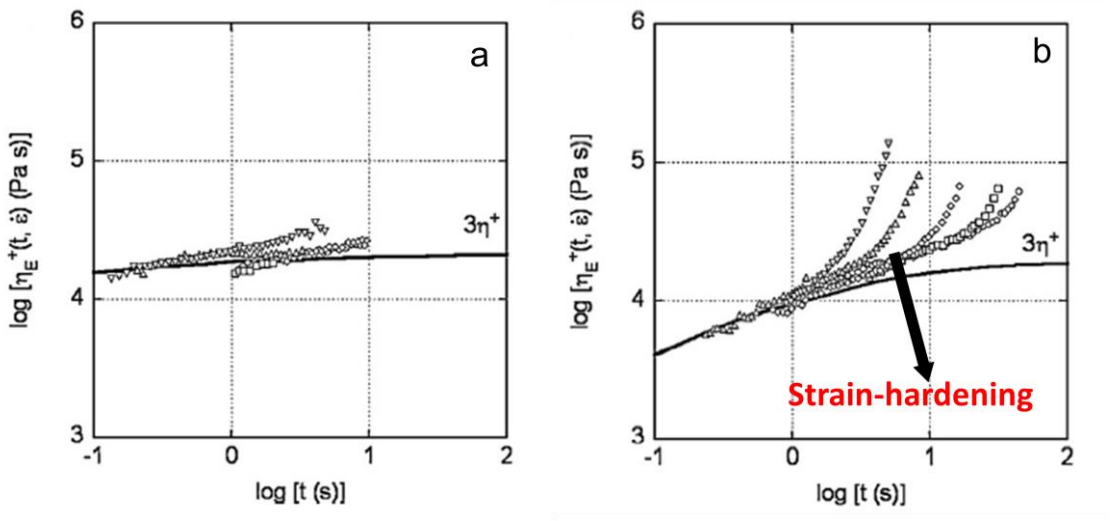

Figure 1-3 Growth curves of uniaxial elongational viscosity $\eta_E^+(t,\dot{\varepsilon})$; (a) LLDPE and (b) LDPE[47]

1.3.3.3 Drawdown force

The force needed to stretch a molten polymer under elongational flow is called "drawdown force". It has been recognized that drawdown force has information on uniaxial elongational viscosity.[48-54] Varying the draw ratio, the information on the elongtional viscosity at various strain rates is collected. The drawdown force at the maximum stretching rate is called "melt strength". A typical experimental set-up for drawdown force is exemplified in Figure 1-4.[50]

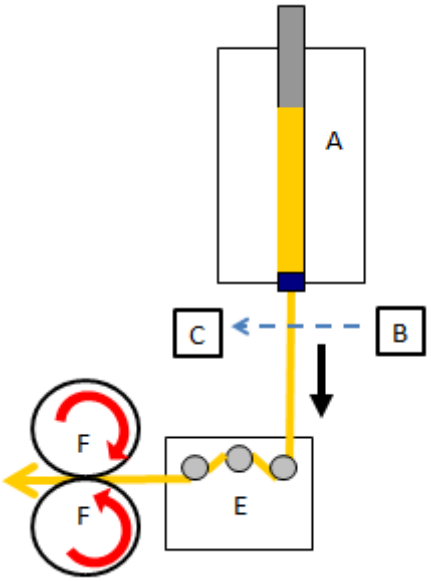

Figure 1-4. Schematic diagram for the measurements of drawdown force; (A) capillary rheometer, (B) and (C) diameter detector, (E) tension detector and (F) rotating wheels

The drawdown force is measured by pulling the strand extruded vertically downward from die in capillary rheometer (A) at constant rate by two rotating wheels (F). Then, the drawdown is measured by a tension detector (E). Furthermore, this machine

enables to evaluate of extensibility, the ultimate draw ratio at the break point of the strand, by increasing the pulling rate constantly. Some capillary rheometers also have an attachment to measure the extrudate swell. The diameter of the extrudates is measured using a laser beam emitted from (B) to (C). The measurements are a useful technique to determine the non-linear behavior of a polymer melt.[4] Further, it is well known that most polymer processing operations involve some kinds of extensional flow by converging flow at a die entry or nozzle. Therefore, the extensional deformation has become favorite to determine the processability of a commercial polymer.[47,55-57]

1.4 Tube model

Linear and non-linear viscoelasticity of entangled polymers are well described by the tube model. The entanglement couplings of polymer chains restrict the diffusion of a polymer chain, especially in the direction perpendicular to the chain due to topological constrains. Edwards introduced a concept that a polymer chain is confined in a tube-like region[58] as shown in Figure 1-5. As a polymer chain is longer than the length of such a virtual tube, de Gennes supposed that the chain moves windingly in the tube. The motion was called reptation named after the Latin *reptare*, to creep.[59]

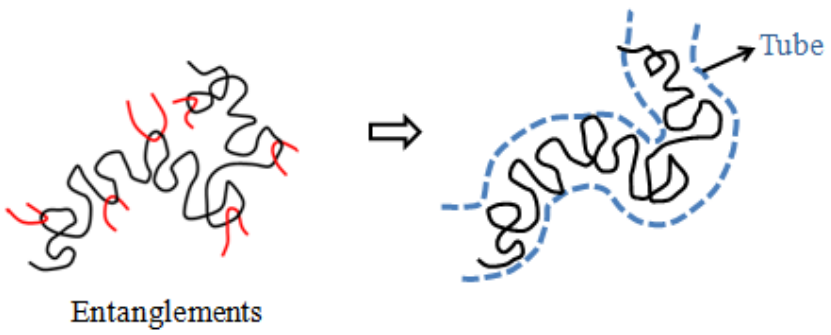

Figure 1-5. A polymer chain entangled by surrounding chains

The Doi-Edwards theory[44] assumes that the diameter of tube a is equivalent to the square root of the mean-square end-to-end distance of the polymer chain whose molecular weight is M_e, as shown in Figure 1-6, to consider the topological restrain caused by entanglements of surrounding polymer chains. The center line of the tube, which offers the shortest path of the chain, is called the primitive chain.

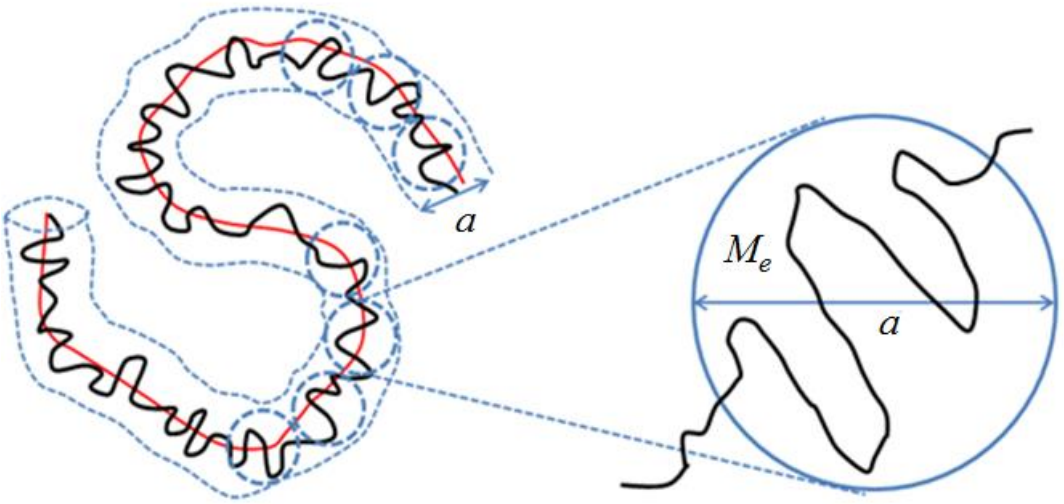

Figure 1-6. Dimension of a tube in the Doi-Edwards theory

Figure 1-7 shows the reptation of a polymer chain having linear structure. The chain fluctuates around the primitive chain. By some fluctuations, it may store some excess mass in a part of the chain. This mass may diffuse along the primitive chain and finally leave the tube. The chain thus creates a new piece of a tube and at the same time destroys a part of the tube on the other side. Further, the time required to escape from the original tube is “reptation time”.

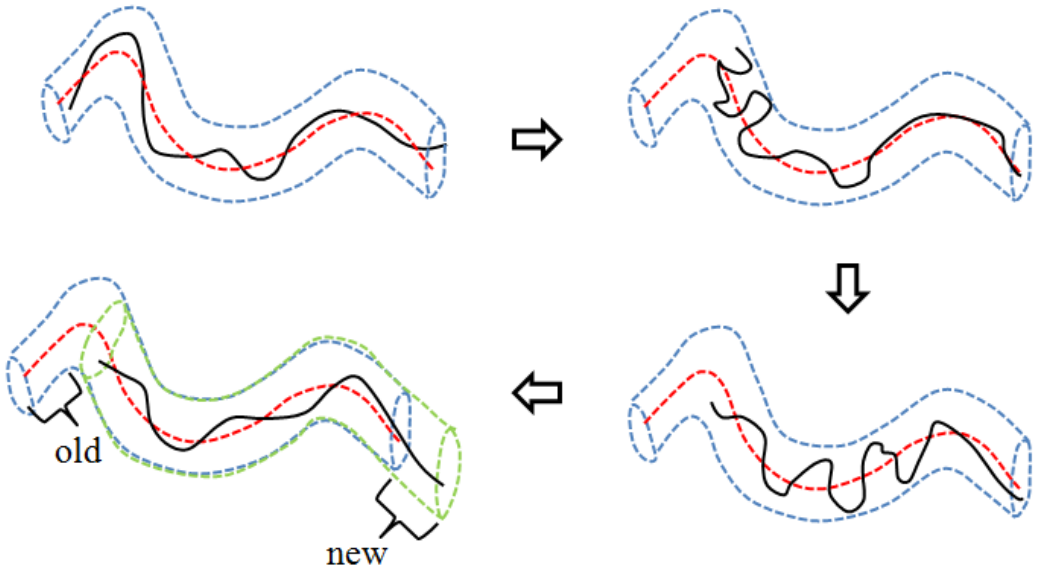

Figure 1-7. Relaxation process in a linear polymer[59]

The existence of branch points interrupts the relaxation of polymer chain. Figure 1-8 shows the stress relaxation mechanism in a star-shaped polymer. Obviously, the simple reptation of a polymer chain is prohibited. Meanwhile, the polymer is able to retract and withdraw a chain from the tube to the branching point, and then the chain goes into a new tube. This phenomenon, called contour length fluctuation, is allowed for stress relaxation in branched polymers.

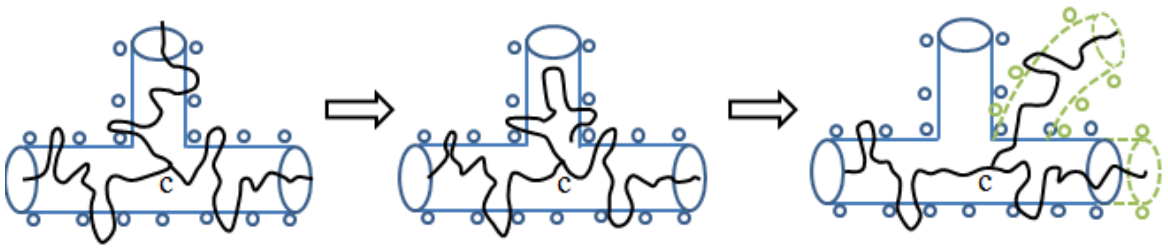

Figure 1-8. Contour length fluctuation in a star-shaped polymer[44]

Further, the main chain is not able to be relaxed until the relaxation of branches occurs in highly branched structure as shown in Figure 1-9. The figure illustrates that the main chain is constrained by a neighbor chain (left). However, the contour length fluctuation of the neighbor chain releases the main chain from the constraint (right).

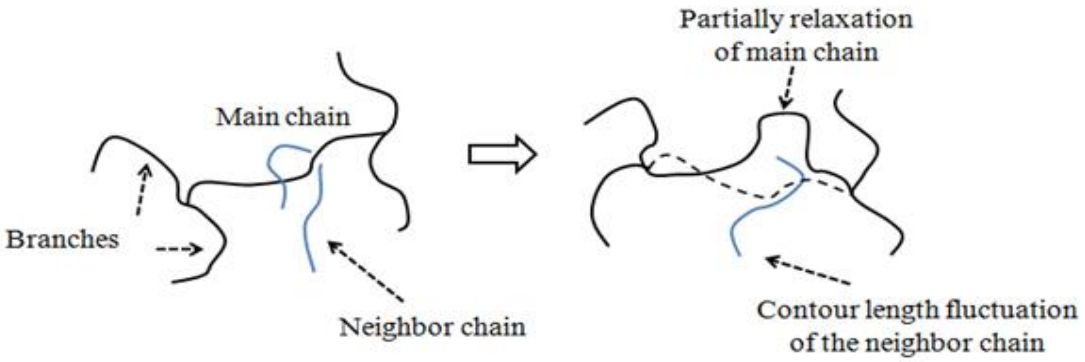

Figure 1-9. Relaxation of a main chain by constraint release[44]

1.5 Polymer processing

Varieties of processing equipments and shaping methods such as extrusion, injection-molding, blow-molding, thermoforming, and calendaring are available to form a desired product in the plastic industry. Before raw materials are transformed into a final plastic product by processing operations, almost all polymers are compounded with other materials such as fillers, reinforcements, other polymers, pigments, flame retardants, thermal stabilizers, and various processing aids for specific purposes. Typically, they are compounded with other materials by melt mixing to produce pellets to be used in subsequent processing operations.[60-64] In this section, following operations, in which their processability are strongly affected by the melt elasticity of material, are explained briefly; extrusion coating**,** thermoforming and blown film.

1.5.1 Extrusion coating

Nowadays, a large amount of LDPE is produced for extrusion coating.[65] The processability is very important to use a raw material efficiently and minimize the waste emission caused by the production loss, otherwise the waste spawns not only industrial loss but also social loss such as wasting fossil resource, excess energy consumption for re-production, and the expenditure to supplement all the loss and replacement.

The PE extrusion started in 1940's in the US. PE was firstly used as a coating material onto a paperboard for milk carton production since 1957 in order to give waterproof function to the paperboard. Since then, the extrusion coating was expanded in the 1960s, and the commercial use of PE coated material has been accelerated in the industry. Nowadays, co-extrusion is frequently applied to extrude a multilayer film. The co-extrusion uses several extruders depending on the layer structure desired. Further, not only a paperboard but also various films are used as substrates at extrusion coating, and extrusion lamination. The extrusion lamination is an extended application of extrusion technology to produce various multilayer lamination structures. In the lamination, a molten polymer is extruded between two substrate films as shown in Figure 1-10.[66]

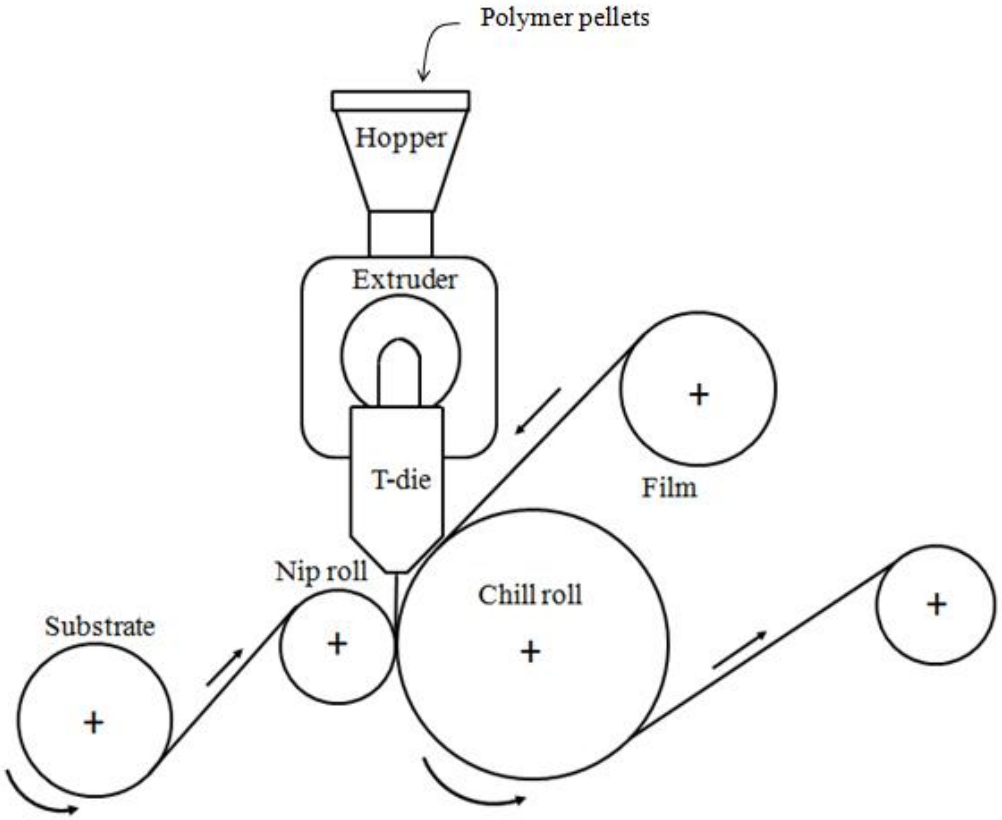

Figure 1-10. Schematic illustration of extrusion lamination station[66]

In T-die forming such as film casting, extrusion coating, and lamination, a polymer melt is extruded through a slit outlet of T-die with a shape of curtain-like film.

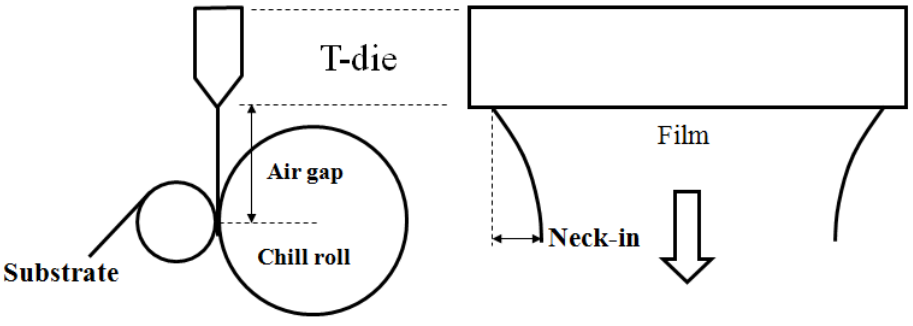

Figure 1-11. Shape of extrudate between T-die and rolls.

Higher speed coating is required for extrusion coating these days for high cost-performance. The stability of a molten polymer in the air gap, *i.e.*, the area between a die exit and a drill roll, and adhesion between the polymer and substrate are the necessary requirement for the extrusion coating. Meanwhile, a molten polymer film reduces its width, called neck-in and edge beads, as illustrated in Figure 1-11. The neck-in occurs in the air gap, resulting in the increase in film thickness at the both edges of the film, *i.e.*, edge beads. Because of neck-in, thicker edges need to be trimmed after coating, leading to the reduction of the film width. Therefore, the level of neck-in must be minimized, considering the productivity and quality of products. The extrudate is drawn by contacting a substrate that is usually running at several hundreds meters per minute.

It is well known that the extrusion coating process requires polymers having marked melt elasticity. In general, melt elasticity is pronounced by broadening MWD and incorporation of LCB. Therefore, LDPE is conventionally employed at extrusion coating.[67,68]

1.5.2 Thermoforming

Thermoforming involves softening of a thermoplastic sheet by heating, followed by forming with vacuum, pressure, or a moving mold core and mold cavity.[69-72] It is a process for converting a flat sheet into a product with thin-wall. Geometries of thermoformed products are usually simple, such as boxes, food trays, various containers, refrigerator linears, and computer cases. At vacuum forming, a sheet is clamped into a frame and exposed to radiant heaters as shown in Figure 1-12. After a sheet becomes soft to a formable condition, it is moved over a mold cavity and forced by air pressure forcing on

the top surface of the mold. As well as extrusion coating process, polymers used at thermoforming process must have marked melt elasticity because a molten sheet is deformed by gravitational force, which is known as “sagging”. The sagging phenomenon causes thinning and uneven thickness. Especially, excess thinning can be a cause of failure of a final product.

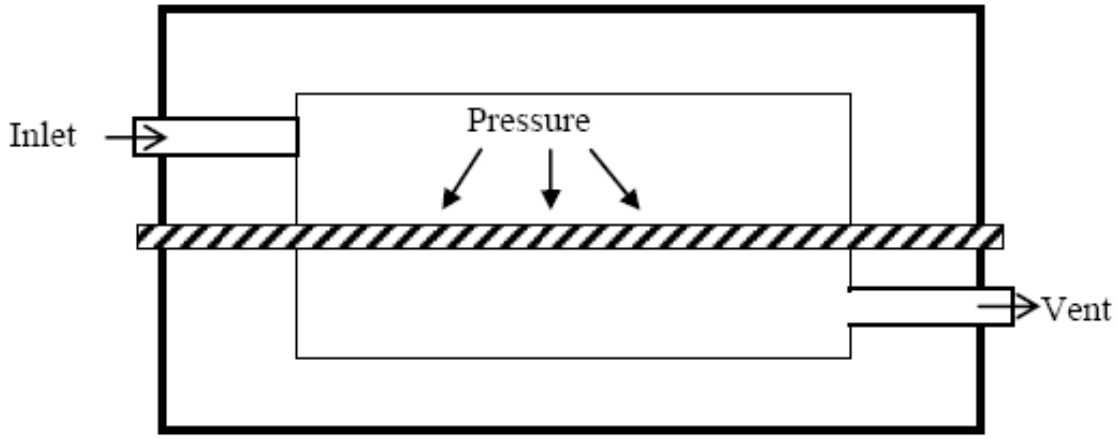

Figure 1-12. Schematic diagram of thermo forming.

At thermoforming, a sheet will not be fully melted at low temperature. Consequently, a formed product will not replicate accurately on the surface of the mold. When the temperature is too high, the sheet loses its dimensional stability and thus flows downward by gravity to a great extent. As a result, a thermoformed product will have uneven wall thickness and may even result in tearing.

1.5.3 Blown film

A blown film is obtained by biaxial stretching of an extruded molten polymer passed through an annular die like a tube and then blowing as a bubble as shown in Figure 1-13. During blowing process, a bubble is cooled by blowing air to expand the bubble outward. The inflation process will stretch a bubble in the transverse direction. This region is very important for bubble formation because poor melt elasticity of a linear polymer will give localized deformation and results in poor processability. However, if a branched polymer is used, a uniform deformation will take place because of marked strain-hardening, as seen in Figure 1-14.[73,74] Then, solidifying process of a bubble film occurs around the freezing line. A solidified bubble film is flattened into a double-layered sheet by nip rollers. After a bubble film has been flattened by nip rollers, a flat film is reeled up under a constant tension as a tubular film.

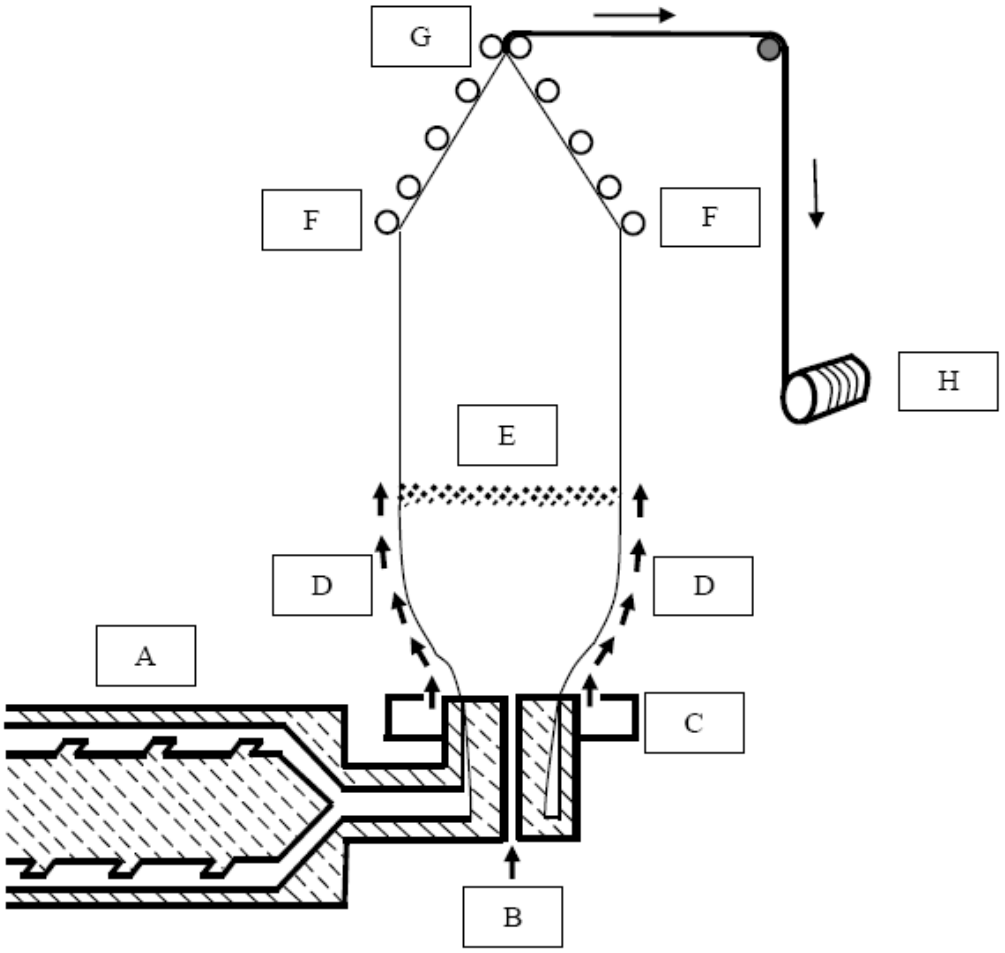

Figure 1-13. Schematic diagram of a blown film: A extruder; B air supply; C air ring; D cooling air flow; E freezing line; F guide rolls; G driven nip rolls; and H winder.[75]

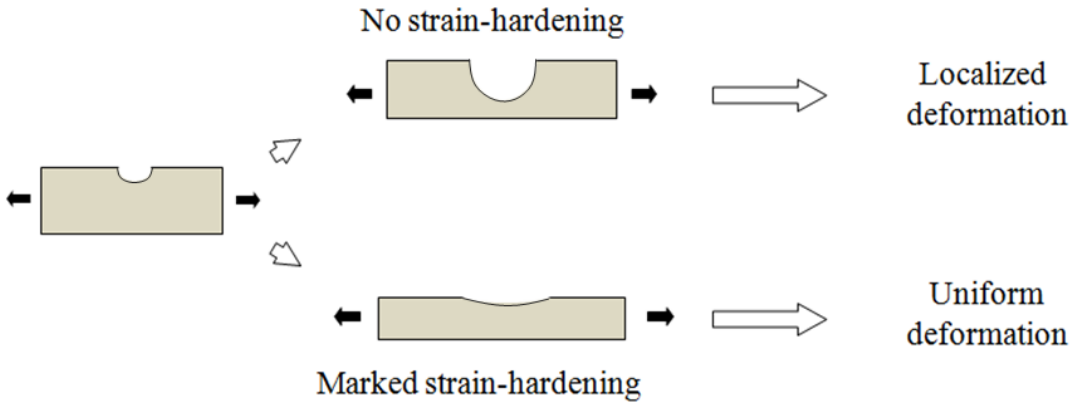

Figure 1-14. Deformation of a polymer melt with free surface

1.6 Rheological modification of PE

For the industry, processability is very important to fully utilize a raw material efficiently and minimize emission of waste caused by production loss, therefore control of rheological properties of a molten PE is an important technology to improve the processability and reduce the production loss.

As well know, many rheological modification techniques to control of rheological properties for PE have been proposed. Most of them have a strong impact on the elongational viscosity which is one of the most important rheological properties at polymer processing. In this section, several techniques to control the melt elasticity of PE, which were proposed by many previous researches, are reviewed briefly.

1.6.1 Shear modification

It is well known that long-chain branches enhance the elastic features greatly in the molten state.[28,44,76-80] Therefore, LDPE having long-chain branches shows higher melt elasticity than LLDPE. However, the elastic property of LDPE in the molten state is found to be depressed by applied processing history, which is known as "shear modification".[81-86] The mechanism of the shear modification was explained by Münstedt[80] based on the tube model.[44] At equilibrium state, branch polymer shows prolonged characteristic time of the longest relaxation mechanism, a because a simple reptation is not allowed by the branch parts. Further, the chain contraction between branch points is prohibited. After processing history, long-chain branches tend to align to the main chain by applied hydrodynamic force.[22,80,86] Consequently, a branch part is dragged into a tube of a main chain, leading to decrease in "active" long-chain branches. Because the alignment of LCB to the main chain,

a simple reptation is allowed. As a result, chain stretching occurs without the hindrance of branch parts as similar to linear polymer. Further, the longest relaxation time, *i.e.*, reptation time, is also reduced.

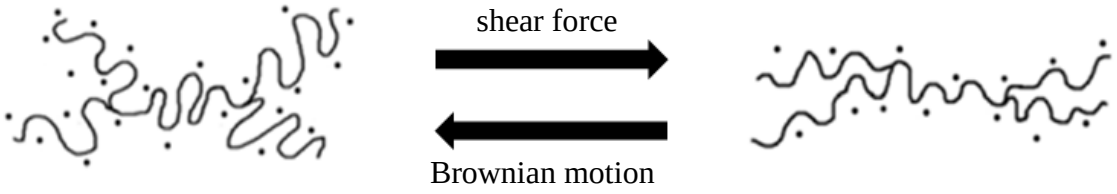

Figure 1-15. Schematics illustration of molecular conformation (left) before and (right) after the shear modification.

However, the branch parts are in a low entropy state. Therefore, the conformation will recover to the initial one by entropic force. Yamaguchi and Gogos evaluated the rheological properties at recovery process from shear modification and found that the rheological properties after applied shear history are determined by the applied shear stress and the duration time of shearing.[1]

1.6.2 LDPE/LLDPE blends

LDPE is often blended with linear PE, including LLDPE, VLDPE and HDPE, to improve the processability. Furthermore, it has been found that LDPE blended with linear PE having high molecular weight shows anomalous behaviors as reported by a number of researches.[3,4,47,87,88] In particular, the melt elasticity of LDPE is enhanced by blending LLDPE or HDPE, although both LLDPE and HDPE have narrow MWD with no LCB. This peculiar phenomenon was firstly detected by Utracki and Schlund.[3,87] They reported

that a positive deviation from the log additive rule is detected for η_0 of LDPE/LLDPE blends under both shear and extensional flow. Later, Ajji et al.[88] found that LLDPE containing 10–20 wt% of LDPE shows marked strain-hardening behavior in elongational viscosity. Wagner et al.[4] also demonstrated that the strain-hardening behavior for LDPE/LLDPE is more pronounced than that for pure LDPE. Further, the deviation of drawdown force from the linear additive rule for LDPE/LLDPE blends was reported by Mieda and Yamaguchi, as shown in Figure 1-16.[47]

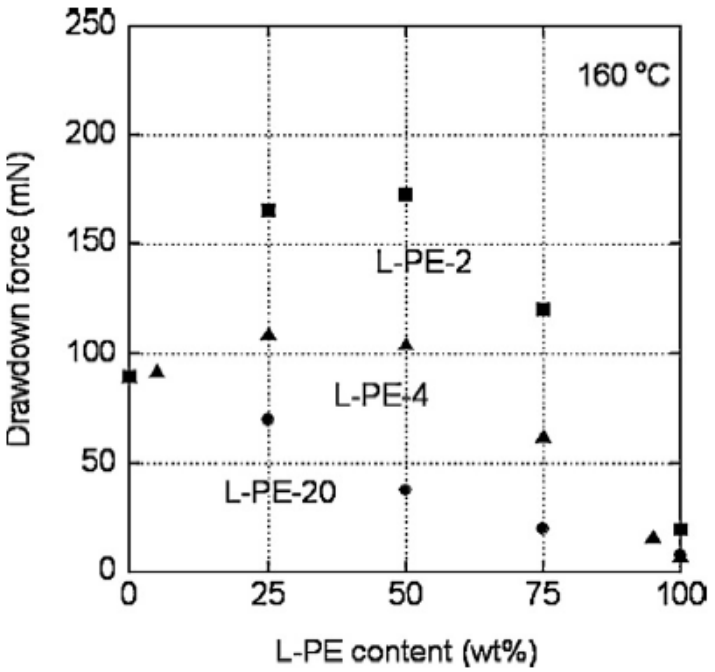

Figure 1-16. Drawdown force of branch-PE/linear-PE blends, B-PE/L-PE, at 160 ^{o}C; (closed circles) B-PE/L-PE-20, (closed triangles) B-PE/LPE-4, and (closed squares) B-PE/L-PE-2 blends. The number in the sample code represents a melt flow rate MFR of L-PE.[47]

The anomalous rheological responses, sometime called “synergetic system”, are pronounced as the molecular weight of linear PE increases. The anomalous phenomenon is

believed to be attributed to the entanglement couplings between a branched polymer and linear polymers.[2,6] In the blend system, the longest relaxation mechanism of the blends will be the relaxation of a backbone of a branch polymer in LDPE. For a branch polymer chain, primitive path fluctuation, dynamic tube dilation, and constraint release of branch parts become important, which have been proposed to predict the viscoelastic properties precisely based on the tube model.[87-90] Since the primitive path fluctuation is affected by the length of a branch, the characteristic time of this motion is unchanged by blending LLDPE.[89-91] On the other hand, the characteristic times of the dynamic tube dilation and constraint release depend on the relaxation of surrounding chains. For pure LDPE, the long-chain branched molecules in LDPE are surrounded by many linear molecules with low molecular weight. Therefore, after mixing with LLDPE having high molecular weight, the average relaxation time of surrounding linear chains will be increased. Consequently, the longest relaxation time of the blend with a linear PE having high molecular weight becomes longer than that of the pure LDPE.[92]

1.6.3 Cross-linking reaction

1.6.3.1 Cross-linking by thermal history

PE trends to show cross-linking reaction, especially at high temperature with prolonged residence time.[93,94] It results in changes of molecular weight, polydispersity, and branch structure. A basic mechanism was proposed by Rideal and Padget,[95] in which alkyl radical diffuses to react with oxygen to generate peroxy radical. Then, the radical abstracts hydrogen from an adjacent polymer chain. Consequently, the branch structure is created. A number of previous researches proposed that the processing history affect the characters of

a material, such as rheological properties, extrusion processability and crystallization rate.[96-98] Ono and Yamaguchi found that the drawdown force of LDPE increases and the drawability decreases with extrusion temperature up to 290 ^{o}C, as shown in Figure 1-17.[99] The result suggests that the extrusion processing leads to a cross-linking reaction, resulting in increased elongational viscosity.

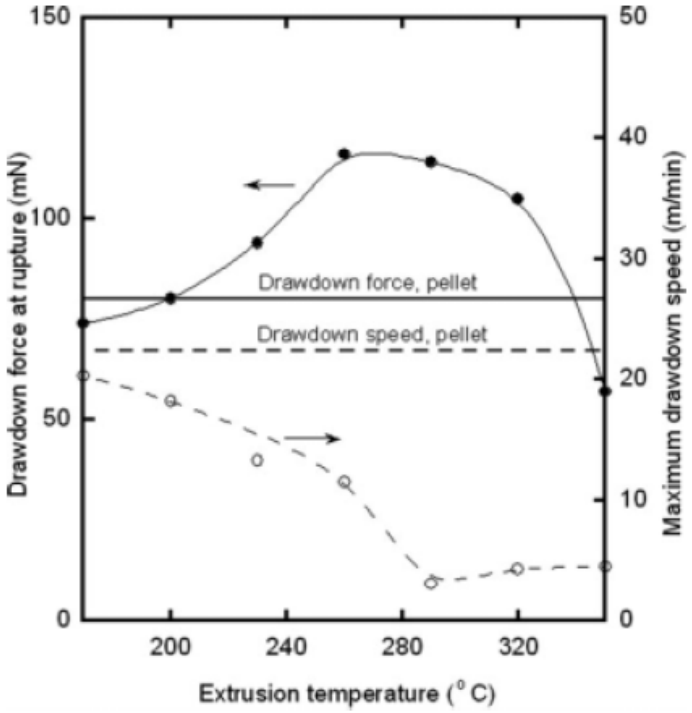

Figure 1-17. Drawdown properties of LDPE at 160 ^{o}C; drawdown force at rupture (filled circle) and maximum drawdown speed (open circle).[99] The samples without thermal stabilizer were extruded using a single-screw extruder at various temperatures.

1.6.3.2 Cross-linking by peroxide addition

Since PE is a thermoplastic material, it can be reprocessed repeatedly. However, it shows poor mechanical properties at high temperature, such as strength, environmental stress crack resistance (ESCR), resistance to slow crack growth, toughness, and abrasion resistance, which limits its applications.[100,101] Therefore, cross-linking is ofen carried out to retain desirable properties at high temperature. The permanent network generated by cross-linking reaction changes the nature of PE from a thermoplastic to a semi-thermoset plastic. The reaction leads to the formation of an insoluble part, in which the intermolecular reaction takes place to form three-dimension network structure,[102,103] This structure change improves impact strength, ESCR, and abrasion resistance without affecting tensile strength.[104,105] However, it reduces elongation at break.

1.7 Objectives of the study

Most studies on the cross-linking reaction were restricted to a single component of PE. Meanwhile, marked elastic properties of LDPE/LLDPE blend, in which LLDPE shows higher shear viscosity, have been reported as mention previously. However, the studies on cross-linking reaction for the LDPE/LLDPE blends have not been reported.

Further, a recent interesting research successfully revealed that molecular weight segregation of PE blends takes place in the molten state.[7] It was found that a fraction with low molecular weight tends to localize at a film surface. This type of segregation was confirmed for poly(styrene),[9,106] styrene-acrylonitrile copolymer,[8] and poly(styreneblock-methyl methacrylate).[107] Based on these researches, the rheological modification of PE by molecular weight segregation under temperature gradient is proposed in this study.

The main objective of this research is to propose several techniques to control the rheological properties of PE. In particular, the rheological modification is focused on the following two topics; (1) Cross-linking of LDPE/LLDPE blends with/without a peroxide compound. The rheological changes in pure LDPE, pure LLDPE and their blends after cross-linking reaction are investigated. Further, the effect of flow field on cross-linking efficiency for LDPE and LLDPE is discussed; (2) Molecular weight segregation of PE under temperature gradient. Firstly, the molecular weight segregation behavior under temperature gradient is studied using HDPE blends. Then, the molecular weight segregation of LDPE is investigated, which may be employed in the industry as a new method to control the viscoelastic properties.

References

1. Yamaguchi M.; Gogos C. G., *Adv. Polym. Tech.* **2001**, *20*, 261.
2. Yamaguchi, M.; Wagner M. H., *Polymer* **2006**, *47*, 3629.
3. Utracki, L. A.; Schlund B., *Polym. Eng. Sci.***1987**, *27*, 1512.
4. Wagner, M. H.; Kheirandish, S.; Yamaguchi M., *Rheol. Acta* **2004**, *44*, 198.
5. Mieda, N., *Effect of Long-chain Branches on Non-linear Rheological Properties for Polyethylene*, Ph.D. Thesis, Japan Advanced Institute of Science and Technology, Japan, **2011**.
6. Mieda, N.; Yamaguchi M., *Adv. Polym. Tech.* **2007**, *26*, 173.
7. Suwa, J.; Kakiage, M.; Yamanobe, T.; Komoto T.; Uehara, H., *Langmuir* **2007**, *23*, 5882.
8. Kim, E.; Kramer, E. J.; Garrett, P. D.; Mendelson, A. R.; Wu W. C., *Polymer* **1995**, *36*, 2427.
9. Tanaka, K.; Takahara, A.; Kajiyama, T., *Macromolecules* **1997**, *30*, 6626.
10. Tamboli, S. M.; Mhaske, S. T.; Kale, D. D., *Indian J. Chem. Technol.* **2004**, *11*, 853.
11. *Polyethylene Technology Book*; Mikami, N., Eds.; Kogyo Chosa Kai: Tokyo, **2001**.
12. JIS K 6922-1, **1997**.
13. Ziegler, K.; Holkampf, E.; Breil, H.; Martin, H., *Angew. Chem.*, **1955**, *67*, 541.
14. Shinn, H.; Kaminsky, W. ;Vollmer, H. J.; Woldt, R., *Angew. Chem. Int. Ed. Engl.*, **1980**, *19*, 390.
15. Peacock, A. J., *Handbook of polyethylene*; Marcel Dekker, Inc.: New York, **2000**.

16. Raff, R. A.; Doak, K. W., *Crystalline Olefin Polymers*; Interscience Publishers; J. Wiley & Sons Inc.: New York, **1964**.

17. McDaniel, M. P., *Polymerization on Phillips Type Catalysts,* in *Handbook of Heterogeneous Catalysis,* 2nd ed.; Ertl, G., Knozinger, H., Schuth, F., Weitkamp, J., Eds.; Chap. 15, Wiley-VCH Verlag: Weinheim, **2008**.

18. Yoshikawa, K.; Tonegi, N.; Mogi, Y.; Takahashi, M. Masuda, R., *J. Soc. Rheol. Jpn*., **1990**, *18,* 80.

19. Yoshikawa, K.; Tonegi, N.; Mogi, Y.; Takahashi, M. Masuda, R., *J. Soc. Rheol. Jpn*., **1990**, *18,* 87.

20. Hogan, J. P.; Levett, **C.** T.; Werkman, R. T., *SPE J.,* **1967**, *23,* **87.**

21. Randall, J. **C.,** In *Polymer Characterization with ESR and NMR, 142,* ACS Symposia: Washington D.C., **1980**.

22. Yamaguchi, M., *Melt Elasticity of Polyolefins; Impact of Elastic Properties on Foam Processing*, in *Polymeric Foam, Mechanisms and Materials*; Lee, S.T.; Ramesh, N., Eds.; Chap. 2, CRC Press: New York, **2004**.

23. Lauprelre, E; Monnerie, L.; Barthelemy, L.; Vairon, J. P.; Sauzeau, A.; Roussel, D., *Polym. Bull.,* **1986**, *15,* 159.

24. Pang. S ;.Rudin, A., *Polym. Mater. Sci. Eng.,* **1991**, *65,* 95.

25. Shroff, R. N.; Mavridis, H., *Macromolecules,* **1999**, *32,* 8454.

26. Chum, P. S.; Kruper, W. J.; Guest, M. J., *Adv. Mater.*, **2000,** *12*, 1759.

27. Laun, H. M.; Schuch, H., *J. Rheol.*, **1989,** *33*, 119.

28. Ferry, J. D., *Viscoelastic Properties of Polymers*; Wiley: New York, **1980**.

29. Van Krevelen, D. W., *Properties of Polymers,* 2nd ed; Elsevier: New York, **1976**.

30. Stadler, F. J.; Münstedt, H., *Macromol. Mater. Eng.*, **2009**, *294*, 25.

31. Garcia-Franco, **C.** A.; Harrington, B. A.; Lohse, D. J., *Macromolecules,* **2006**, *39*, 2710.

32. Tschoegl, N. W., *Rheol. Acta*, **1971**, *10*, 582.

33. Graessley, W., *Adv. Polym. Sci.*, **1974**, *16*, 1.

34. ASTM D 238.

35. Bannie, S.; Pokowski, C.; Kingston, J., *Characterization and Failure Analysis of Plastics*; ASM International: New York, 2003.

36. Macosko, C. W., *Rheology: Principles, Measurements, and Applications*; John Wiley & Sons: New York, **1994**.

37. Suzuki, M.; Mohd Amran, M. A.; Okamoto, K.; Taniike, T.; Terano, M.; Yamaguchi, M., *Adv. Polym. Technol.*, **2009**, *28*, 185.

38. Huang, J. C.; Leong, K. S., *J. Appl. Polym. Sci.* **2002**, *84*, 1269.

39. Tapadia, P. S.; Joshi, Y. M.; Lele, A. K.; Mashelkar, R. A., *Macromol.*, **2000**, *33*, 250.

40. Meissner, J., *Trans. Soc. Rheol.*, **1972**, *16*, 405.

41. Trouton, F. T., *Proc. Roy. Soc.*, **1906**, *A77*, 426.

42. Barnes, H. A.; Hutton, J. F.; Walter, K., *An Introduction to Rheology*; Elsevier Science: New York, **1993**.

43. Osaki, K.; Murai, A.; Besshi, N.; Kim, B. S., *J. Rheol.*, **1976**, *4*, 166.

44. Doi, M; Edwards, S .F., *The Theory of Polymer Dynamics*; Oxford University Press: New York, **2007**.

45. Wagner, M. H.; Yamaguchi, M.; Takahashi, M., *J. Rheol*., **2003**, *147*, 779.

46. Inkson, N. J.; McLeish, T. C. B., *J. Rheol.*, **1999**, *43*, 873.

47. Mieda, N.; Yamaguchi, M., *J. Non-Newtonian Fluid Mech.*, **2011**, *166*, 231.

48. Bernnat, A., *Polymer Melt Rheology and the Rheotens Test.* Ph.D. Thesis, University of Stuttgart, Stuttgart, **2001**.

49. Yamaguchi, M.; Takahashi, M., *Polymer*, **2001**, *42*, 8663.

50. Wanger, M. H.; Bastian, H.; Hachmann, P.; Meissner, J.; Kurzbeck, S.; Münstedt, H.; Langouche, F., *Rheol. Acta*, **2000**, *39*, 1.

51. Wanger, M. H.; Bernnat, A.; Schulze, V., *J. Rheol.*, **1998**, *42*, 917.

52. Yamaguchi M., *J. Polym. Sci. Polym. Phys. Ed.*, **2001**, *39*, 228.

53. Hameed, T.; Hussein, I. A., *Polymer*, **2002**, *43*, 6911.

54. Hussein, I. A.; Hameed, T.; Sharkh, B. F. A.; Mezghani, K., *Polymer*, **2003**, *44*, 4665.

55. Arakawa, K.; Yokohara, T.; Yamaguchi, M., *J. Appl. Polym. Sci.*, **2007**, *107*, 1320.

56. Deadly, J. M.; Larson, R. G., *Structure and Rheology of Molten Polymers: from Structure to Flow Behavior and Back Again*; Hanser Publishers: Munich, **2006**.

57. Clifford, K. S.; Peter, K., *Kirk-Othmer Encyclopedia of Chemical Technology*, **2000**, *11*, 473.

58. Edwards, S .F., *Proc. Phys. Soc.*, **1967**, *92*, 9.

59. de Gennes, P. G., *J. Chem. Phys.*, **1971**, *55*, 572.

60. Grulke, E. A., *Polymer Process Engineering*; PTR Prentice-Hall: New Jersey, **1994**.

61. Progelhof, R. C.; Throne, J. L., *Polymer Engineering Principles: Properties, Processes and Tests for Design*; Hanser Publishers: Munich, **1993**.

62. Chabot, J. F., *The Development of Plastics Processing Machinery and Methods*; Society of Plastics Engineers: Connecticut, **1992**.

63. Charrier, J. M., *Polymeric Materials and Processing: Plastics, Elastomers and Composites*; Hanser Publishers: Munich, **1991**.

64. Morton-Jones, D. H., *Polymer Processing*; Chapman and Hall: New York, **1989**.

65. *Next generation polyolefins,* vol.3; The society of Polyolefin Science and Industry Japan, Eds.; Sankeisha: Tokyo, **2009**.

66. Ono, K., *Study on Modification of Polyolefin by Extraneous Factors during Polymer Processing*, Ph.D. Thesis, Japan Advanced Institute of Science and Technology, Japan, **2010**.

67. Dobroth, T., Erwin, L., *Polym. Eng. Sci.*, **1986,** *26*, 462.

68. Kouda, S., *Polym. Eng. Sci*., **2008**, *48*, 1094.

69. Klien, P. W., *Fundamentals of Plastics Thermoforming*; Morgan & Claypool Publisher: New York, **2009**.

70. Illing, A., *Thermoforming: A Practical Guide*; Hanser Publishers: Munich, **2000**.

71. Throne, J. L., *Technology of Thermoforming*; Hanser Publishers: Munich, **1996**.

72. Florian, J., *Practical; Thermoforming: Principles and Applications*; Marcel Dekker: New York, **1996**.

73. Han, C. D.; Park, J. Y., *J. Appl. Polym. Sci.*, **1975**, *19*, 3291.

74. Yamaguchi, M., *Polym. Eng. Sci.*, **2006**, *46*, 1284.

75. Tadmor, Z.; Gogos, C. G., *Principles of Polymer Processing*, 2nd ed.; John Wileys & Sons, Inc.: New York, **2006**.

76. Boghetich, L.; Kratz, R. F., *Trans. Soc. Rheol.*, **1965**, *9*, 255.

77. Mendelson, R. A.; Bowles, W. A.; Finger, F. L., *J. Polym. Sci. Polym. Phys. Ed.*, **1970**, *8*, 105.

78. Vega, J. F.; Santamaria, A., *Macromolecules* **1998**, *31*, 3639.

79. Gotsis, A. D.; Zeevenhoven , B. L. F.; Tsenoglou, C., *J. Rheol.*, **2004**, *48*, 895.

80. Münstedt, H. *Soft Matter*, **2011**, *7*, 227.

81. Howells, E. R.; Benbow, J., *J. Trans J. Plast. Inst.*, **1962**, *30*, 240.

82. Hanson, D. E., *Polym. Eng. Sci.*, **1969**, *9*, 405.

83. Fujiki, T., *J. Appl. Polym. Sci.*, **1969**, *13*, 233.

84. Münstedt, H., *Colloid Polym. Sci.*, **1981**, *259*, 966.

85. Rudin, A.; Schreiber, H. P., *Polym. Eng. Sci.*, **1983**, *23*, 422.

86. Leblans, P. J. R.; Bastiaansen, C., *Macromolecules*, **1989**, *22*, 3312.

87. Schlund, B.; Utracki, L. A., *Polym. Eng. Sci.*, **1987**, *27*, 1523.

88. Ajji, A.; Sammut, P.; Huneault, M. A., *J. Appl. Polym. Sci.*, **2003**, *88*, 3070.

89. Lohse, D. J.; Milner, S. T.; Fetters, L. J.; Xenidou, M.; Hadjichristidis, N.; Mendelson, R. A.; Garcia-Franco, C. A.; Lyon, M. K., *Macromolecules*, **2002**, *35*, 3066.

90. Delgadillo-Velázquez, O.; Hazikirakos, S. G.; Sentmanat, M., *Rheol. Acta*, **2008**, *47*, 19.

91. Valenza, A.; Manitia, F. P. L.; Acierno, D., *J. Rheol.*, **1986**, *30*, 1085.

92. Tuminello, W. H., *Polym. Eng. Sci.*, **1986**, *26*, 1339.

93. Butler, T. I., *J. Plast. Film Sheet*, **1990**, *6*, 247.

94. Hinsken, H.; Moss, S.; Pauquet, J. R.; Zweifel, H., *Polym. Degrad. Stab*, **1991**, *34*, 279.

95. Rideal, G. R.; Padget, J. C., *J. Polym. Sci. Symp.* **1976**, 57, 1.

96. Satoh, N.; Tomiyama, H. T.; Kajiwara, T., *Polym. Eng. Sci.* **2001**, *41*, 1564.

97. Zahavich, A. T. P.; Latto, B.; Takacs, E.; Vlachopoulos, J., *Adv. Polym. Technol.* **1997**, *16*, 11.

98. Rybnikar, F., *J. Polym. Sci. Polym. Symp.* **1976**, *57*, 101.

99. Ono, K.; Yamaguchi M., *J. Appl. Polym. Sci.*, **2009**, *113*, 1462.

100. Samburski, G.; Narkis, M., *J. Macromol. Sci. Phys. B*, **1996**, *35*, 843.

101. Dakin, Y. I., *J. Appl. Polym. Sci.*, **1996**, *59*, 1355.

102. Sawatari, C.; Mastuo, M., *Polym. J.*, **1987**, *19*, 1365.

103. Houde, M.; Schreiber, H. P., *J. Appl. Polym. Sci.*, **1992**, *46*, 2049.

104. Miltz, J.; Nakis, M., *Polymer*, **1968**, *9*, 173.

105. Nakis, M.; Miltz, J., *J. Appl. Polym. Sci.*, **1968**, *12*, 1030.

106. Keddie, J. L.; Jones, R. A. L.; Coury, R. A., *Europhys. Lett.*, **1994**, *27*, 59.

107. Tanaka, K.; Takahara, A.; Kajiyama, T., *Acta Polym.* **1995**, *46*, 476.

Chapter 2

Rheological Modification by Cross-linking Reaction

2.1 Introduction

As explained in Chapter 1, LDPE is profitably employed in extrusion-coating because of its marked melt elasticity. The chemical structure of LDPE is, however, changed at processing operation because extrusion-coating is performed at higher temperature to enhance the adhesive strength with a base material. Moreover, LDPE used in extrusion coating does not contain any thermal stabilizer. Therefore, chemical reaction such as cross-linking and chain scission occurs significantly. This is very important to control the processablity.

According to previous reports,[1-4] the cross-linking reaction occurrs more readily at relatively high temperatures, *e.g.*, 250-320 °C. In these reactions, free radicals generated during processing play an important role. Kuroki *et al*.[1] revealed that the rate of cross-linking reaction is 3-5 times larger than that of chain scission at temperatures below 350 °C. Andersson *et al.* found that the cross-linking reaction is dominant at temperatures below 325 °C during extrusion coating.[2] The same result was obtained by Ono and Yamaguchi at extrusion processing.[3] Rangarajan,[4] in contrast, reported that chain scission takes place randomly at temperatures between 450 and 490 °C. Further, it was reported that repeated extrusions affects to polymer structure and mechanical properties of LDPE.[5,6]

Because chain scission is generally not desired, various techniques are used to improve the cross-linking efficiency of PE, such as irradiation,[7] addition of peroxide compounds as free radical initiators, or addition of silane coupling agents. According to Ghosh *et al.*,[8] the addition of a proper amount of a peroxide compound results in the acceleration of the cross-linking reactions. This technique is applicable to control the shear viscosity and its non-Newtonian behavior.

In the cross-linking reaction, macroradicals generated by the abstraction of a hydrogen atom in the chain, which often occurs at tertiary carbon atoms, show intermolecular reaction:[9] X-type branch points are provided by the reaction of two macroradicals, whereas Y-type branch points are provided by the reaction between a macroradical and a double bond at the chain end (terminal vinyl).[10-12] Moreover, a high degree of cross-link density leads to a three-dimension network structure which greatly changes the rheological properties of a material.[13,14]

To the best of our knowledge, however, most studies on the rheological changes resulting from rheological modification through the cross-linking reaction were restricted to a single component of PE. Meanwhile, the marked elastic properties of LLDPE/LDPE blends, in which the LLDPE shows higher shear viscosity, have been reported by a number of researchers.[15-20] However, the rheological modification through the cross-linking reaction of LLDPE/LDPE blends has not been studied, even though the blends have been employed in industry. In this study, therefore, the effects of cross-linking/chain scission reaction with/without peroxide compound on the rheological properties of LLDPE, LDPE, and their blends are investigated. Moreover, the effect of flow field on the cross-linking efficiency is also studied using a peroxide compound.

2.2 Experimental

2.2.1 Materials

Commercially available LDPE, produced in an autoclave reactor, and LLDPE, synthesized by a metallocene catalyst, were used in this study. Neither sample contained thermal stabilizer. Molecular characteristics are summarized in Table 2-1. The contents of unsaturated bonds at chain ends (terminal vinyl) and in the middle of chains (vinylene and vinylidene) were measured by proton nuclear magnetic resonance spectroscopy (^{1}H-NMR). The short- and long- ($\geq C_6$) chain branches per 1000 backbone carbon atoms were characterized by carbon nuclear magnetic resonance spectroscopy (^{13}C-NMR). The number of long- ($\geq C_6$) chain branches of LDPE is a typical one for conventional LDPE.[5,21-23] Further, the molecular weights were evaluated by gel permeation chromatography (GPC) (Waters, Alliance GPC 2000) as linear PE standard, using TSK_{gel} GMH_6-HT and TSK_{gel} GMH_6-HTL, with ortho-dichlorobenzene at 140 ºC as an eluant at a flow rate of 1.0 mL/min. The sample concentration was 0.15 wt.%.

Table 2-l Molecular characteristics of PE used in this work

	GPC			^{1}H-NMR (per 1000 carbon atoms)			^{13}C-NMR (per 1000 carbon atoms)			
	Mn (Da)	Mw (Da)	Mz (Da)	terminal vinyl	vinylene	vinylidene	C2	C4	C5	C6 or more
LDPE	13,000	192,000	1080,000	0.06	0.07	0.33	1	-	8	2
LLDPE	33,200	98,900	220,000	0.06	0.05	0.05	-	36	-	-

2.2.2 Sample Preparation

2.2.2.1 Sample without thermal modification

LDPE, LLDPE and their blends at various blend ratios were prepared by melt-mixing at 130 °C with thermal stabilizers, such as pentaerythritol tetrakis(3-3,5-di-tert-butyl-4-hydroxyphenyl propionate) (Ciba, Irganox1010) and tris(2,4-di-tert-butylphenyl)phosphate (Ciba, Irgafos168), in a 60 cc internal batch mixer (Toyoseiki, Labo-plastmil) for 3 min. The total amount was 48 g. The blade rotation speed was 30 rpm. The content of each additive was 5000 ppm. The obtained samples are used as reference samples.

2.2.2.2 Thermal modification

LDPE and LLDPE were melt-blended at various blend ratios in the same internal batch mixer for 3 min at 280 °C to perform the thermal modification. The total amount was 48 g. The blade rotation speed was 30 rpm. Thermal stabilizers at the same content with the reference sample were added after 3 min and further mixed for 30 s. The same thermal history was also applied to pure LDPE and LLDPE.

2.2.2.3 Thermal modification under flow field

The samples were mixed with a cross-linking agent, α,α'–di(t-butylperoxy)diiso-propylbenzene (Perbutyl-P, 338.48 g mol^{-1}), 1 % wt.%, at 130 ^{o}C by the same internal batch mixer. The haft time of decomposition of peroxide compound is 1 min at 175.4 ^{o}C. Then, the polymer was compressed at 130 ^{o}C under 10 MPa for 3 min. The obtained sample composed of 1 wt.% peroxide was used a master batch. The master batch was cut into small pieces and diluted by melt-mixing with LDPE or LLDPE at 190 ^{o}C at a blade

rotation speed of 30 rpm, for 15 min in a 30 cc internal batch mixer (Toyoseiki, Labo-plastmil) to perform the cross-linking reaction under flow field. The total amount was 24 g. Then, the thermal stabilizers were added and mixed for 30 s. Finally, the concentration of peroxide was controlled to be 0.1 and 0.05 wt.%.

.

2.2.2.4 Thermal modification without flow field

The master batch, 1 wt.% peroxide, was cut and diluted by melt-mixing with LDPE or LLDPE at 130 ^{o}C by the 30 cc internal batch mixer. The total amount was 24 g. The obtained samples with various concentrations of the peroxide were compressed at 190 ^{o}C with a compression stress of 1 MPa for 15 min by the compression-molding (Imoto Machinery Co., Ltd) to perform the cross-linking reaction without flow field. The thickness of the sample sheet was 1 mm.

Further, the cross-linked LDPE/LLDPE (50/50) without flow field was prepared by the same protocol. The final contents of the peroxide for the blend were controlled to be 0.05 and 0.5 wt.%.

All samples, except for the cross-linked samples without flow field, were compressed into a flat sheet by the compression-molding machine at 230 °C under 10 MPa for 10 min. Then, the sample was cooled down at 30 °C. Because of the long annealing time in the compression-molding machine, the applied shear history, which has strong impact on the rheological properties of long-chain branched polymers, known as “shear modification”,[24,25] was removed from the samples. It was revealed that the rheological properties such as drawdown force and oscillatory modulus were not changed by prolonged annealing in the compression-molding machine, which will be shown later. Consequently, the oscillatory modulus in the molten state was stable during the

measurement, confirmed by repeat measurements of the frequency dependence of the oscillatory modulus

2.2.3 Measurements

The frequency dependence of the oscillatory shear moduli was measured at 130, 160 and 190 °C in a rotational-type rheometer (TA Instruments, AR2000) under a nitrogen atmosphere using cone-and-plate and parallel-plate geometries. The time dependence of the oscillatory modulus at 0.01 Hz was also evaluated at 190 °C to confirm thermal stability. The both diameters of cone-and-plate and parallel-plate were 25 mm. The cone angle was 4°. Further, the shear stress and primary normal stress difference under steady-shear were measured at various shear rates at 190 °C using the cone-and-plate rheometer. The measurements were performed three times to evaluate the experimental scatter.

Capillary extrusion was performed on a capillary rheometer (Yasuda Seiki Seisakusyo, 140 SAS-2002) at 190 °C to evaluate the steady-state shear viscosity and the appearance of the extruded strands. The molten polymer was extruded through a die of dimensions: 1 mm diameter, 10 mm long and an entrance angle of 180°. The swell ratio was measured by a laser detector fixed 5 cm below the die exit.

The drawdown force measurement was carried out at 190 °C with the capillary rheometer, equipped with a tension detector and a set of rotating wheels. The molten polymer was extruded through the same die used to evaluate the capillary extrusion properties. The draw ratio was 9.2, which was empirically chosen because it gave reliable values of force. Furthermore, the value is less sensitive to the draw ratio when the draw ratio is larger than 5.[23,26] The apparent shear rate at the die wall was 21.9 s^{-1}.

The growth curves of uniaxial elongational viscosity were evaluated at 160 °C on the rotational rheometer, equipped with a universal testing platform (Xpansion instruments, SER2-G). Flat sheet samples, 10 mm wide, 15 mm long, and 0.5 mm thick, were used.

The recovery behavior of the oscillatory modulus after applied shear history was evaluated to obtain the information on the branch structure. Under the applied hydrodynamic force, the long-chain branches are aligned to the main chain. The modulus recovery after the cessation of flow is a result of an increase in entropy around the branch points, as this alignment relaxes. Therefore, the process is sensitive to the branch structure. The samples were sheared at a stress level of 24.5 kPa by the cone-and-plate rheometer at 160 °C for 30 min. After cessation of the shear flow, an oscillatory strain at 0.01 Hz was applied immediately to the sample at 160 °C. Then, the growth curves of the shear storage modulus were evaluated as a function of the residence time in the rheometer. The details of this method were explained in a previous paper.[24]

2.3 Results and discussion

2.3.1 Rheological modification of PE by thermal history

2.3.1.1 LDPE and LLDPE

The molecular weight and its distributions for the samples before and after thermal modification are shown in Figure 2-1. The GPC curves are barely changed by the thermal modification at 280 °C for 3 min in the internal mixer. Moreover, the contents of double bonds in the processed samples, evaluated by NMR, are the same as those in the original polymers within experimental error, as seen in Table 2-2.

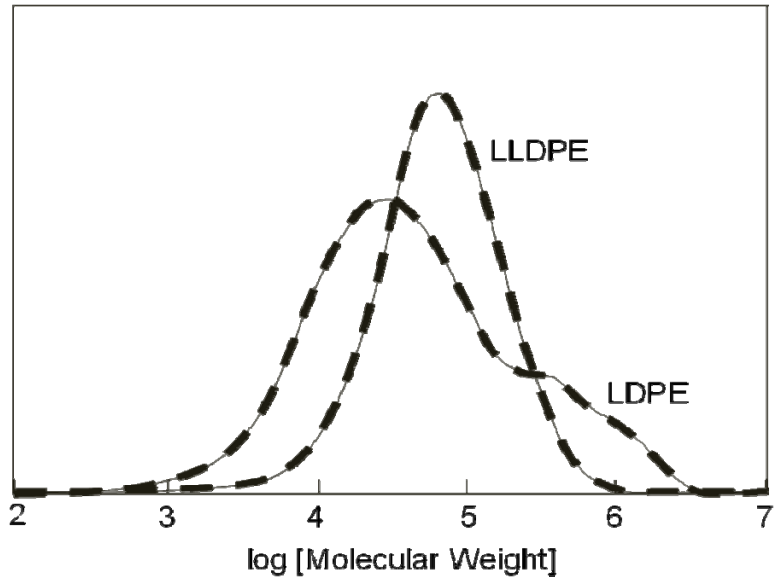

Figure 2-1 GPC curves of LDPE and LLDPE; (dotted lines) before and (solid lines) after thermal modification

Table 2-2 Molecular characteristics of PE after thermal modification

	GPC			^{1}H-NMR (per 1000 carbon atoms)		
	Mn (Da)	Mw (Da)	Mz (Da)	terminal vinyl	vinylene	vinylidene
LDPE	13,000	192,000	1,080,000	0.06	0.07	0.33
LDPE after modification	13,500	195,000	1,130,000	0.06	0.07	0.32
LLDPE	33,200	98,900	220,000	0.06	0.05	0.05
LLDPE after modification	30,400	99,000	227,000	0.05	0.05	0.05

Although the poor sensitivity (1/1000 carbon atoms for branches) has to be considered, these results indicate that the thermal history should not be severe enough to affect their primary molecular structure. This behavior was previously reported and well summarized by Janzen and Colby.[27] It has been well known for PE that thermal modification barely affects the number of short-chain branches.[3,12,28]

Prior to the measurement of the frequency dependence of the oscillatory shear modulus, the time dependence of the oscillatory shear modulus was evaluated at 190 °C to confirm the thermal stability during the measurement. As shown in Figure 2-2, the shear storage modulus *G'* is a constant irrespective of the residence time in the rheometer at 190 °C, suggesting that the samples are thermally stable, presumably as a result of the sufficient thermal stabilizers. Furthermore, the figures also demonstrate that the samples are free from shear history. It has been reported that the oscillatory moduli of a long-chain branched polymer are strongly reduced by applied shear history and increase with annealing time in the molten state without shear flow.[24,25,29,30] All the samples used in this study show constant values of both moduli irrespective of the residence time in the rheometer, demonstrating that the effect of the applied shear history was removed during the compression-molding at 230 °C for 10 min.

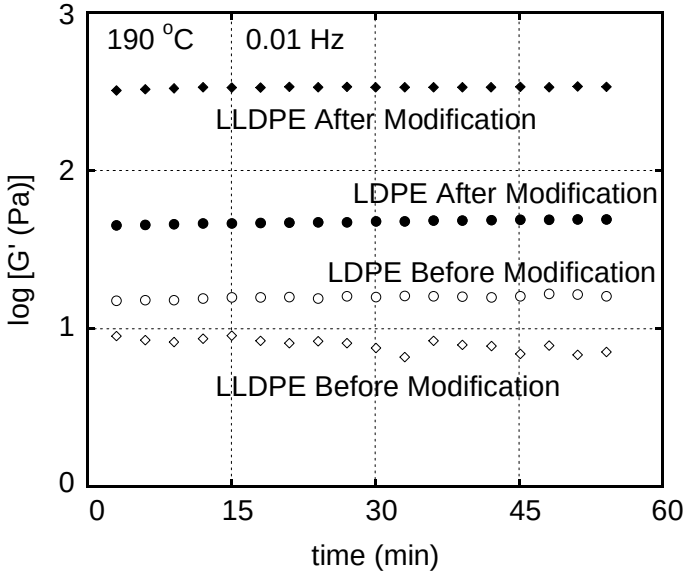

Figure 2-2 Time dependence of shear storage modulus *G'* at 0.01 Hz at 190 °C for the samples (open symbols) before and (closed symbols) after thermal modification; (circles) LDPE and (diamonds) LLDPE

The angular-frequency dependence of the oscillatory moduli for LDPE and LLDPE is shown in Figure 2-3. As indicated in Figure 2-2, both moduli for LLDPE are greatly enhanced by the applied thermal history. Because the GPC curve, based on a linear PE standard, is not changed by the history, the generation of a small amount of long-chain branches must affect the rheological properties as shown later. Because the contents of double bonds in the original LLDPE are unchanged, the cross-linking reaction of two macro-radicals produced by the removal of a hydrogen atom in the backbone, which was revealed by Kriston[31] in detail, is the dominant mechanism to provide long-chain branches. A large number of short-chain branches in the LLDPE used in this study is responsible for the marked rheological change, because the hydrogen atoms attached to the tertiary carbon are easily abstracted. However, the effect of the applied thermal history on the linear viscoelastic properties is not obvious for LDPE, suggesting that linear viscoelastic properties of LDPE are less sensitive to the applied thermal history. Because of the broad distribution of relaxation times of the original LDPE, as compared with the original LLDPE, prolonged relaxation mechanisms cannot be detected clearly. This is reasonable because a small amount of long-chain branches created by the thermal modification should have minimal effect on the linear viscoelastic properties of LDPE.[27] Even for LDPE, however, *G'* in the low frequency region is slightly enhanced, indicating that the characteristic time of the longest relaxation mechanism is prolonged. Moreover, GPC curves and oscillatory modulus at high frequencies indicate that chain scission during the thermal history can be ignored for both samples.

The enhancement of *G"* by thermal modification is, of course, responsible for the increase in η_0: from 19,000 [Pa s] at 190 °C for the original LLDPE to 190,000 [Pa s] for the modified LLDPE. Considering that there is almost no change in the weight-average

molecular weight M_w as seen in Table 2-2, this result also supports the generation of long-chain branches.

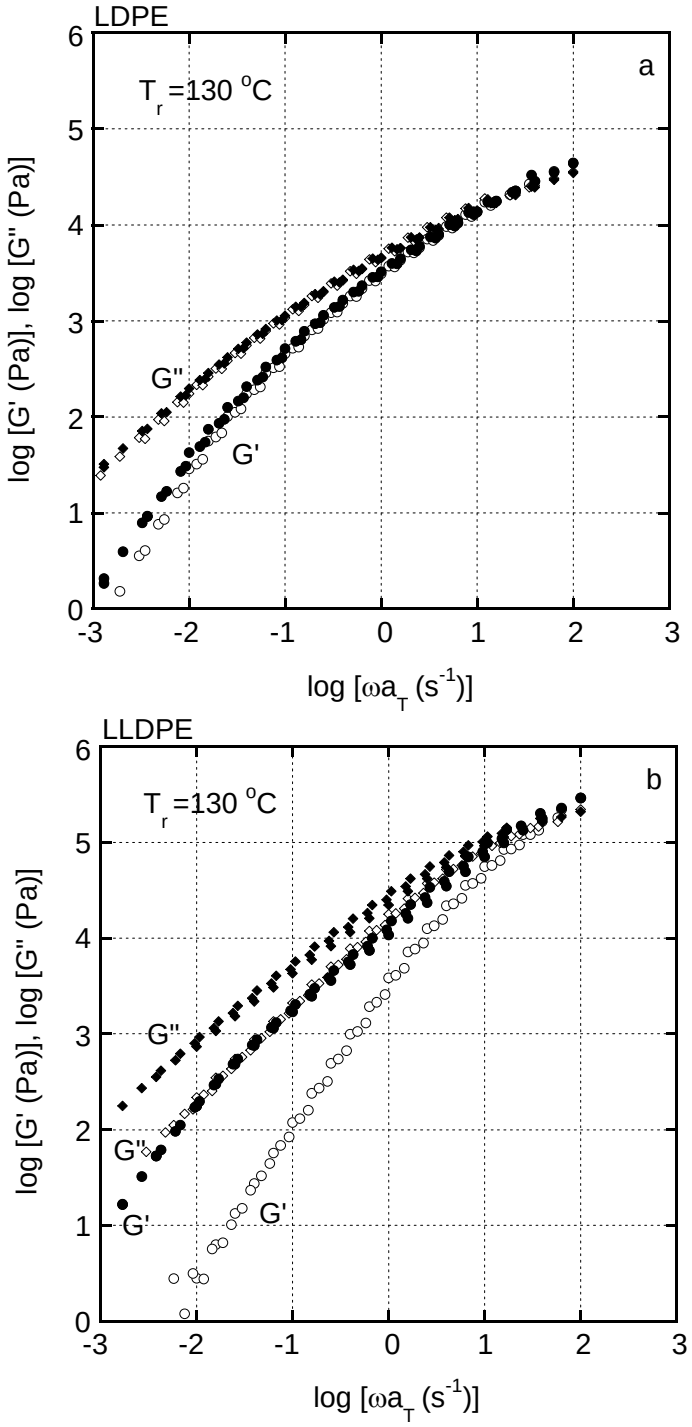

Figure 2-3 Master curves of frequency dependence of (circles) shear storage modulus *G'* and (diamonds) loss modulus *G"* at 130 °C for (a) LDPE and (b) LLDPE; (open symbols) before and (closed symbols) after thermal modification.

The master curves in Figure 2-3 are obtained by a simple horizontal shift without a vertical one. Strictly speaking, however, it is impossible to superpose all data for LDPE, because molten LDPE is known to be a thermo-rheologically complex material.[16,20] Keßner and Münstedt[32] reported a similar result for a metallocene-based LLDPE having long chain branches (LCB).

The van Gurp-Palmen plot is known to be very sensitive to polydispersity, LCB and molecular weight distribution (MWD).[33] Therefore, it will be a useful method to monitor the changes of molecular architecture after modification. In the Van Gurp-Palmen plot, the plot of phase angle δ is plotted against the absolute values of complex shear modulus $|G^*|$. If the time temperature superposition principle (TTS) is acceptable to a material, the isothermal curves can merge into a common line. However, if the TTS principle is not acceptable, the curves cannot be superposed onto each other. Further the low value of δ suggests a broad relaxation time distribution.

The van Gurp-Palmen plots for pure polymers are shown in Figure 2-4. Although all data are on a single curve for LLDPE prior to the thermal modification, the complex thermo-rheological behavior is clearly detected after the thermal modification. Moreover, the data measured at low temperature are located below those at high temperature, as is also the case for LDPE. The phase angle becomes smaller as a result of the thermal modification, especially for LLDPE. This result is attributed to the broadening of the relaxation time distribution. Furthermore, the shoulder at $|G^*| = 10^4$ Pa in the modified LLDPE demonstrates that there is a long-time relaxation mechanism with a relatively narrow distribution of characteristic times, which is presumably attributed to the relaxation of the long-chain branches.

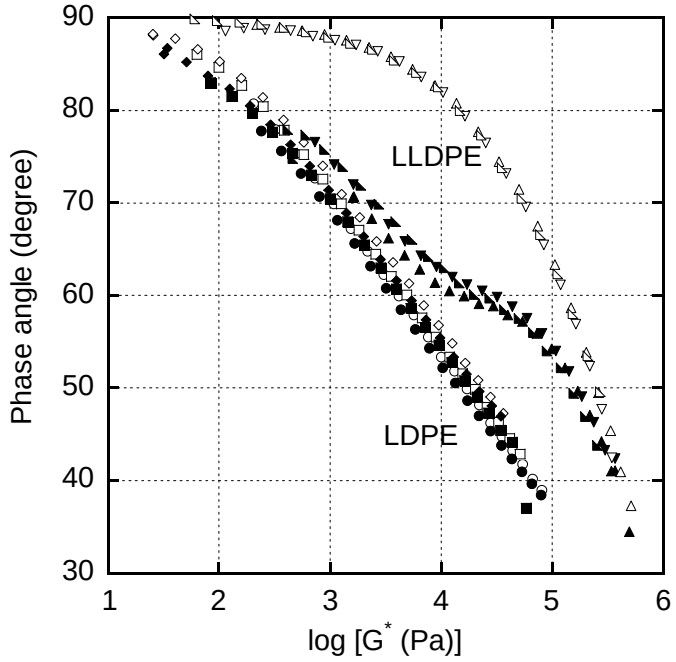

Figure 2-4 van Gurp-Palmen plots for the samples (open symbols) before and (closed symbols) after thermal modification; (circles) LDPE at 130 °C, (diamonds) LDPE at 160 °C, (squares) LDPE at 190 °C, (triangles) LLDPE at 130 °C, (inverted triangles) LLDPE at 160 °C and (right triangles) LLDPE at 190 °C.

The apparent flow activation energy E_a is calculated as a function of the loss moldulus, at the same level of *G"* using an Arrhenius-type equation as shown in the following equation.

$$a_T \propto \exp\left[\frac{-\Delta E_a}{RT}\right] \tag{2-1}$$

As shown in Figure 2-5, E_a is almost unchanged by the thermal history for LDPE. The high value at low modulus is attributed to the high E_a of the relaxation process associated with long-chain branches. In contrast, for LLDPE, E_a prior to the thermal modification is constant, irrespective of *G"*. This is reasonable because a conventional

LLDPE is thermo-rheologically simple, like other simple polymer melts. Exposure to the thermal history in the mixer, however, affects this thermo-rheological simplicity. After thermal modification, E_a increases with decreasing G'', showing similar behavior to that seen for pure LDPE. The result indicates that long-chain branches are now present.

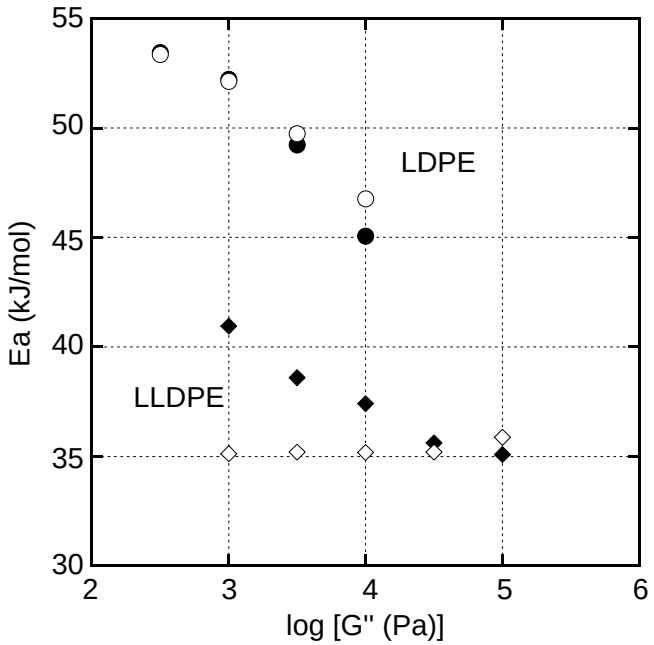

Figure 2-5 Relation between shear loss modulus G'' and flow activation energy E_a for (circles) LDPE and (diamonds) LLDPE; (open symbols) before and (closed symbols) after thermal modification

2.3.1.2 LDPE/LLDPE blends

The molecular weights and their distributions for the blend of LDPE/LLDPE (50/50) before and after thermal modification are shown in Figure 2-6. The GPC curves are barely changed by the applied thermal history. Moreover, the contents of double bonds in the processed samples are almost the same as the blend before modification, as seen in Table 2-3. The result supports the primarily structure of the blend is barely changed by the applied thermal history.

Table 2-3 Molecular characteristics of LDPE/LLDPE (50/50)

	GPC			^{1}H-NMR (per 1000 carbon atoms)		
LDPE/LLDPE (50/50)	Mn (Da)	Mw (Da)	Mz (Da)	terminal vinyl	vinylene	vinylidene
Before modification	18,500	149,000	809,000	0.06	0.06	0.19
After modification	18,100	155,000	111,000	0.05	0.08	0.17

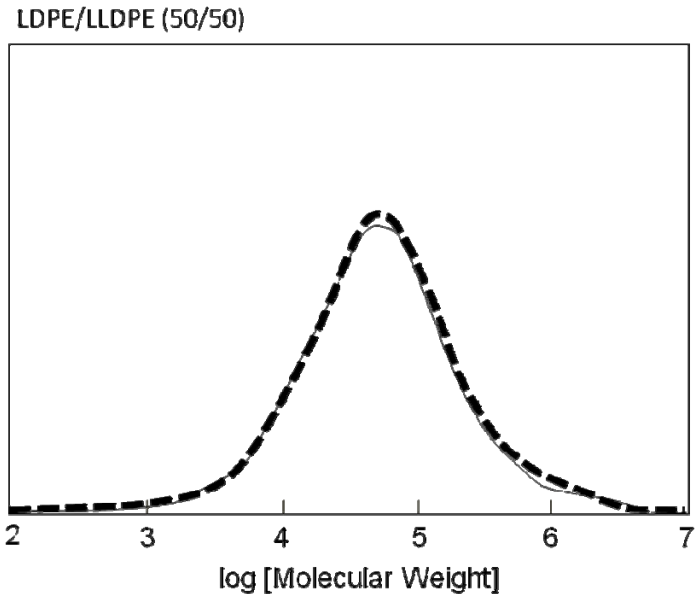

Figure 2-6 GPC curves of the blend of LDPE/LLDPE (50/50); (dotted lines) before and (solid lines) after thermal modification

The master curves of *G'* and *G"* at 130 °C for the blends before/after the thermal modification are plotted in Figure 2-7. Prior to modification, the blends exhibit higher values than those of the pure components in the low frequency region, as also seen in the previous reports.[15,16,19] According to the earlier reports, the oscillatory modulus is enhanced by the addition of high molecular weight linear PE. Moreover, the blends exhibit

marked melt elasticity, such as strain hardening in elongational viscosity. Some researchers concluded that the anomalous rheological behavior can be attributed to phase separation as summarized in references,[16,20] mostly based on thermal analysis. However, the melting and/or crystallization behavior of PE blends have been known to induce segregation. Therefore, the miscibility in the molten state should not be discussed based on the results of characterization in the solid state (such as thermal analysis), although there has been controversial discussion on the miscibility of PE blends.[34,35] Moreover, Wagner *et al.* reported that an advanced molecular model based on the molecular stress function (MSF) theory successfully predicts the rheological properties in the molten state, assuming phase separation.[16] Meanwhile, it was found that the enhancement of strain hardening in elongational viscosity as well as zero-shear viscosity was observed in blends of LDPE and linear PEs, irrespective of the number of short-chain branches in the linear PEs.[19] Because the number of short-chain branches affects the miscibility, the anomalous behavior is not attributed to phase separation in the molten state. The suggestion was made that the prolonged relaxation time of the linear chains surrounding a branched polymer, which restricts dynamic tube dilation and constraint release, is responsible for the anomalous rheological behavior.[36,37] Because similar results are obtained for the present blends prior to modification, the LDPE and LLDPE used in this study are assumed to be miscible in the molten state.

After the thermal modification, as shown in Figure 2-7(c) and (d), both *G'* and *G"* are enhanced, which become more pronounced with increasing LLDPE content. Consequently, LDPE shows the lowest values among all the samples.

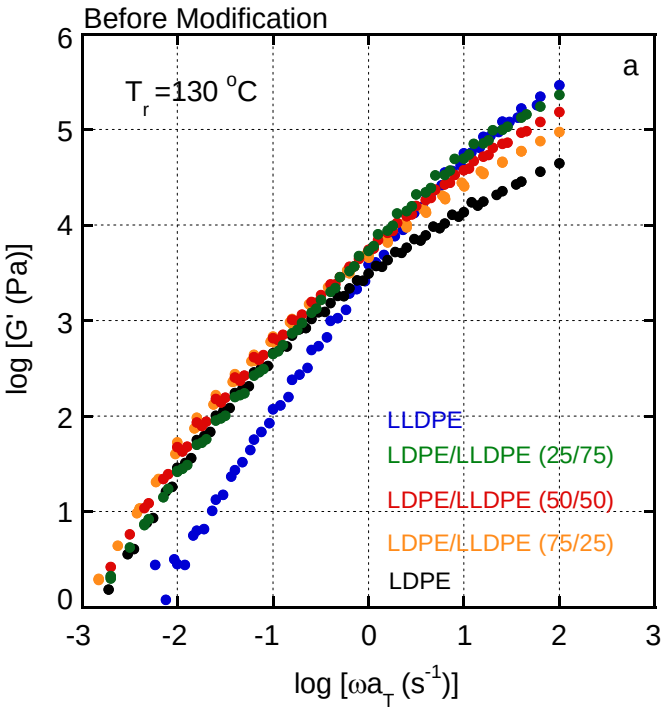
Before Modification
a
T r =130 °C
log [G' (Pa)]
log [ωa T (s-1)]
LLDPE
LDPE/LLDPE (25/75)
LDPE/LLDPE (50/50)
LDPE/LLDPE (75/25)
LDPE

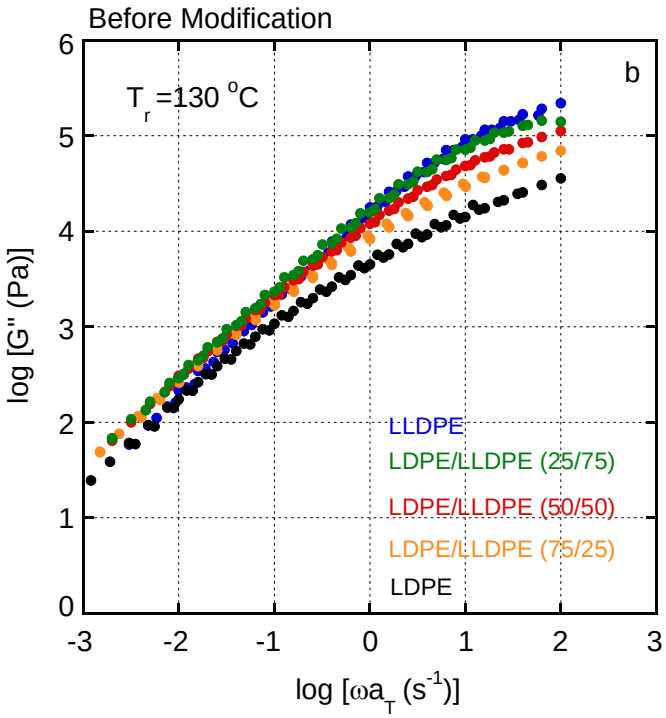
Before Modification
b
T r =130 °C
log [G'' (Pa)]
log [ωa T (s-1)]
LLDPE
LDPE/LLDPE (25/75)
LDPE/LLDPE (50/50)
LDPE/LLDPE (75/25)
LDPE

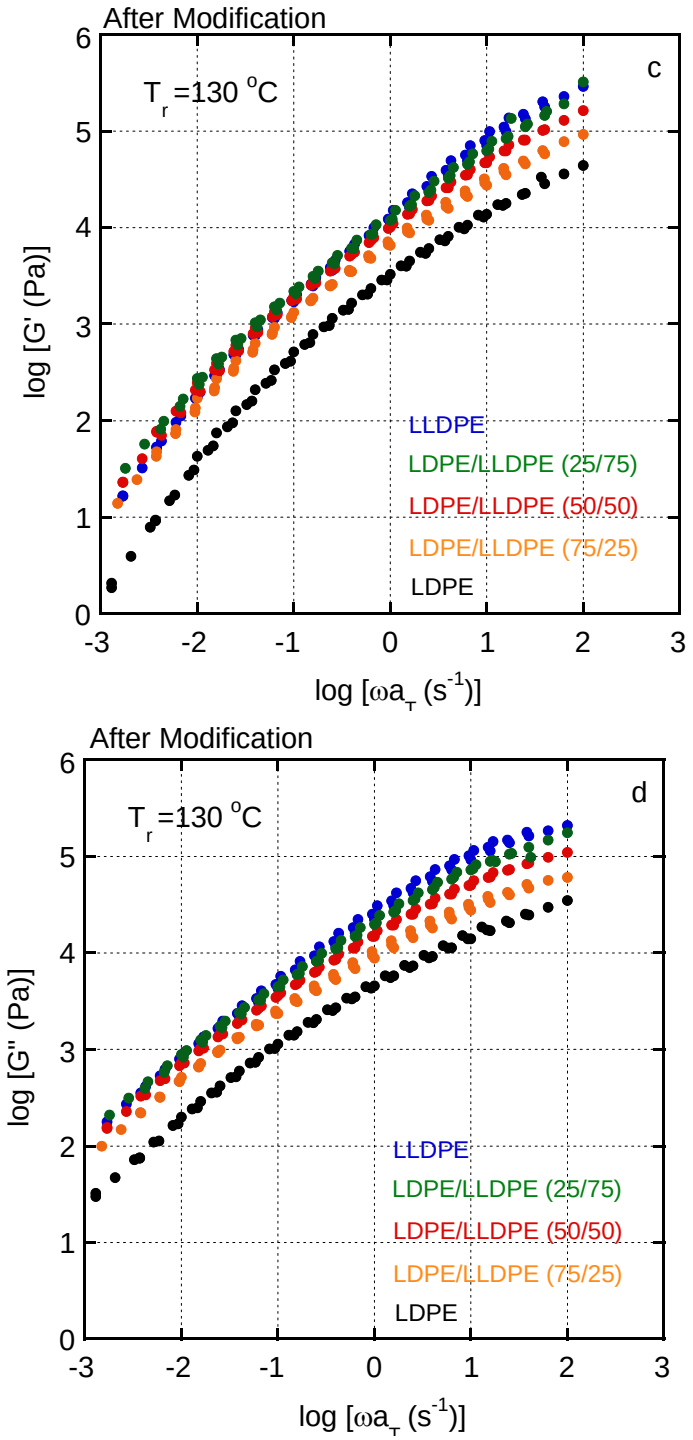

Figure 2-7 Master curves of frequency dependence of shear storage modulus *G'* and *G"* at 130 °C for LDPE/LLDPE blends before and after thermal modification; (a) *G'* of the blends before modification, (b) *G"* of the blends before modification, (c) *G'* of the blends after modification and (d) *G"* of the blends after modification; (black) LDPE, (orange) LDPE/LLDPE (75/25), (red) LDPE/LLDPE (50/50), (green) LDPE/LLDPE (25/75) and (blue) LLDPE.

The zero-shear viscosity η_0 at 130 °C is calculated from *G"*, as shown in eq. 2-1, and is plotted as a function of the LLDPE content in Figure 2-8. Prior to thermal modification, the values of the blends are higher than those of the individual components, which correspond with previous papers.[18-20] Even after the thermal modification, the values are slightly greater than those expected from the log-additive rule, although η_0 increases monotonically with the LLDPE content. The result suggests that the anomalous behavior, *i.e.*, enhancement of η_0, is less distinct after the thermal history, at least from the viewpoint of linear viscoelastic properties. In other words, the thermal history is the main factor affecting the zero-shear viscosity.

$$\eta_0 = \lim_{\omega \to 0} \frac{G''(\omega)}{\omega} \tag{2-2}$$

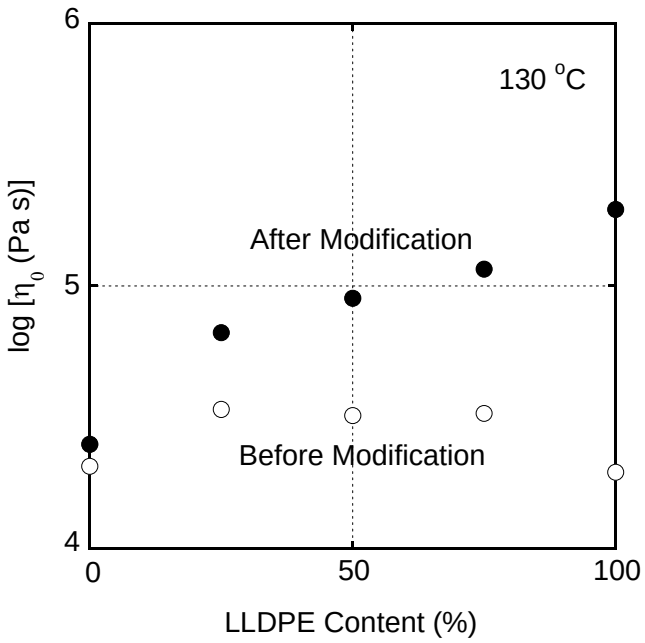

Figure 2-8 Zero-shear viscosity η_0 at 130 °C for LDPE/LLDPE blends (open circles) before and (closed circles) after thermal modification

Figure 2-9 and Figure 2-10 shows the shear stress σ and primary normal stress difference N_1, respectively, at 190 °C measured by the cone-and-plate rheometer. The measurements were carried out three times to confirm the results. In the figure, $|G^*|$ curves are plotted against the angular frequency ω. Prior to the thermal modification, both LDPE and LLDPE show almost the same level of normal stress difference, although LDPE has long-chain branches. This is attributed to the difference in their molecular weights. In fact, the shear stress of the LLDPE, which has higher molecular weight, is considerably higher than that of LDPE. The level of shear stress σ is almost the same as $|G^*|$, suggesting that the Cox-Merz rule,[38] *i.e.*, an empirical rule which states that the dependence of the steady shear viscosity on the shear rate can be estimated from the dynamic viscosity as a function of frequency, is applicable to these systems. Furthermore, it is clearly seen that both shear stress and normal stress difference are enhanced by the thermal modification: the greatest enhancement is seen for the normal stress difference, and becomes more obvious with increasing LLDPE content.

Prior to the modification, the shear stresses of the blends containing 50 or 75% LLDPE are similar to that of pure LLDPE. After the thermal modification, however, LLDPE exhibits the highest shear stress, *i.e.*, shear viscosity. Moreover, the shear stress increases with the LLDPE content, as similar to the linear viscoelastic properties.

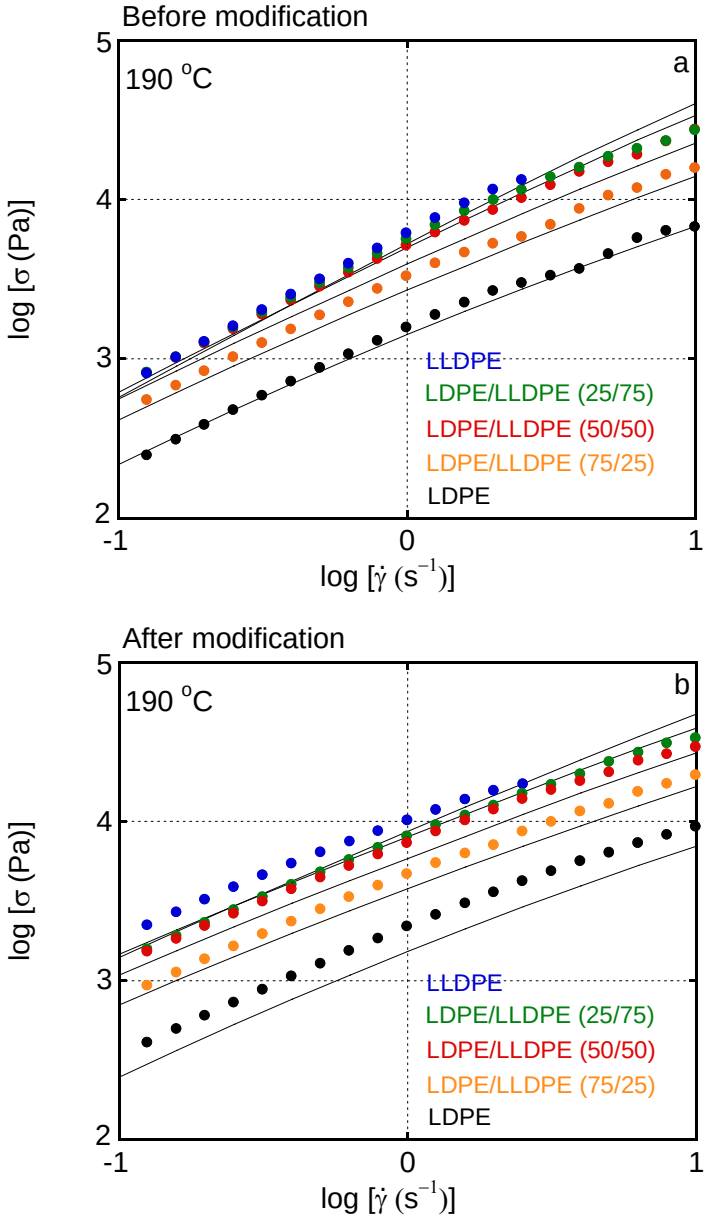

Figure 2-9 Shear stress σ at various shear rates $\dot{\gamma}$ at 190 °C for the samples (a) before and (b) after thermal modification; (black circles) LDPE, (orange circles) LDPE/LLDPE (75/25), (red circles) LDPE/LLDPE (50/50), (green circles) LDPE/LLDPE (25/75) and (blue circles) LLDPE. The solid lines denote the shear stress predicted by the Cox-Merz rule.[38]

In contrast, the blends show still higher primary normal stress difference N_1 than the pure components even after the thermal modification. The results demonstrate that the blends show higher melt elasticity than the pure components.

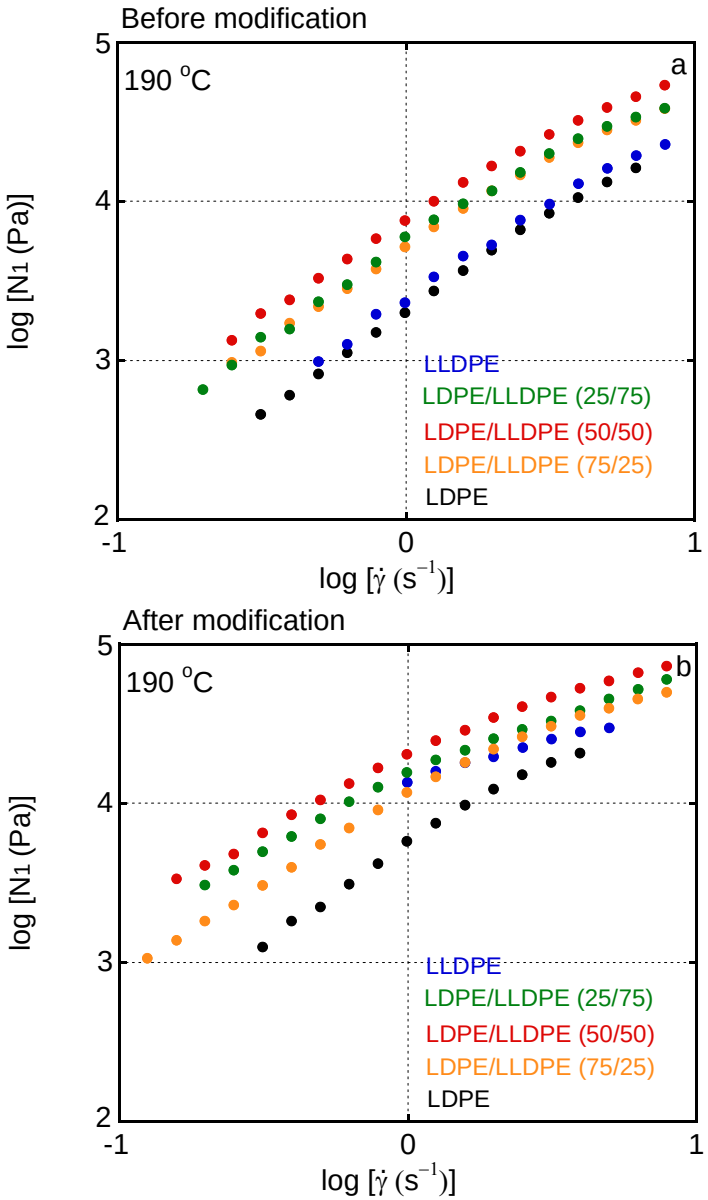

Figure 2-10 Normal stress difference N_1 at various shear rates $\dot{\gamma}$ at 190 °C for the samples (a) before and (b) after thermal modification; (black circles) LDPE, (orange circles) LDPE/LLDPE (75/25), (red circles) LDPE/LLDPE (50/50), (green circles) LDPE/LLDPE (25/75) and (blue circles) LLDPE.

The enhanced N_1 after the thermal modification indicates the marked strain hardening behavior in transient elongational viscosity which is responsible for good processability at various processing operations.[39-47] However, the material having marked strain hardening always shows flow instability at high output production. In other words, the enhanced strain hardening can be predicted by the appearance of flow instability.

The mechanism of flow instability at capillary extrusion has been studied for a long time.[48-64] The gross melt fracture is the flow instability occurred at die entrance, which is prominent for a polymer melt with high melt elasticity, such as LDPE and poly(vinyl chloride).[64,65] Meller found that elongational stress generated by contraction flow at die entrance decides the occurrence of gross melt fracture.[55] As increasing the output rate, gross melt fracture occurs when the elongational stress is beyond the critical one. Since LDPE exhibit marked strain hardening in elongational viscosity, leading to high elongational stress, gross melt fracture is always detected. Recently, Mieda and Yamaguchi revealed that binary blends of LDPE and LLDPE with high molecular weight exhibit severe gross melt fracture owing to enhanced elongational stress.[64] On the contrary, LLDPE and HDPE show shark-skin failure before gross melt fracture when shear stress is beyond the critical value. Roughly speaking, two types of mechanism have been proposed for shark-skin failure; one is owing to cohesive rupture at surface of extrudates by sudden large deformation at die exit, originally proposed by Cogswell;[49] and the other is due to the detachment of a melt from die surface accompanied with cracks by adhesive failure, which was summarized in recent works by Kulikov et al.[58,62]

In the study, extrusion properties of samples were evaluated by the capillary rheometer at 190 °C. The photographs taken by an optical microscope (Leica 2, DMLP) of the extruded strands are shown in Figure 2-11. The blends after the thermal modification

exhibit gross melt fracture at a lower shear rate than before modification, especially for LDPE/LLDPE (75/25), in which the onset shear rate greatly decreases from 1000 s^{-1} to 277 s^{-1}. As LLDPE content increases, helical distortion, instead of chaotic distortion, is detected in the high shear rate region. In the case of pure LLDPE, shark-skin failure appears prior to gross melt fracture, irrespective of the thermal modification. The onset shear stress is around 0.25 MPa, which seems to be independent of thermal modification and agrees with values reported previously.[66] Further, the strand diameters become larger after thermal modification, as illustrated in Figure 2-12. The enhancement of the Barus effect is clearly seen in LLDPE, which is consistent with the increase in the normal stress difference observed for this sample.

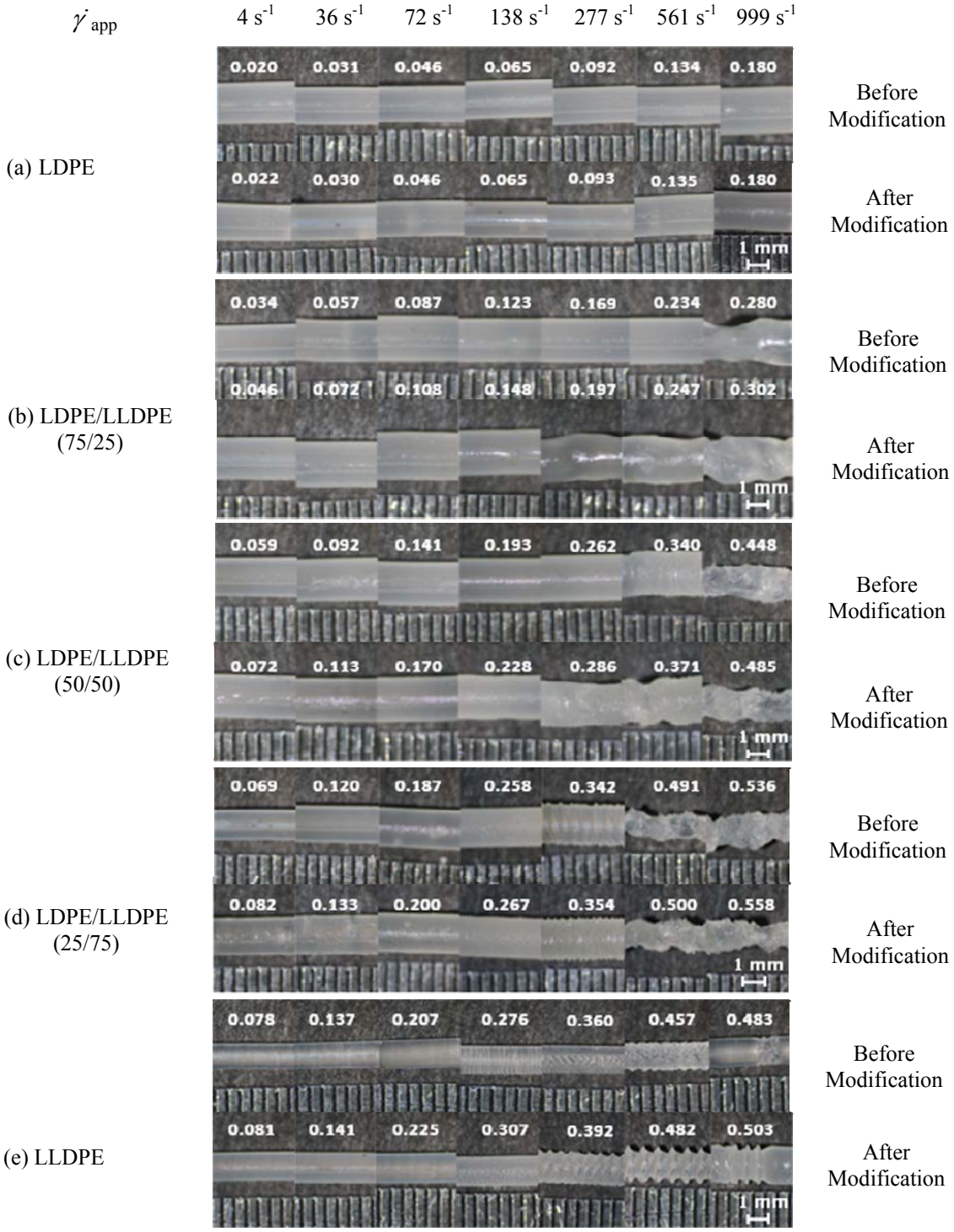

Figure 2-11 Optical photographs of extruded strands at 190 °C through a circle die with L/D = 10/1 (mm): (a) LDPE, (b) LDPE/LLDPE (75/25), (c) LDPE/LLDPE (50/50), (d) LDPE/LLDPE (25/75) and (e) LLDPE. The numerals in the figure represent the apparent shear stress (MPa).

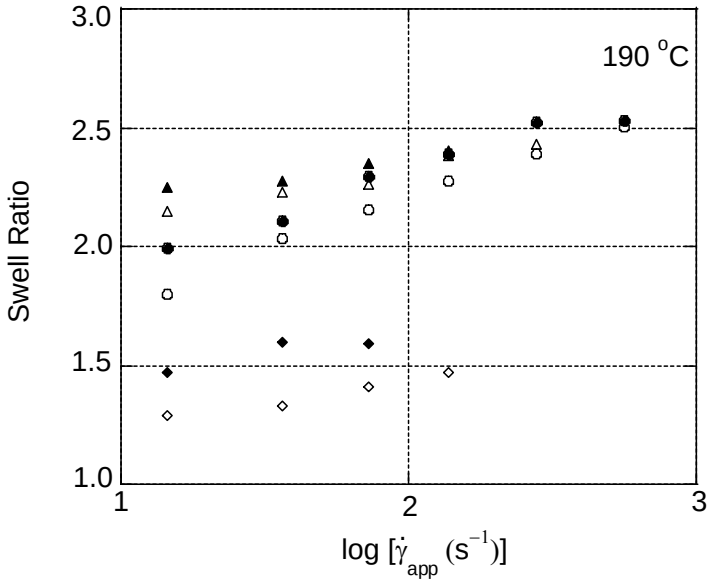

Figure 2-12 Swell ratio plotted against shear rate $\dot{\gamma}$ at 190 °C for (circles) LDPE, (triangles) LDPE/LLDPE (50/50) and (diamonds) LLDPE; (open symbols) before and (closed symbols) after thermal modification.

The origin of the gross melt fracture is believed to be the flow instability at the die entrance.[58,67,68] As previously explained, a polymer liquid having marked strain hardening in elongational viscosity, such as LDPE, is apt to show gross melt fracture even at a low output rate, as compared with a polymer melt without strain-hardening. The present result suggests that elongational viscosity is pronounced for the blend systems because of thermal modification, although the onset elongational stress for gross melt fracture cannot be evaluated from the present results. Precise evaluation of the entrance angle is required to predict the elongational strain, and thus the elongational stress, at the die entry.

To obtain the information on the elongational stress of the samples, the drawdown force, *i.e.*, the force required to stretch a strand,[26,69] is evaluated as shown in Figure 2-13. It is apparent that the drawdown force is greatly enhanced by the thermal modification, especially for the blends. It should be noted that enhancement of drawdown force is not so

obvious for LLDPE, even though its linear viscoelastic properties and rheological properties under steady-state shear are greatly affected by the thermal modification. The results suggest that the strain hardening behavior, *i.e.*, upwards deviation from the linear value, is not obvious for LLDPE, even after the modification. In addition, the symbol (x) in the figure will be explained later.

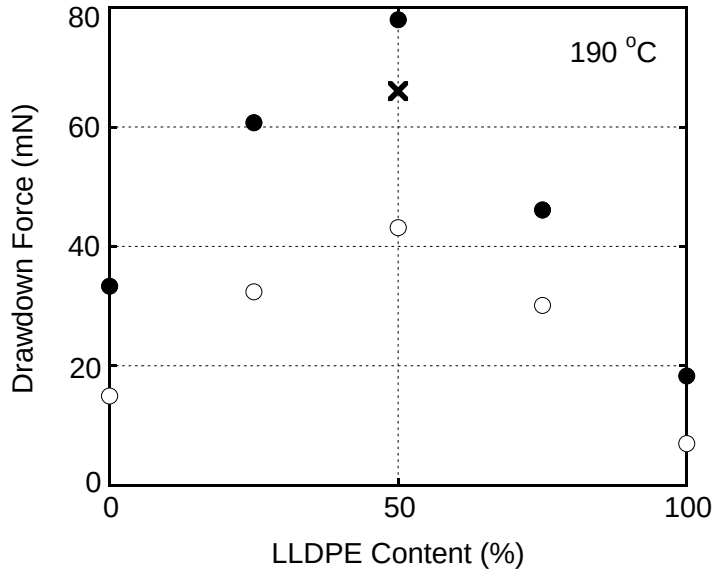

Figure 2-13 Drawdown force at 190 °C for LDPE/LLDPE blends; (open circles) before and (closed circles) after thermal modification. In the figure, (x) denotes the drawdown force of the LDPE/LLDPE (50/50) blend prepared by mixing the thermally-modified pure components.

To evaluate the strain hardening behavior directly, the growth curves of uniaxial elongational viscosity are measured (Figure 2-14). The solid line in the figure represents three times of the growth curve of shear viscosity in the linear region $3\eta^+$, which is calculated by the approximate equation proposed by Osaki *et al*.[70]

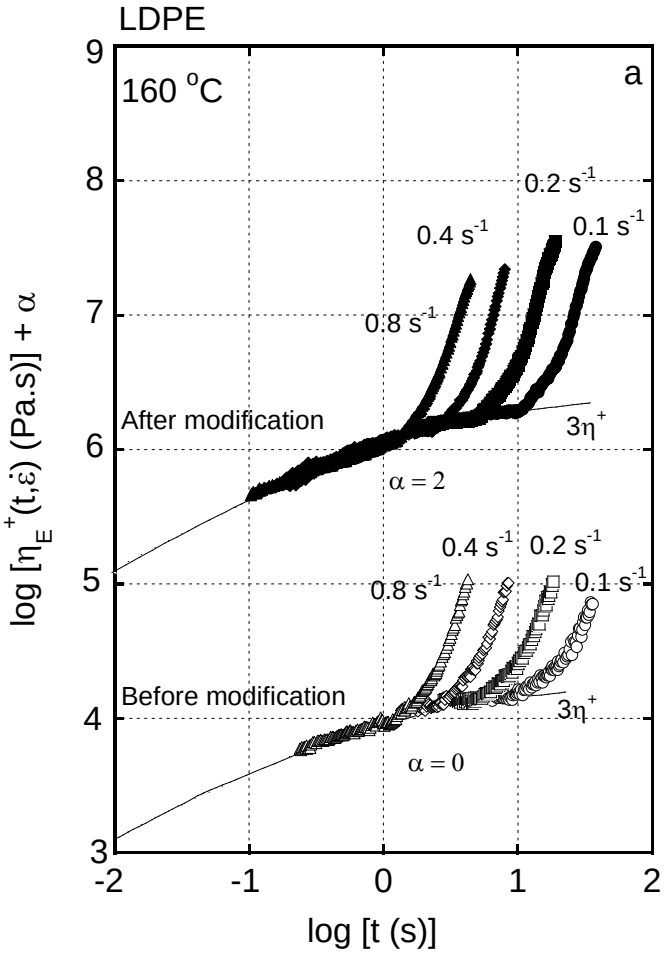
LDPE
160 °C
a
0.2 s-1
0.4 s-1
0.1 s-1
0.8 s-1
After modification
3η+
α = 2
0.4 s-1
0.2 s-1
0.8 s-1
0.1 s-1
Before modification
3η+
α = 0
log [η+E(t,ε̇) (Pa.s)] + α
log [t (s)]
9
8
7
6
5
4
3
-2
-1
0
1
2

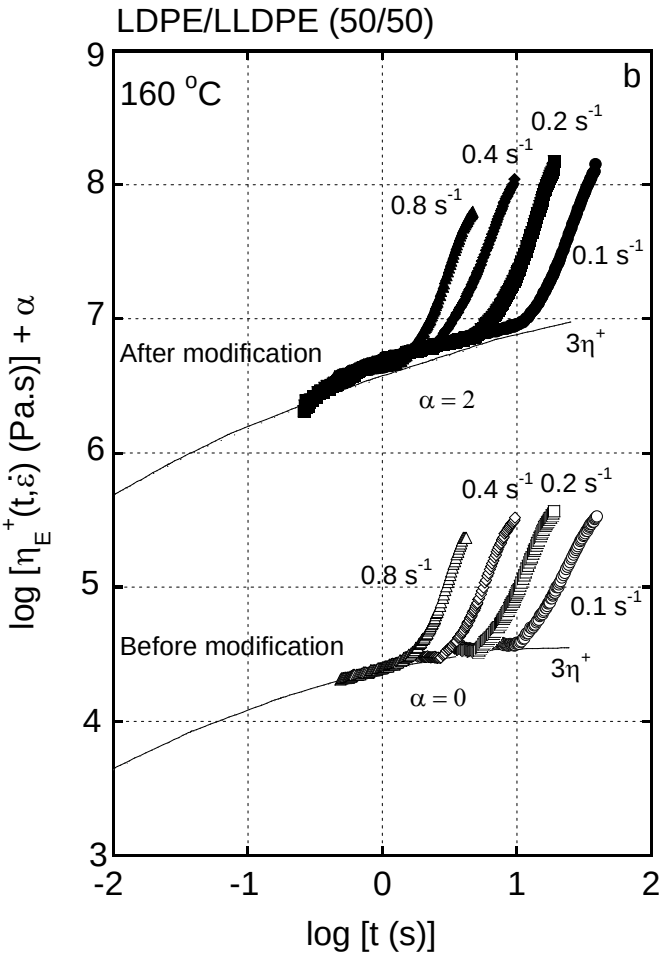
LDPE/LLDPE (50/50)
160 °C
b
0.2 s-1
0.4 s-1
0.8 s-1
0.1 s-1
After modification
3η+
α = 2
0.4 s-1
0.2 s-1
0.8 s-1
0.1 s-1
Before modification
3η+
α = 0
log [η+E(t,ε̇) (Pa.s)] + α
log [t (s)]
9
8
7
6
5
4
3
-2
-1
0
1
2

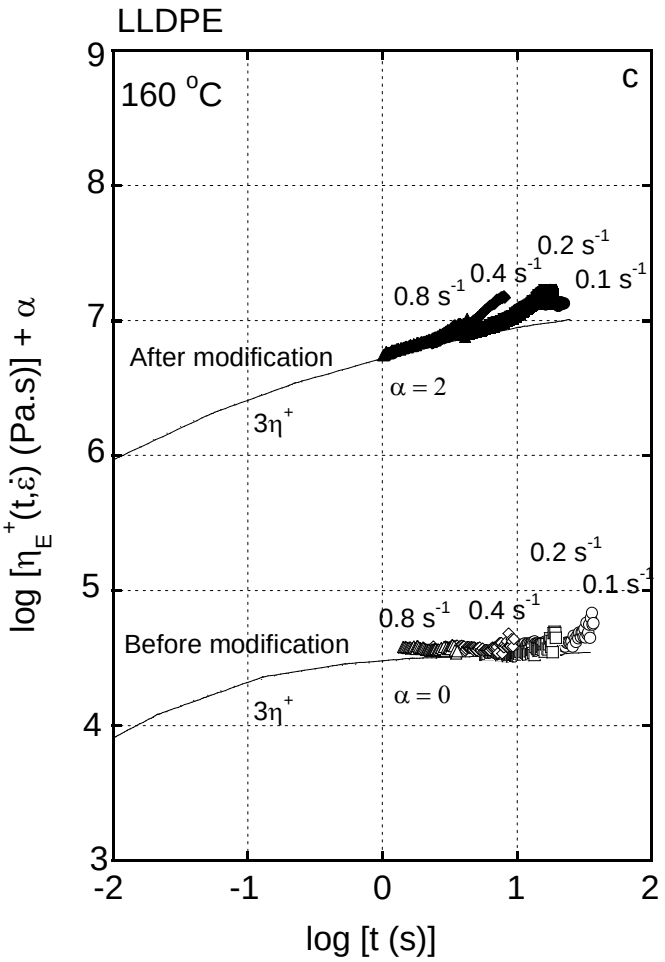

Figure 2-14 Growth curves of uniaxial elongational viscosity $\eta_E^+(t,\dot{\varepsilon})$ at 160 °C; (a) LDPE, (b) LDPE/LLDPE (50/50) and (c) LLDPE; (open symbols) before and (closed symbols) after thermal modification at various strain rates, (circles) 0.1 s^{-1}, (squares) 0.2 s^{-1}, (diamonds) 0.4 s^{-1} and (triangles) 0.8 s^{-1}. The solid line denotes the growth curve of elongational viscosity at a low strain rate asymptote $3\eta^+(t)$.

As seen in the figure, the modified blend shows a steep curve of $3\eta^+$ and marked strain hardening. Both features are responsible for the enhanced drawdown force. Moreover, the strain hardening behavior also occurs at smaller strains, as demonstrated in Figure 2-15. In the case of LDPE, strain hardening is also pronounced, with a slight increase in $3\eta^+$, while the elongational strain required for strain hardening is not changed

greatly by the thermal modification. Finally, the strain hardening behavior is not clearly detected for LLDPE, even after the thermal modification; this will be explained later.

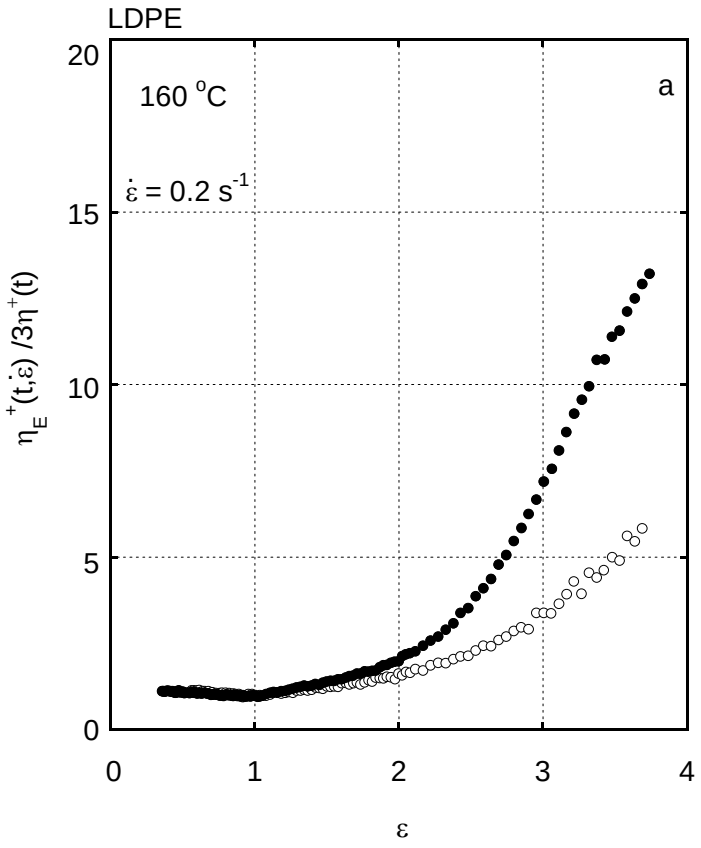

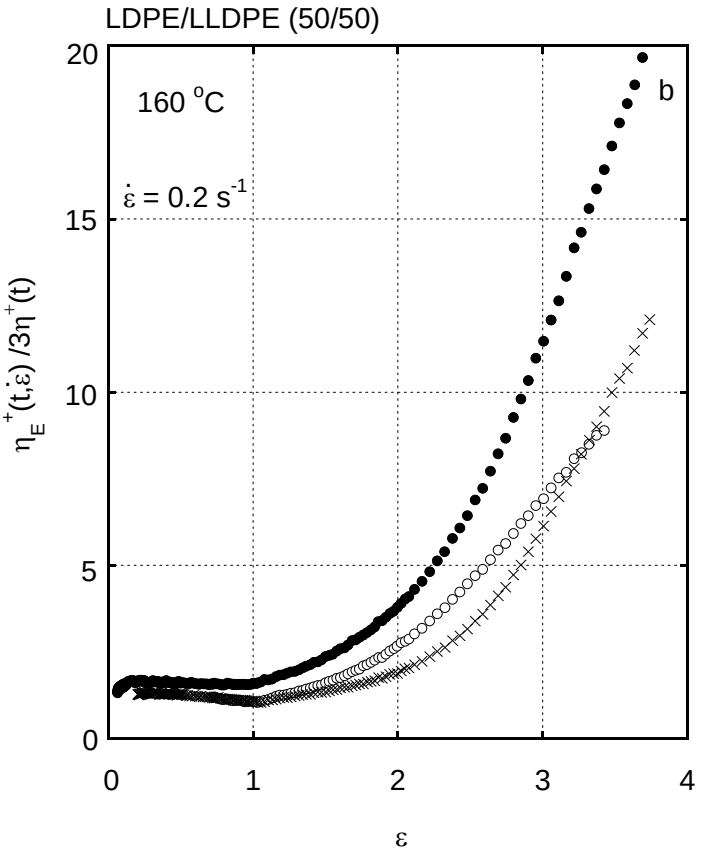

Figure 2-15 Ratio of uniaxial elongational viscosity $\eta_E^+(t,\dot{\varepsilon})$ to that at the low strain rate asymptote $3\eta^+(t)$ as a function of elongational strain ε at a strain rate $\dot{\varepsilon}$ of 0.2 s^{-1} for (a) LDPE and (b) LDPE/LLDPE (50/50); (open circles) before and (closed circles) after thermal modification. The symbols (x) represent the data of the LDPE/LLDPE (50/50) blend prepared by mixing the thermally-modified pure components.

The present experimental results indicate that polymer chains having more than two branch points are generated in the blend. In the case of LLDPE, a polymer chain has to be attacked by at least two macroradicals to become comb-shaped branch structure. As demonstrated by the GPC curve, however, the thermal history applied in this experiment is not so severe to change the molecular weight or its distribution. Moreover, the van Gurp-Palmen plot of the thermally-modified LLDPE indicates that the distribution of relaxation times associated with long-chain branches is not so broad. These results indicate that most

branched chains generated by the thermal modification of LLDPE will have star-shaped branch structure. For the blends, in contrast, intermolecular reaction between LLDPE and LDPE will take place, as well as the reaction between two LLDPE molecules, because the cross-linking reaction occurs randomly when the blend is miscible. As a result, the number of branched polymers having more than two branch points in a chain will increase because of reaction of LLDPE with LDPE. Further, prolonged relaxation times of polymer chains surrounding a branched chain will enhance the chain stretching. To confirm the intermolecular reaction between LLDPE and LDPE, another blend was prepared by mixing the thermally-modified pure components, *i.e.*, modified LLDPE and modified LDPE, at 130 °C as a reference sample. After compression-molding at 230 °C, the rheological properties were evaluated. As indicated by x in Figure 2-13, the drawdown force of the reference sample blended after the thermal modification is lower than that of the blend modified during mixing. Correspondingly, the upturn only occurs at a large elongational strain, and is smaller for the reference sample compared with that of the blend modified during mixing. In other words, the thermal modification during mixing is more effective to enhance the elastic properties.

Finally, recovery curves of the shear storage modulus from the shear-modified state were evaluated to discuss the branch structure. Yamaguchi and Gogos[24] found that the shear modification phenomenon, which is observed clearly for branched polymers, can be evaluated by examining the recovery process of the oscillatory modulus after cessation of shear flow. Furthermore, the degree of shear modification is determined by the applied shear stress, duration of shearing, and flow pattern. When the applied flow field is chaotic, the rheological properties are barely affected by the shear history.[69] This is reasonable because the shear modification occurs by the alignment of branch chains along main

chains. Therefore, the oscillatory modulus greatly decreases as a result of the shear flow in a cone-and-plate rheometer. Moreover, the branch structure can be predicted from the recovery curves to some degree[21,71] because a longer branch will need a longer recovery time to return its equilibrium state.

Figure 2-16 shows the recovery curves of *G'* and its normalized values, *i.e.*, $G'(t)/G'(t=0)$, after removal of the shear stress at 24.5 kPa. As seen in the figure, *G'* increases with the elapsed time in the rheometer for all samples (except for LLDPE prior to the modification). Although the *G'* change provided by the shear history is clear for the modified LLDPE, the modified blends require a longer time to recover to their plateau values, as does the modified LDPE. Because the recovery time is closely related to the length of long-chain branches,[30] the thermally-modified blends have long or hierarchical branches compared with the thermally-modified LLDPE. This result also supports the idea that, in the blends, intermolecular crosslinking reactions between LLDPE and LDPE take place during the thermal modification. In contrast, depression of the initial *G'*, which is presumably attributed to the number of long-chain branches,[42,30] is prominent for the thermally-modified LLDPE.

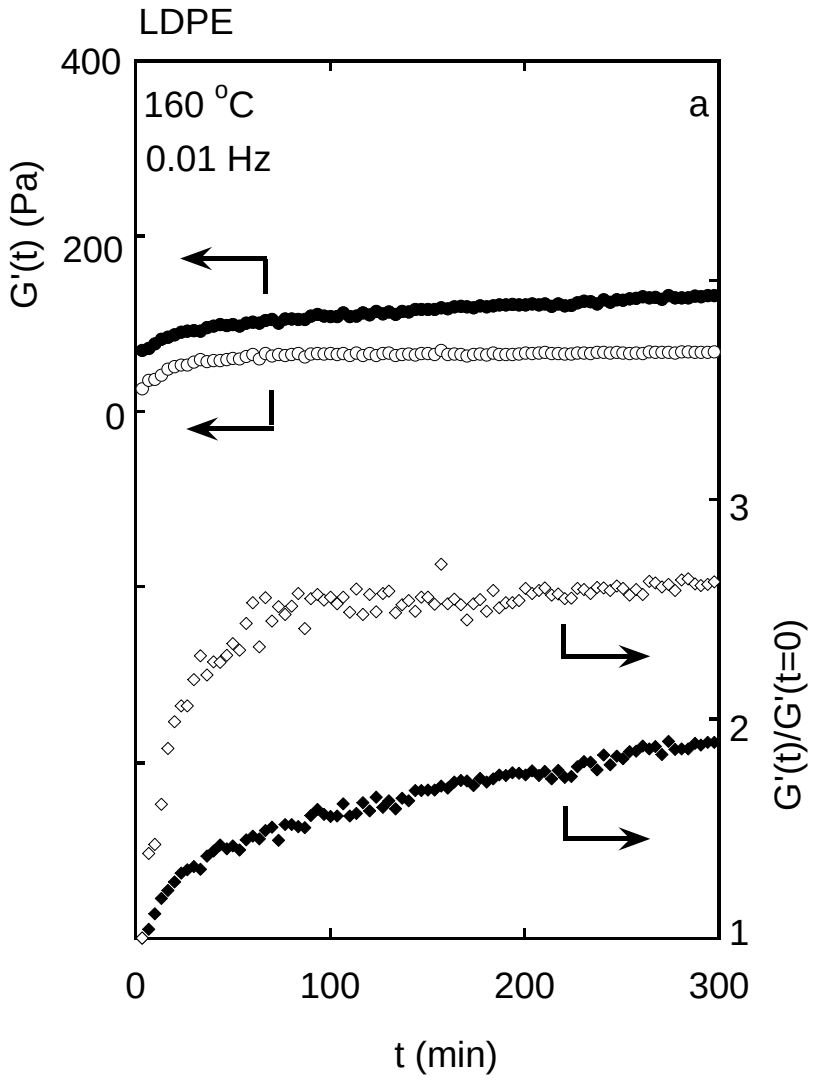
LDPE
160 °C
0.01 Hz
a
G'(t) (Pa)
G'(t)/G'(t=0)
t (min)
400
200
0
3
2
1
0
100
200
300

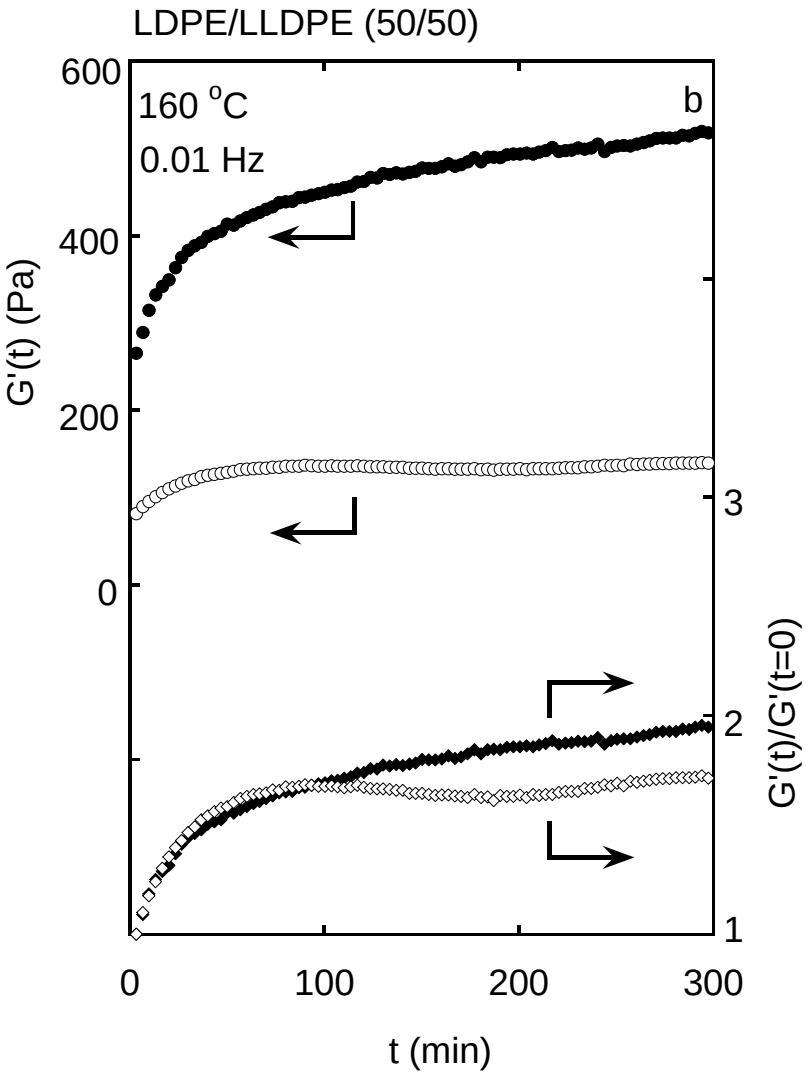
LDPE/LLDPE (50/50)
160 °C
0.01 Hz
b
G'(t) (Pa)
G'(t)/G'(t=0)
t (min)
600
400
200
0
3
2
1
0
100
200
300

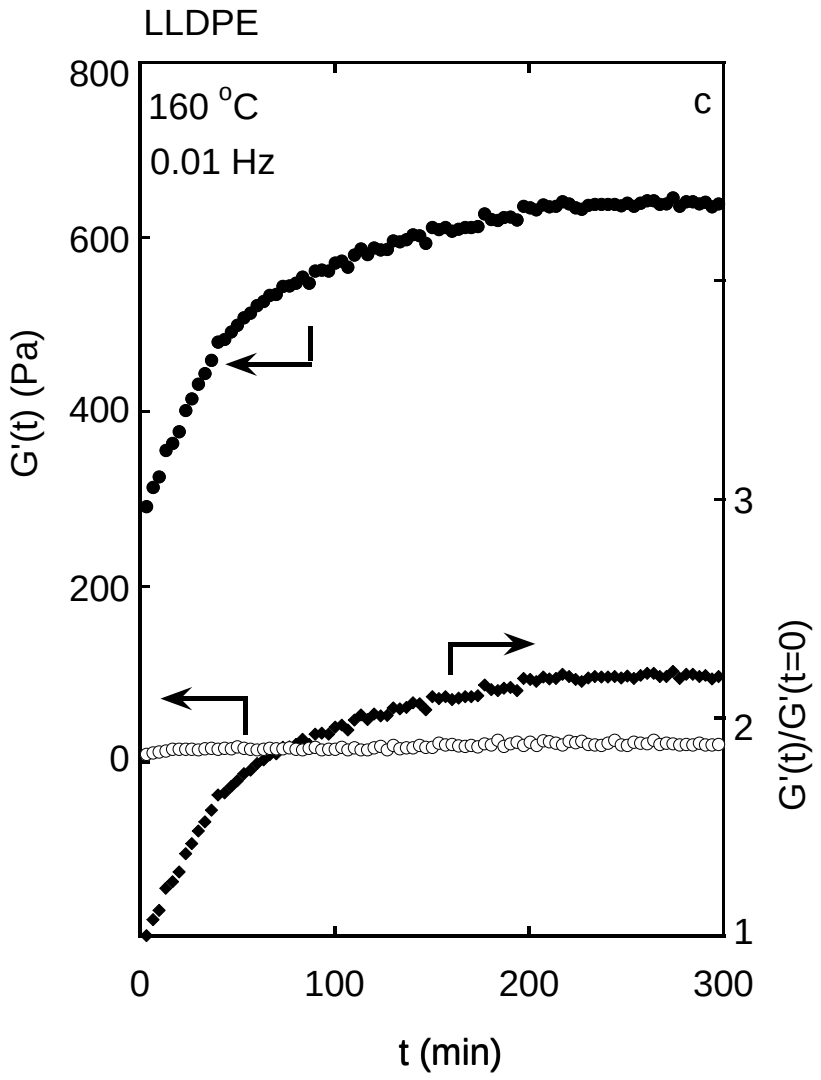

Figure 2-16 Time dependence of (circles) shear storage modulus *G'* and (diamonds) its normalized values *G'*(*t*)/*G'*(*t*=0) at 0.01 Hz after the removal of shear stress (24.5 kPa for 30 min) at 160 °C; (open symbols) before and (closed symbols) after thermal modification for (a) LDPE, (b) LDPE/LLDPE (50/50) and (c) LLDPE.

The effect of shear modification was further studied using a commercial LDPE produced by a radical polymerization method in an autoclave reactor (MFR = 1.6 g/10 min) for a primary study. The processing histories were applied to LDPE in the internal mixer at 160 ^{o}C for 2 hrs at 30 rpm of the blade rotation speed. The sample amount was 48 g in the 60 cc mixer. Then the processed LDPE was extruded by the same capillary rheometer. Figure 2-17 shows the apparent wall shear stress with pictures of the extruded strands. Both samples exhibit smooth surface without any distortion at low shear stress. As increasing the shear rate and thus the output rate, the virgin LDPE exhibits volumetric distortion with smooth surface at 73 s^{-1} (1.9 x 10^5 Pa) and 140 s^{-1} (2.4 x 10^5 Pa). Beyond 280 s^{-1}, surface of the distorted strand becomes rough. The magnified pictures observed by a scanning electron microscope (machine name) are shown in Figure 2-18. On the contrary, the processed sample can be extruded without melt fracture at 140 s^{-1} (1.9 x 10^5 Pa), even though the shear stress is slightly higher than that at 73 s^{-1} for the virgin LDPE. Considering that the gross melt fracture appears beyond the critical elongational stress, the processed sample shows lower elongational stress. Moreover, shark-skin failure is detected at 280 s^{-1} (2.4 x 10^5 Pa) without volumetric distortion for the processed sample. It must be noted, because it has been believed that LDPE shows gross melt fracture prior to sharkskin failure. As seen in Figure 2-18(c), it seems that the crack of adhesive failure at the die wall propagates to large scale roughness, which is a similar result reported by Kulikov *et al.*[58,62] Beyond 560 s^{-1}, the processed sample also shows gross melt fracture with rough surface. As explained in previous report,[24] because of the alignment of branch chains along main chains by the applied shear history, the rheological properties of processed LDPE are similar to those of LLDPE from a viewpoint of flow instability.

The applied processing history, leading to low elongational stress, avoids the onset of the gross melt fracture.

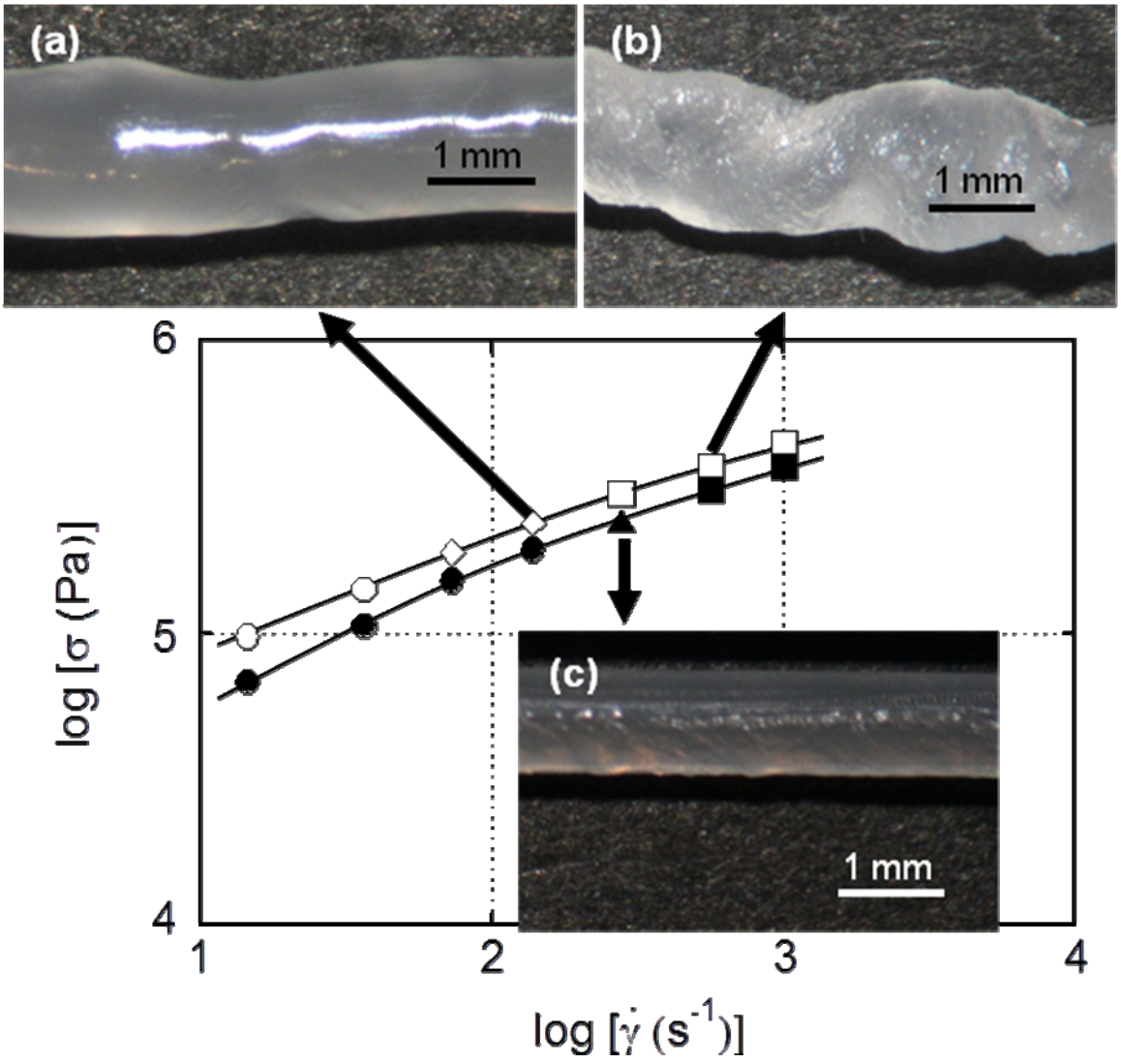

Figure 2-17 Shear stress as a function of shear rate at 160 °C with pictures of extrudates for (open symbols) LDPE and (closed symbols) LDPE processed for 120 min; (circles) smooth surface without gross melt fracture, (triangles) shark-skin failure without gross melt fracture, (diamonds) gross melt fracture with smooth surface, and (squares) gross melt fracture with rough surface.

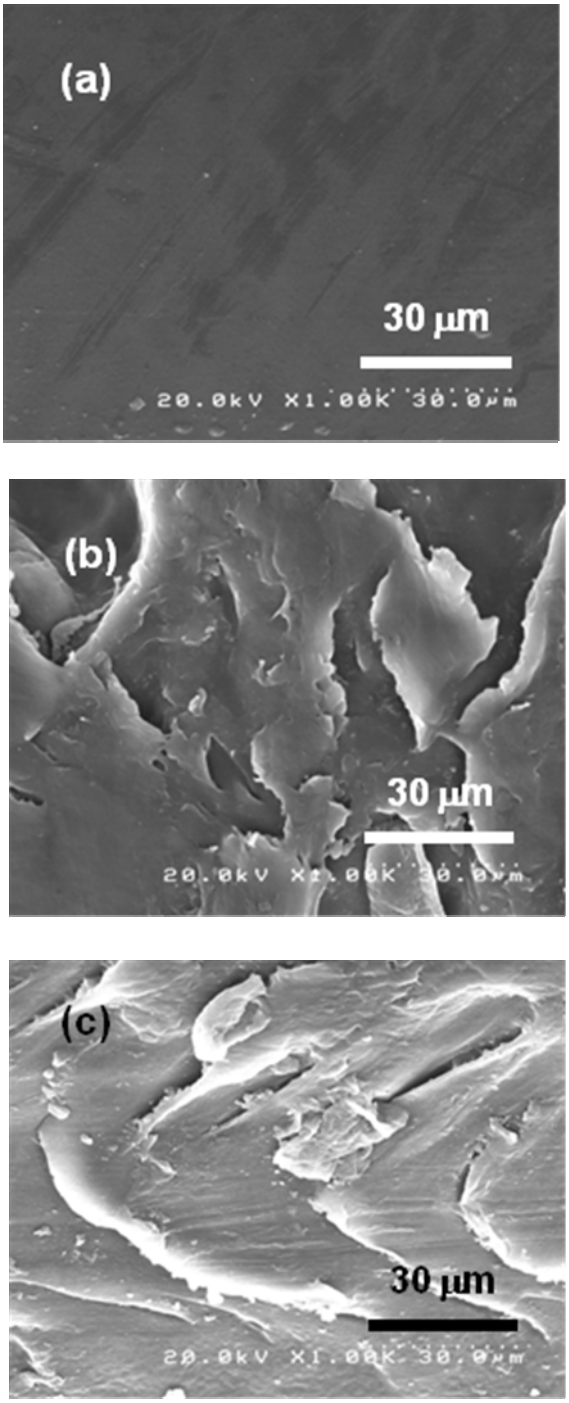

Figure 2-18 SEM pictures of the extrudate's surface; (a) 140 s^{-1} for virgin LDPE, (b) 560 s^{-1} for virgin LDPE, and (c) 280 s^{-1} for LDPE processed for 120 min.

According to previous study reported by Lohse *et al.*,[72] the molecular structure of materials, such as molecular weight average of total molecule M_{tot} and molecular weight of branched chain M_{arm}, can be predicted using zero shear viscosity η_0. However, it should be noted that the values have to be considered under these following conditions; (1) The new star-shape branch structures in modified LLDPE are assumed that they are 4-arm symmetry star-shape structure; (2) It is not clear that there is any simple relation between η_0 and multi-branched polymer, as LDPE and LDPE/LLDPE blends, in the case of M_{arm} because many factors, such as muti-branched structure, amount and length of LCB or the length of main chain between branch point, affect to the η_0. This means that a measure of η_0 alone cannot be used as a measure of LCB. Therefore, the values reported in this study cannot present the actual molecular structure of materials. However, it can be used to roughly consider the structural changes of materials after thermal modification as seen in the Table 2-4.

Table 2-4 Molecular weight average of total molecule M_{tot} and molecular weight of branched chain M_{arm} predicted by the relationship between zero shear viscosity η_0 and molecular weight of polyethylene reported by Lohse *et al.*[72]

Samples		molecular weight average of total molecule M_{tot} (g/mol)	molecular weight of branched chain M_{arm} (g/mol)
LDPE	Before modification	65.3	cannot be predicted
	After modification	65.3	cannot be predicted
LDPE/LLDPE (75/25)	Before modification	67.7	cannot be predicted
	After modification	70.2	cannot be predicted
LDPE/LLDPE (50/50)	Before modification	68.9	cannot be predicted
	After modification	75.3	cannot be predicted
LDPE/LLDPE (25/75)	Before modification	67.7	cannot be predicted
	After modification	80.9	cannot be predicted
LLDPE	Before modification	158.5	-
	After modification	147.6	34.6

2.3.2 Rheological modification of PE by peroxide addition

2.3.2.1 LDPE and LLDPE

It is found from the previous section that LLDPE is very sensitive to the cross-linking reaction. The modification leads to the significant changes in the rheological properties. In this section, the cross-linking reaction of LDPE and LLDPE is further studied using peroxide addition.

Figure 2-17 shows the curves of frequency dependence of oscillatory shear moduli, such as *G'* and *G"* for LDPE before and after peroxide modification, in which the cross-linking reaction was performed under flow field in the mixer or without flow field. It is found that the cross-linking reaction enhances both *G'* and *G"*. Moreover, the values increase with a peroxide content. However, it seems that the modification under flow field gives a poor cross-linking efficiency. In other words, the enhancement of *G'* and *G"* is more pronounced for samples cross-linked without flow.

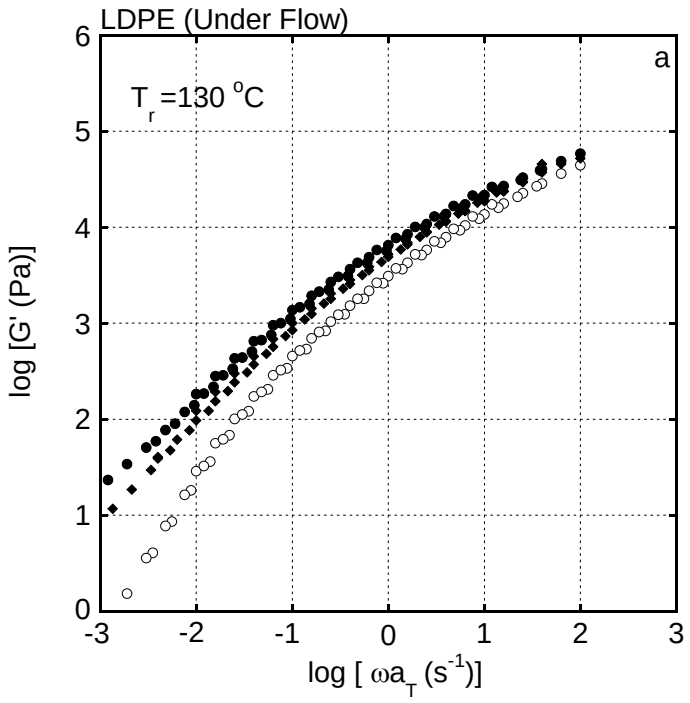
LDPE (Under Flow)
a
T_r =130 °C
log [G' (Pa)]
log [ωa_T (s^-1)]
0
1
2
3
4
5
6
-3
-2
-1
0
1
2
3

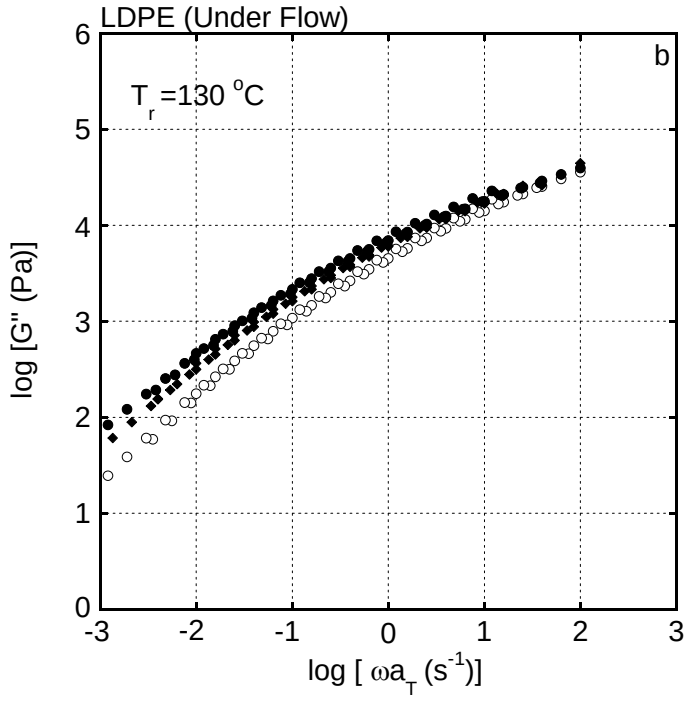
LDPE (Under Flow)
b
T_r =130 °C
log [G'' (Pa)]
log [ωa_T (s^-1)]
0
1
2
3
4
5
6
-3
-2
-1
0
1
2
3

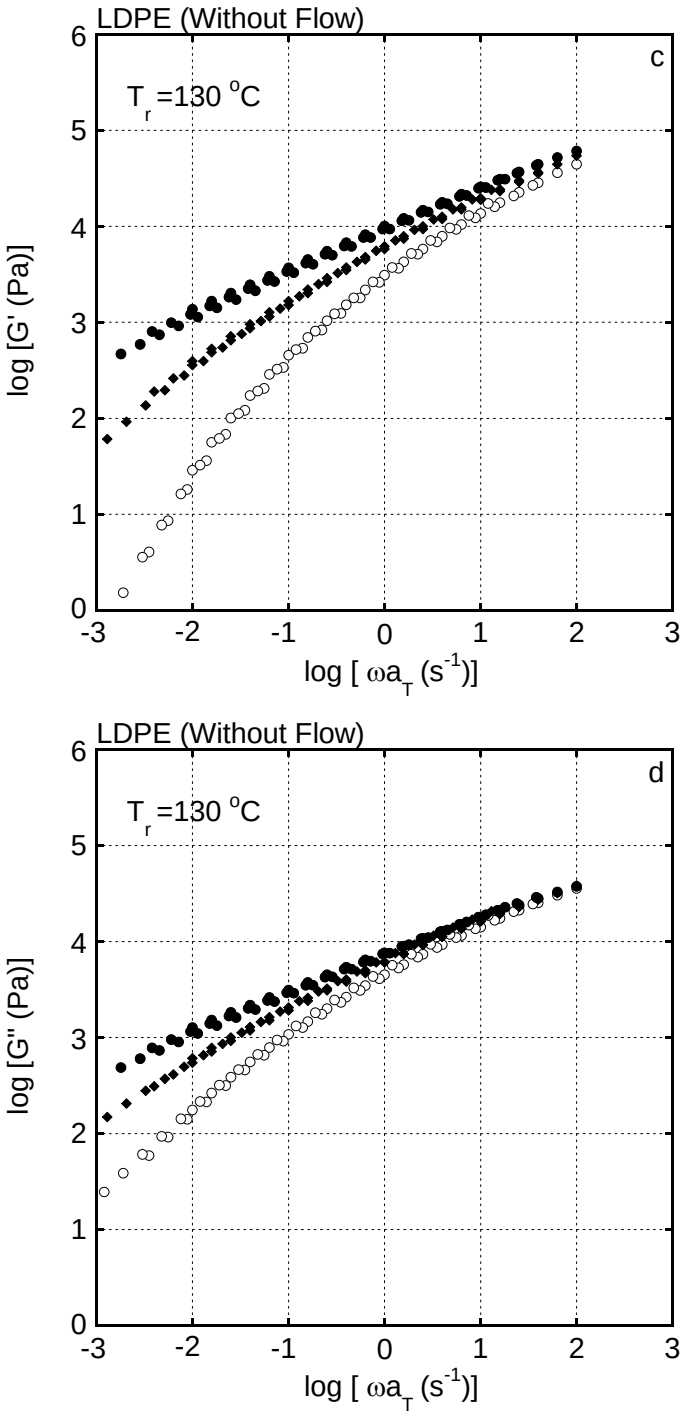

Figure 2-17. Master curves of frequency dependence of shear storage modulus *G'* and loss modulus *G"* at 130 °C for LDPE; (open circles) before modification, (closed circles) 0.1 wt.% and (closed diamonds) 0.05 wt.% peroxide; (a) *G'* of LDPE (under flow), (b) *G"* of LDPE (under flow), (c) *G'* of LDPE (without flow) and (d) *G"* of LDPE (without flow).

Figure 2-18 shows the oscillatory shear moduli *G'* and *G"* curves for LLDPE, before and after the peroxide modification, under and without flow field, respectively. As seen in the figure, both moduli for the modified samples are greatly higher than those of LLDPE prior to the modification. However, the cross-linking efficiency of the modification without flow filed is slightly lower than the modification under flow field. It is found that the applied flow field differently affects to cross-linking behaviors of LDPE and LLDPE.

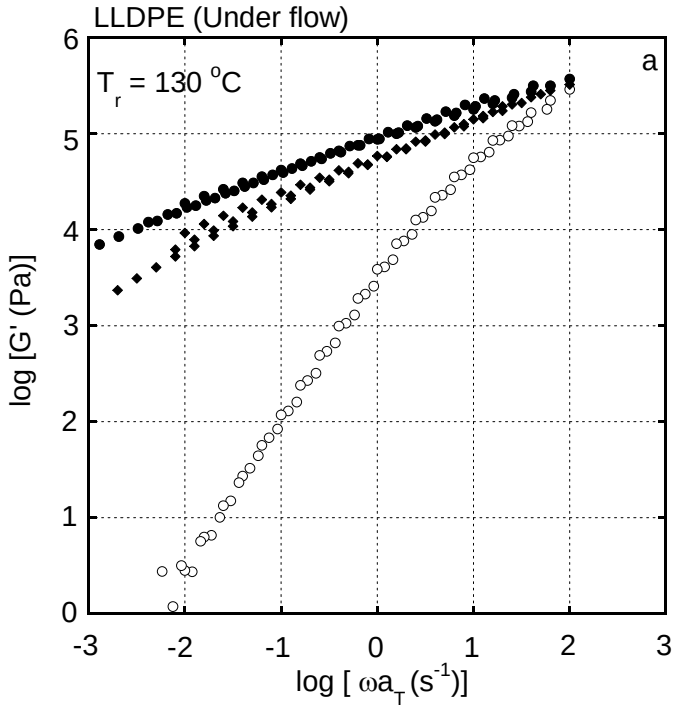

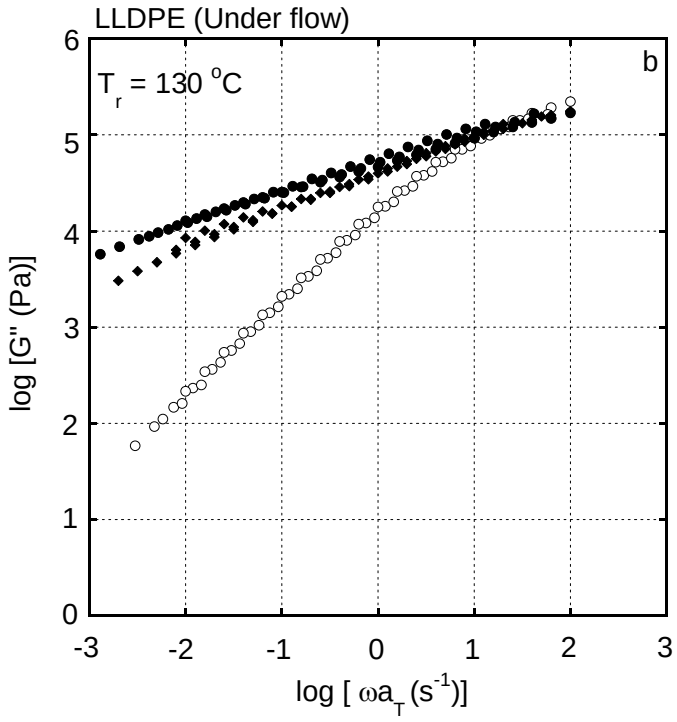
LLDPE (Under flow)
b
T_r = 130 °C
log [G'' (Pa)]
log [ωa_T (s^-1)]
0
1
2
3
4
5
6
-3
-2
-1
0
1
2
3

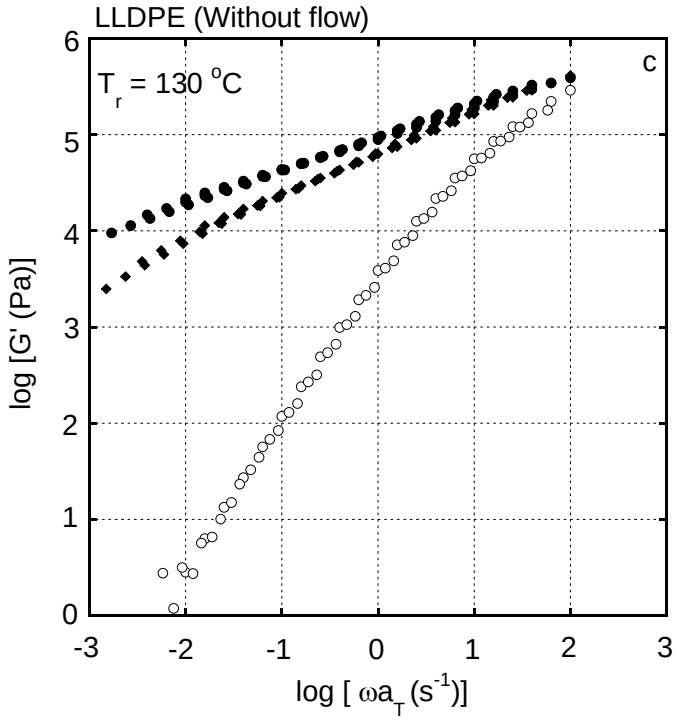
LLDPE (Without flow)
c
T_r = 130 °C
log [G' (Pa)]
log [ωa_T (s^-1)]
0
1
2
3
4
5
6
-3
-2
-1
0
1
2
3

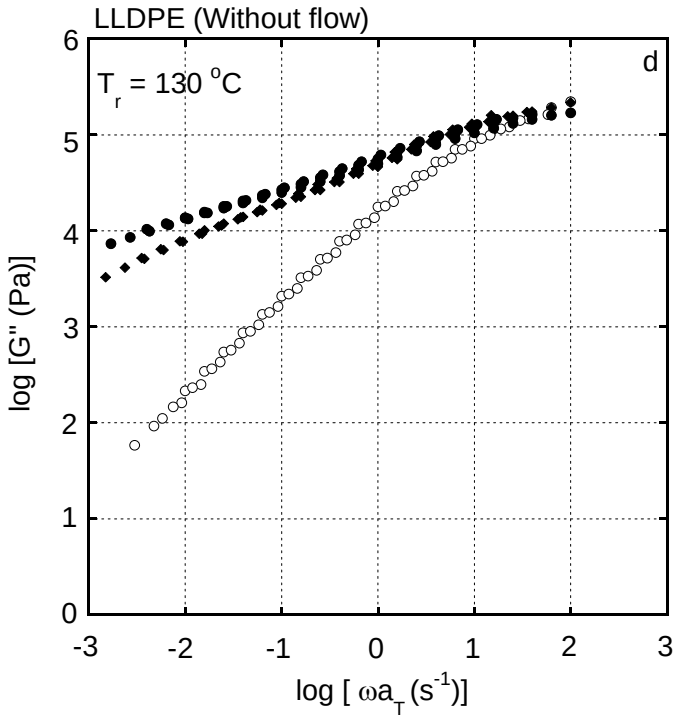

Figure 2-18. Master curves of frequency dependence of shear storage modulus *G'* and loss modulus *G"* at 130 °C for LLDPE; (open circles) before peroxide modification, (closed circles) 0.1wt.%, and (closed diamonds) 0.05 wt.% peroxide; (a) *G'* of LLDPE (under flow), (b) *G"* of LLDPE (under flow), (c) *G'* of LLDPE (without flow) and (d) *G"* of LLDPE (without flow).

It is clearly shown in the van Gurp-Palmen plot (Figure 2-19). In the case of the modified LDPE, the magnitude of δ for LDPE cross-linked under flow flied is higher than that without flow field. This is attributed to broad relaxation time distribution for LDPE cross-linked without flow field. The information suggests that the cross-linking efficiency in LDPE is greatly affected by applied flow field.

Meanwhile, the flow field slightly affects cross-linking behavior of LLDPE. It is found that the relaxation time distribution of LLDPE cross-linked under flow field is slightly broad. The result is consistent with the oscillatory modulus.

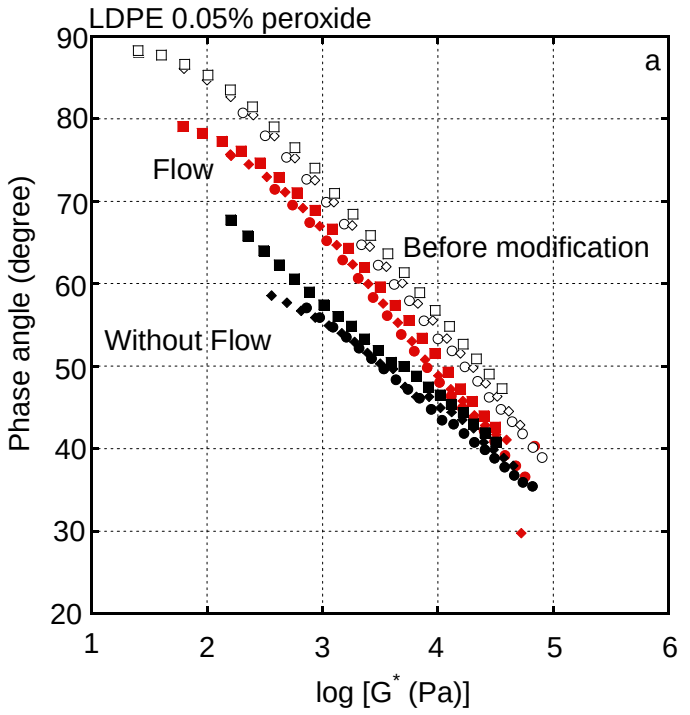
LDPE 0.05% peroxide
a
Flow
Before modification
Without Flow
Phase angle (degree)
log [G* (Pa)]
90
80
70
60
50
40
30
20
1
2
3
4
5
6

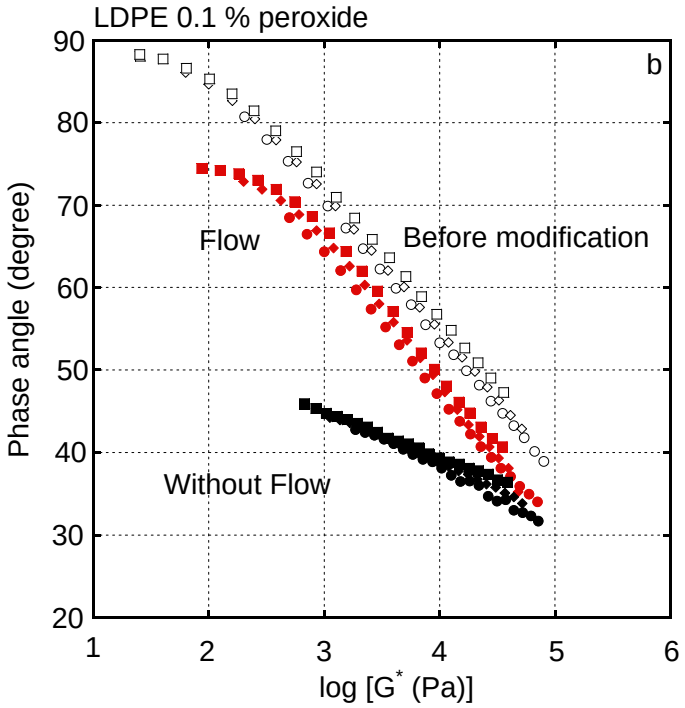
LDPE 0.1 % peroxide
b
Flow
Before modification
Without Flow
Phase angle (degree)
log [G* (Pa)]
90
80
70
60
50
40
30
20
1
2
3
4
5
6

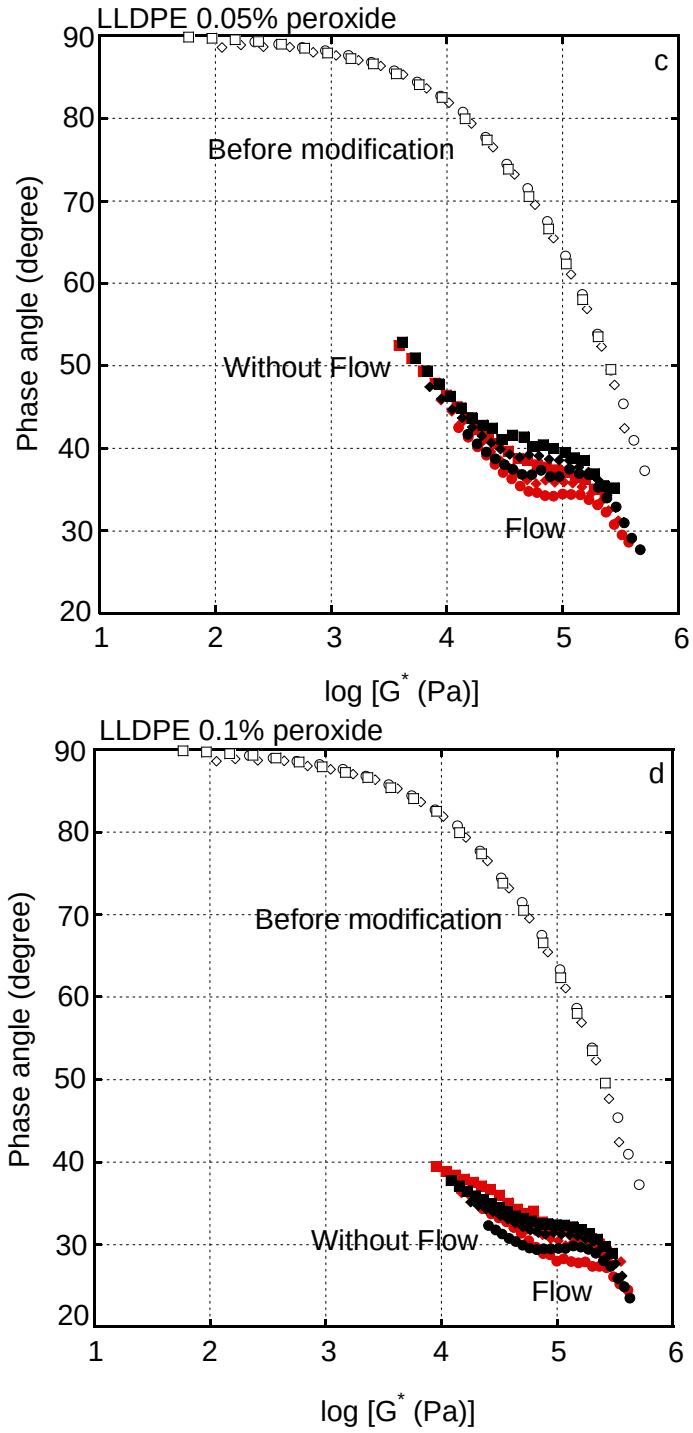

Figure 2-19. van Gurp-Palmen plots for samples (open symbols) before modification and after modification (closed symbols) under flow field and (red symbols) without flow field; at (circles) 130 °C, (diamonds) 160 °C and (squares) 190 °C; (a) LDPE 0.05 wt.%, (b) LDPE 0.1wt.%, (c) LLDPE 0.05 wt.% and (d) LLDPE 0.1 wt.% peroxide.

Further, the effect of flow field to cross-linking behaviors of LDPE and LLDPE is confirmed by the enhancement of shear stress σ and normal stress difference N_1, as seen in Figure 2-20. It is clearly seen that both σ and N_1 are enhanced with peroxide content. However, the values of LDPE cross-linked under flow field are close to those of the sample before modification, whereas they are greatly enhanced by cross-linking without field. In the case of LLDPE, both σ and N_1 for the sample cross-linked under flow field are slightly higher than these without flow field.

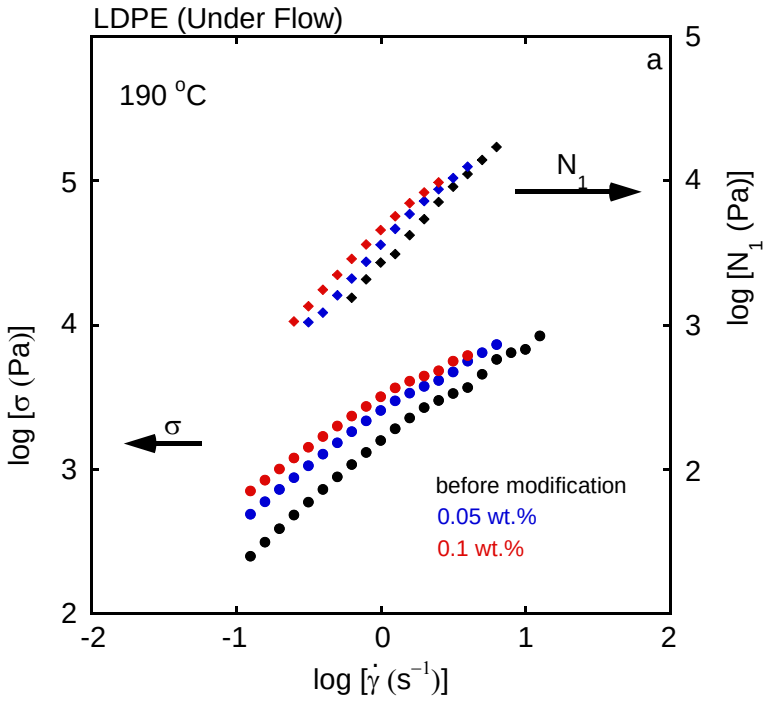

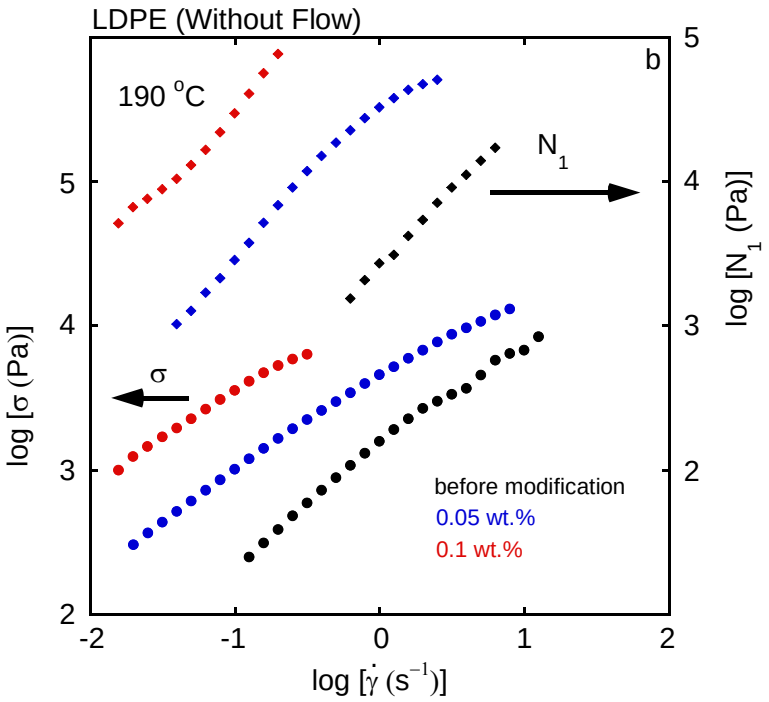
LDPE (Without Flow)
b
190 °C
N1
σ
before modification
0.05 wt.%
0.1 wt.%
log [σ (Pa)]
log [N1 (Pa)]
log [γ̇ (s−1)]

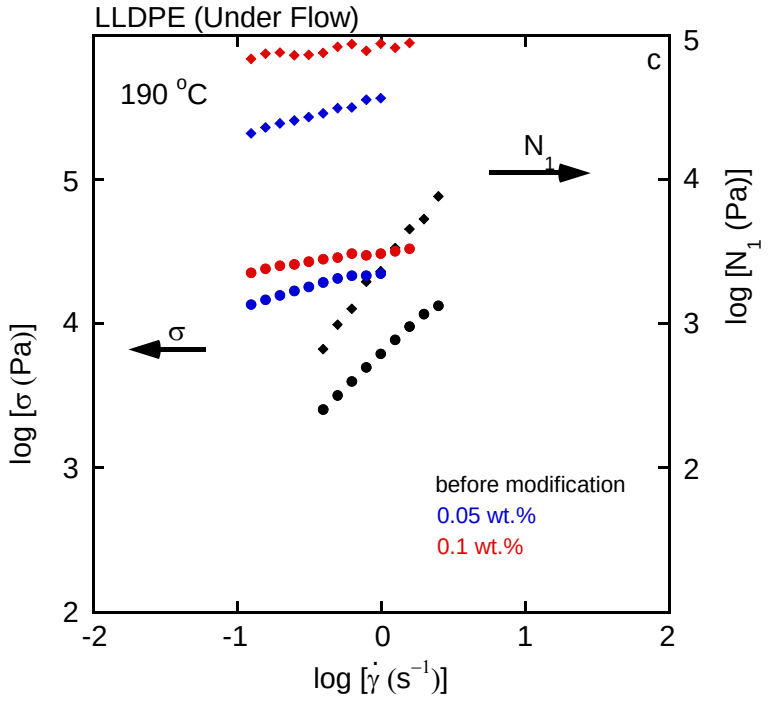
LLDPE (Under Flow)
c
190 °C
N1
σ
before modification
0.05 wt.%
0.1 wt.%
log [σ (Pa)]
log [N1 (Pa)]
log [γ̇ (s−1)]

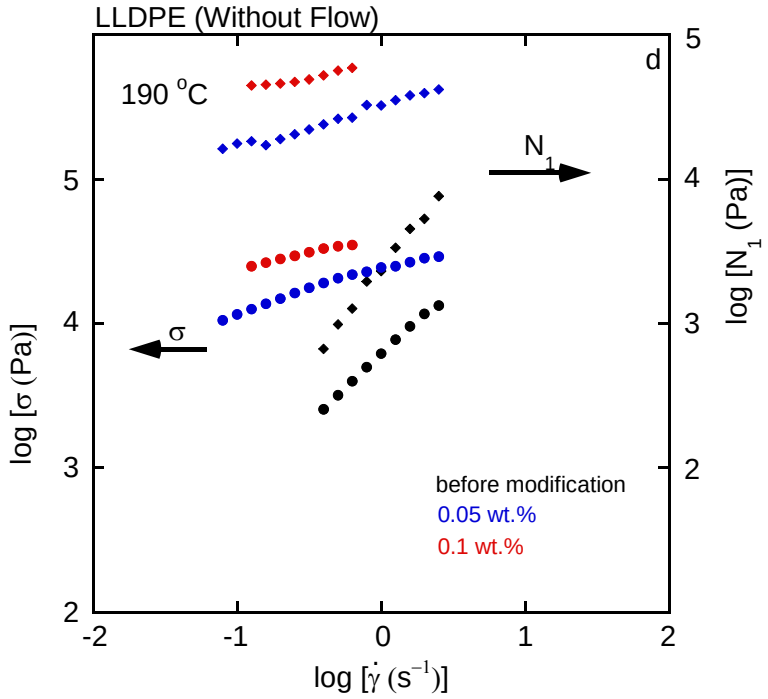

Figure 2-20. Steady-state properties such as (circles) shear stress σ and (diamonds) primary normal stress difference N_1 plotted against shear rate $\dot{\gamma}$ at 190 °C for the samples after peroxide modification; (a) LDPE under flow (b) LDPE without flow, (c) LDPE under flow and (d) LDPE without flow; (black symbols) before modification, (blue symbols) 0.05 wt.% and (red symbols) 0.1 wt.% of peroxide.

It is known that a branch polymer has small gyration radius compared to a liner polymer having the same molecular weight.[73] Therefore, the intramolecular cross-linking reaction is predominate than inter molecular one for LDPE. Once the intramolecular cross-linking occurs, the gyration radius of chain is reduced. Consequently, intramolecular cross-linking, not intermolecular, increases its possibility. Furthermore, the molecules trend to rotate in the applied shear flow and thus reduce the entanglement coupling with surrounding chains as the reaction processeds. Therefore, intramolecular cross-linking

reaction further occurs easily. Meanwhile, in the case of LLDPE, the possibility of intermolecular cross-linking reaction is higher than the intramolecular one. Because LLDPE has linear structure, intramolecular reaction barely occurs compared to LDPE, therefore the intermolecular cross-linking reaction is predominant for LLDPE cross-linked under flow field.

The peroxide modification of LDPE and LLDPE is further studied using the samples having a high cross-linking density. For the measurement, the modified samples cross-linked without flow field are chosen. The gel fraction ϕ and degree of swelling q for the cross-linked LDPE and LLDPE were measured by immersing the samples into hot xylene for 12 hours and drying up the solvent in a vacuum oven for 10 hours.

$$\phi = \frac{W_2}{W_1} \times 100\,(\%) \tag{2-3}$$

where W_1 is the initial weight of the sample before immerge to solvent, W_2 is the dried weight after immerge to solvent.

$$q = \frac{W_3}{W_2} \tag{2-4}$$

where W_3 is the weight of a swollen gel.

Figure 2-21 and Figure 2-22 show swelling ratio and gel fraction plotted against the peroxide content for LDPE and LLDPE, respectively. The results suggest that LLDPE shows higher gel fraction with lower swelling ratio than LDPE at high peroxide content. However, it found that the gel fraction is very low at the low peroxide content. Considering that rheological properties of LLDPE are easily affected by the radicals, it is presumed that the network structure of a weak gel was destroyed by the swelling pressure.

It often occurs for a network polymer immersed in a good solvent. Therefore, the data in Figure 2-21 and 2-22 in the low peroxide content are not reliable. In actual, LLDPE will form permanent network with a lower amount of peroxide than LDPE, and the swell ratio density should be very high.

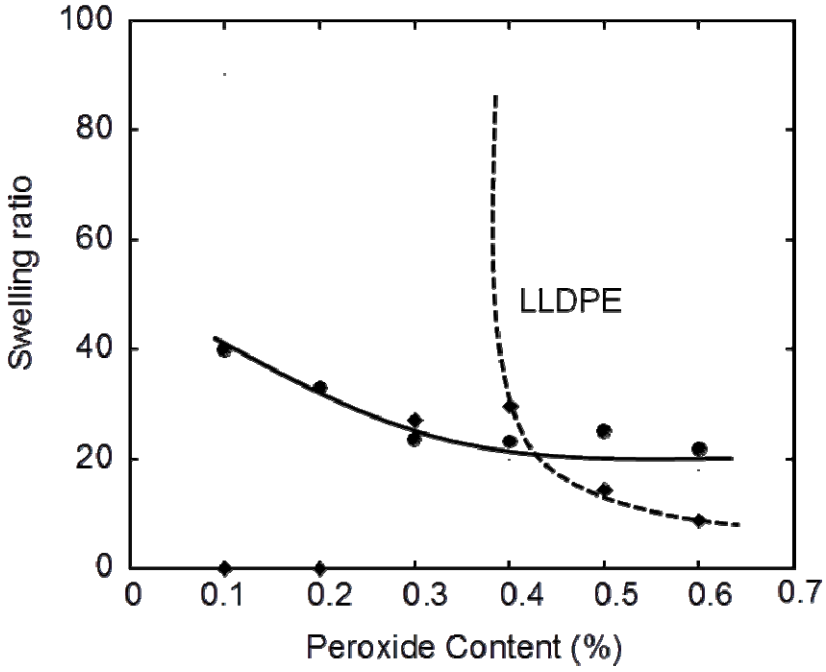

Figure 2-21. Swelling ratio of LDPE and LLDPE at various peroxide concentrations; (solid lines) LDPE and (dotted lines) LLDPE

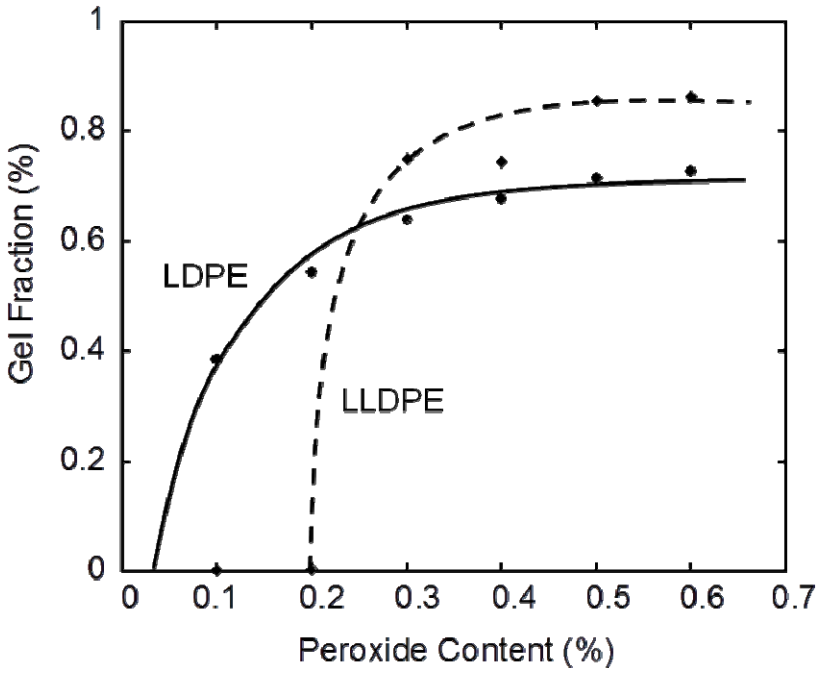

Figure 2-22. Gel fractions of LDPE and LLDPE at various peroxide concentrations; (solid lines) LDPE and (dotted lines) LLDPE

For the sample at high peroxide concentration, the cross-link density is high enough. Therefore, the system behaves like a cross-linked rubber above the melting point. Here, the stress-strain curves were measured by a tensile machine. Figure 2-23 shows the relationship between the stress and strain measured at 160 ^{o}C. At the same peroxide amount, the stress of LLDPE is located higher than that of LDPE which suggests that the cross-link density of LLDPE is higher than LDPE. The result corresponds to the gel fraction and swelling ratio. Further, the initial slope of the stress-strain curve correlates to the tensile storage modulus *E'*.

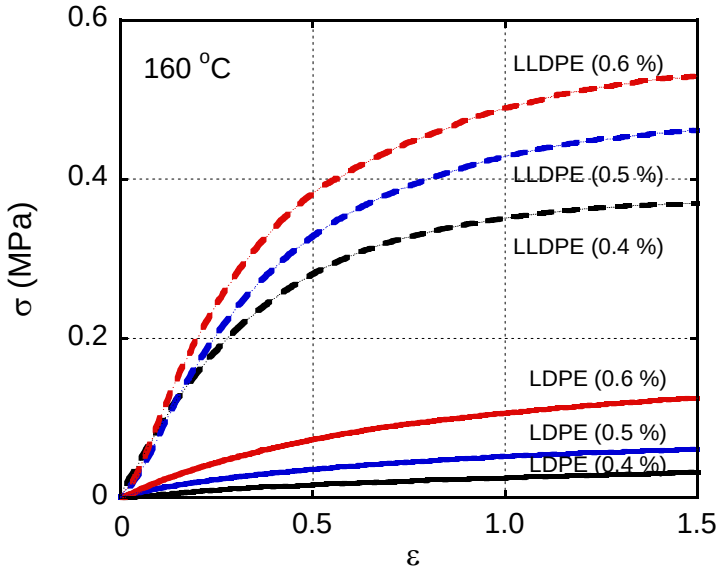

Figure 2-23. Tensile stress σ plotted against strain ε at 160 °C for the samples (solid lines) LDPE and (dotted lines) LLDPE at various peroxide concentration; (black) 0.4, (blue) 0.5 and (red) 0.6 wt.%

Figure 2-24 shows the temperature dependence of tensile storage modulus *E'*, loss modulus *E'*, and loss tangent tan δ at 10 Hz for LDPE and LLDPE with 0.4, 0.5 and 0.6 wt.% of the peroxide. The plateau region is observed beyond the melting point due to the generation of network structure. As well known, the plateau modulus provides the average molecular weight between cross-linking points M_c (Equation 2-4). It is found that M_c of LDPE is higher than that of LLDPE: 78.64 [kg mol^{-1}] for LDPE and 14.03 [kg mol^{-1}] for LLDPE. The result shows that cross-link density for LLDPE is higher than LDPE.

$$G_{plateau} = \frac{3RT}{M_c} \qquad (2\text{-}4)$$

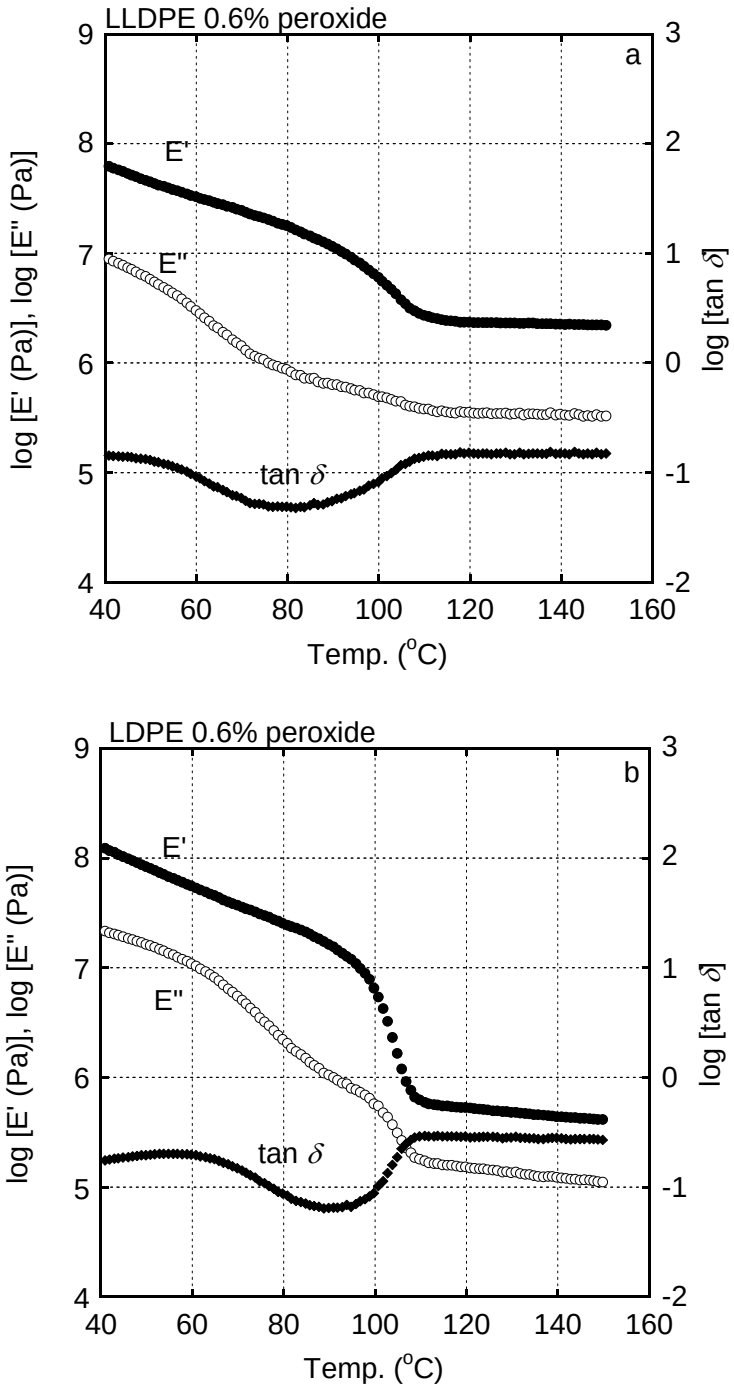

Figure 2-24 Temperature dependence of tensile (closed circles) storage modulus *E'*, (open circles) loss modulus *E*" and (closed diamonds) loss tangent tan δ at 10 Hz for (a) LDPE and (b) LLDPE at peroxide concentration of 0.6 wt.%

It is found that the cross-linking performance is increased with peroxide content. The applied flow field differently affects cross-linking behaviors in LDPE and LLDPE. In the case of LDPE, the intramolecular cross-linking is predominant during flow field. Once the intramolecular cross-linking reaction occurs, the gyration radius of chain decreases. Consequently, the possibility of intramolecular cross-linking is further enhanced. It results in low efficiency to form network structure under flow field. Meanwhile, the applied flow field leads to the opposite result in the case of LLDPE, the intermolecular cross-linking reaction is predominant. Further, the results suggest that cross-link density in LLDPE is higher than that in LDPE.

2.3.2.2 LDPE/LLDPE blends

The cross-linking reaction by peroxide addition is further studied using LDPE/LLDPE blends. The oscillatory modulus of the sample at low peroxide content is performed by shear mode using cone-and-plate and parallel plat geometries. However, at the high peroxide content, *e.g.*, 0.5 wt.%, it is difficult to cut the sample out. Therefore the tensile modulus measurement was performed instead of the shear modulus. In order to compare with other data, the shear modulus is calculated assuming Poisson's ratio of 0.5.

Figure 2-25 shows the curves of frequency dependence of oscillatory shear moduli, such as *G'* and *G"* for the blends after peroxide modification, in which the cross-linking reaction occurs without flow field. It is found that at low peroxide content, 0.05 wt.%, the *G'* for LDPE / LLDPE (25/75) is almost the same level to that of LLDPE in the low frequency region. The same phenomenon is observed in the thermally modified blends, as seen in Figure 2-10 (c) and (d). Furthermore, the phenomenon disappears at the high peroxide content, 0.5 wt.%.

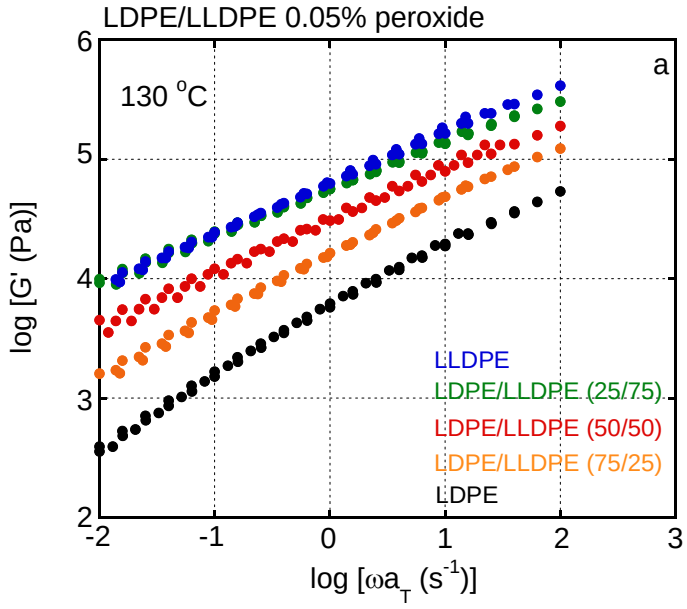
LDPE/LLDPE 0.05% peroxide
130 °C
a
log [G' (Pa)]
log [ωa_T (s^-1)]
LLDPE
LDPE/LLDPE (25/75)
LDPE/LLDPE (50/50)
LDPE/LLDPE (75/25)
LDPE

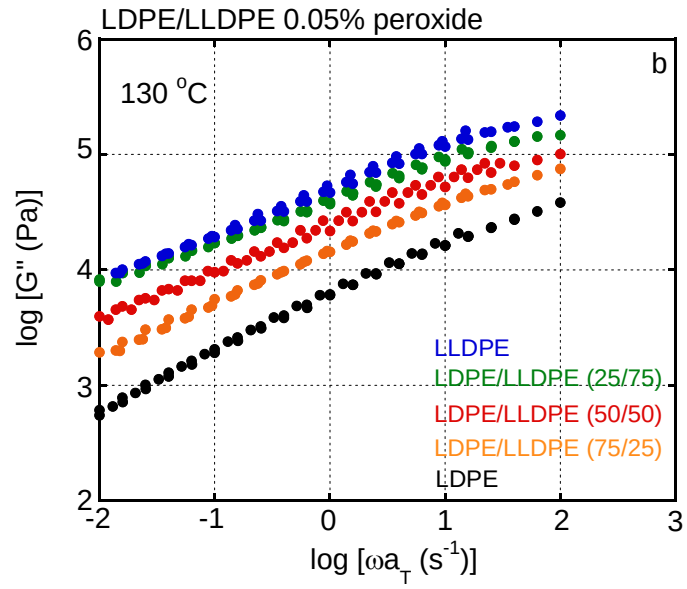
LDPE/LLDPE 0.05% peroxide
130 °C
b
log [G'' (Pa)]
log [ωa_T (s^-1)]
LLDPE
LDPE/LLDPE (25/75)
LDPE/LLDPE (50/50)
LDPE/LLDPE (75/25)
LDPE

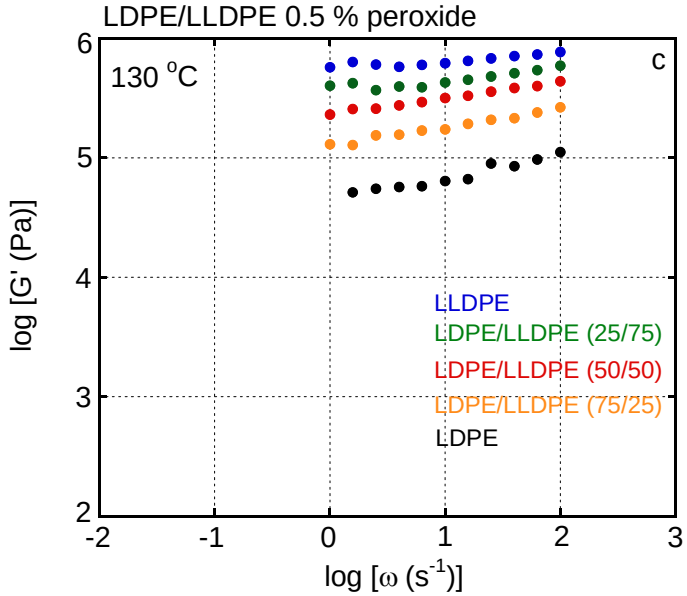
LDPE/LLDPE 0.5 % peroxide
130 °C
c
log [G' (Pa)]
log [ω (s^-1)]
LLDPE
LDPE/LLDPE (25/75)
LDPE/LLDPE (50/50)
LDPE/LLDPE (75/25)
LDPE

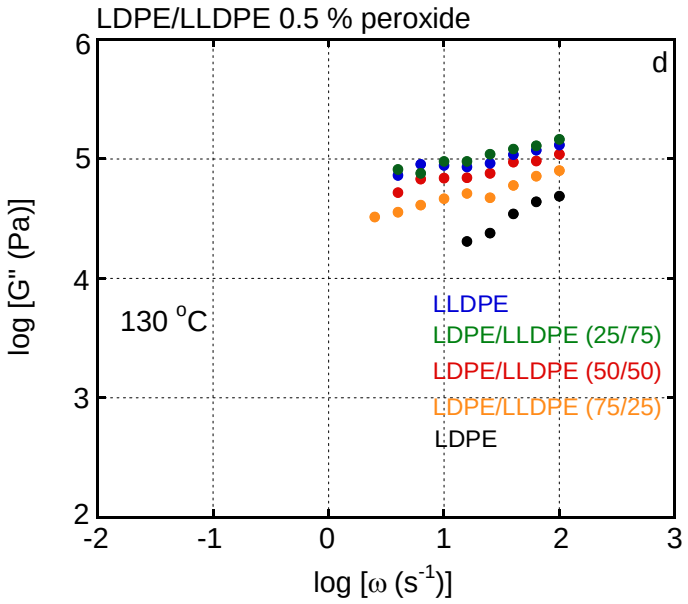

Figure 2-25 Master curves of frequency dependence of shear storage modulus *G'* and loss modulus *G"* at 130 °C for the samples; (a) *G'* of the blends 0.05 wt.% peroxide, (b) *G"* of the blends 0.05 wt.% peroxide, (c) *G'* of the blends 0.5 wt.% peroxide and (d) *G"* of the blends 0.05 wt.% peroxide; (black) LDPE, (orange) LDPE/LLDPE (75/25), (red) LDPE/LLDPE (50/50), (green) LDPE/LLDPE (25/75) and (blue) LLDPE.

Figure 2-26 shows the shear stress σ and primary normal stress difference N_1, respectively, at 190 °C. It is found that the σ increases with peroxide content and LLDPE exhibits the highest σ, whereas N_1 of the blends are higher than those of their pure components. This is similar to the result obtained for the thermally modified blends (Figure 2-9 to 10).

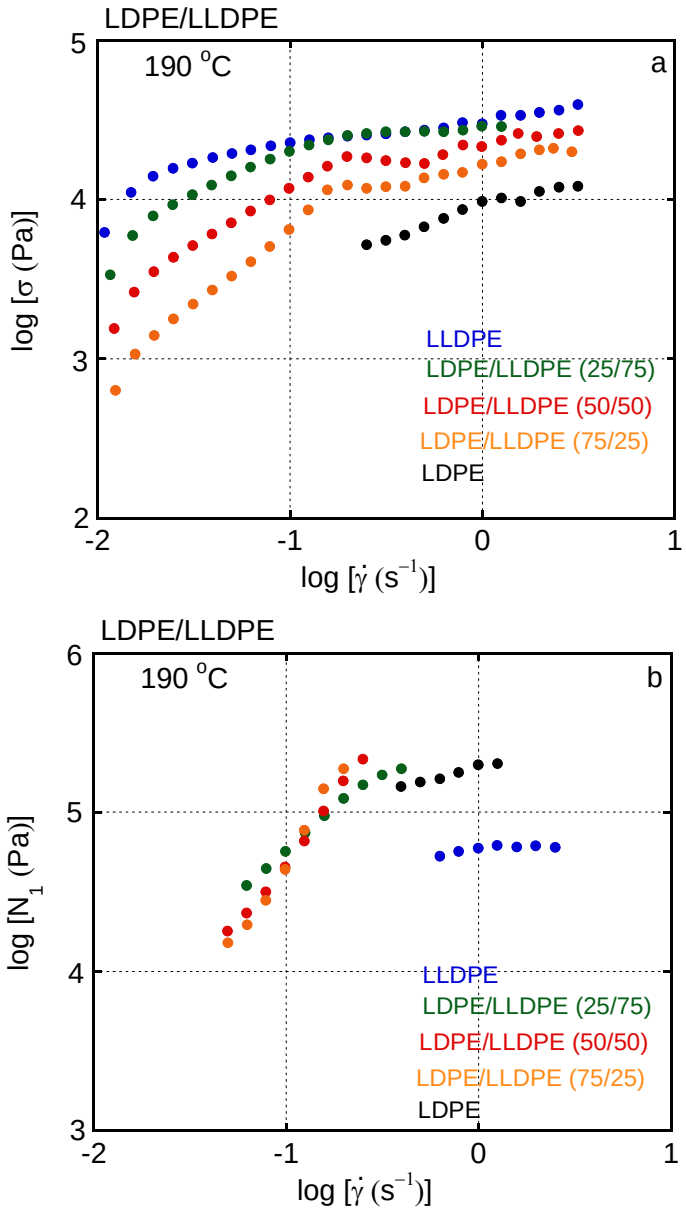

Figure 2-26. Steady-state properties such as (a) shear stress σ and (b) primary normal stress difference N_1 plotted against shear rate $\dot{\gamma}$ at 190 °C for the blends at peroxide concentration of 0.05 wt.%; (black) LDPE, (orange) LDPE/LLDPE (75/25), (red) LDPE/LLDPE (50/50), (green) LDPE/LLDPE (25/75) and (blue) LLDPE.

Further, the extrusion properties are investigated. Because the degree of cross-linking reaction is greater, the similar considerations, such as draw down force and extensional viscosity, are difficult to perform. Even though, the flow instability takes place

at the experiment condition for the blends containing low peroxide amount, the significant differences are observed in the flow instability of strands.

LDPE, LLDPE and their blends contenting 0.05 wt.% were extruded by the capillary rheometer at 190 °C with a apparent shear rate $\dot{\gamma}$ of 21.9 s^{-1}. The photographs of the extruded strands are shown in Figure 2-27. As seen in the figure, LDPE shows the melt fracture slightly, whereas LLDPE shows the shark sharkskin. In contrast, the gross melt fracture is clearly observed for the blends. The apparent flow instability for the blend suggests the marked strain hardening in elongational viscosity.[55,64] Further, the deviation from the additive rule of apparent shear stress is not obvious compared to the blend before the modification. The result suggests that the synergistic effect is detected for the blends having low peroxide amount.

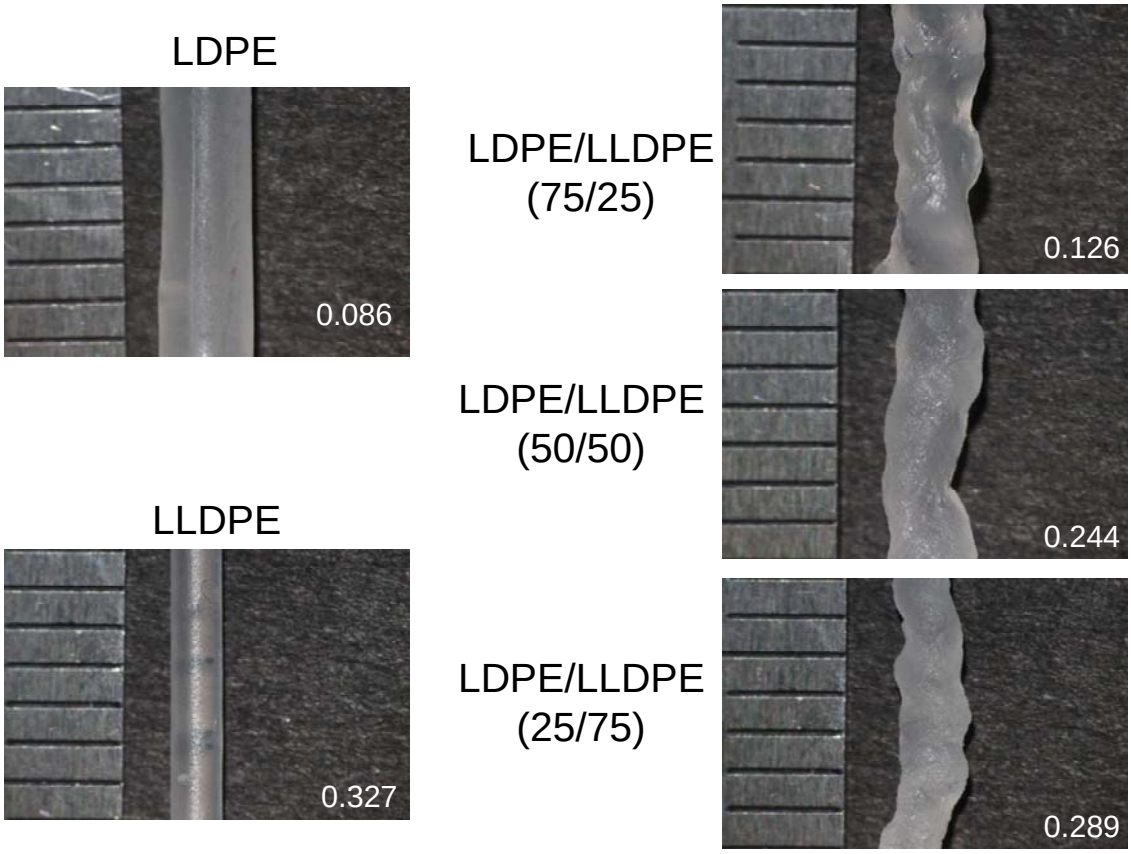

Figure 2-27. Optical photographs of extruded strands for LDPE/LLDPE blend at peroxide concentration of 0.05 wt.% at 190 °C through a circle die with L/D = 10/1 (mm): (a) LDPE, (b) LDPE/LLDPE (75/25), (c) LDPE/LLDPE (50/50), (d) LDPE/LLDPE (25/75) and (e) LLDPE. The numerals in the figure represent apparent shear stress (MPa).

The tensile test was performed at 160 ^{o}C using the blends contenting 0.5 wt.% peroxide. Both stress σ and strain ε are the engineering values. It is found that the stress of LLDPE is the highest due to the high level of cross-linking efficiency, whereas those of the blends are lactated between LDPE and LLDPE. The result suggests that the synergistic effect becomes disappear at high peroxide concentration.

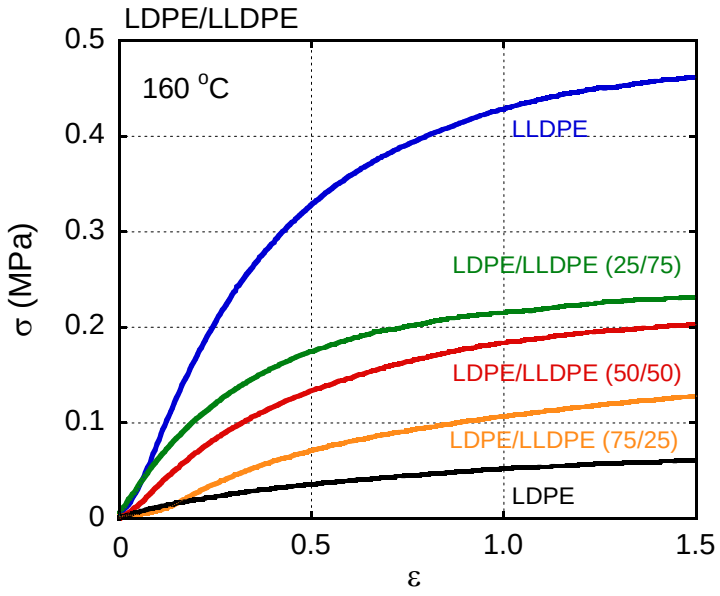

Figure 2-28. Tensile stress σ plotted against strain ε at 160 °C for the blends at peroxide concentration of 0.5 wt.%; (black) LDPE, (orange) LDPE/LLDPE (75/25), (red) LDPE/LLDPE (50/50), (green) LDPE/LLDPE (25/75) and (blue) LLDPE.

The gel fraction ϕ and swelling ratio q were measured and plotted against the LLDPE content, as shown in Figure 2-29 and 2-30, respectively. It is found that LLDPE shows the highest ϕ with the lowest q and vice versa for LDPE, whereas both ϕ and q blends are between those of the individual components, which is consistent with oscillatory modulus and tensile test obtained from the blend contain 0.5 wt.% of the peroxide. In the figure, ϕ and q of the blend at 75% LLDPE are not reliable.

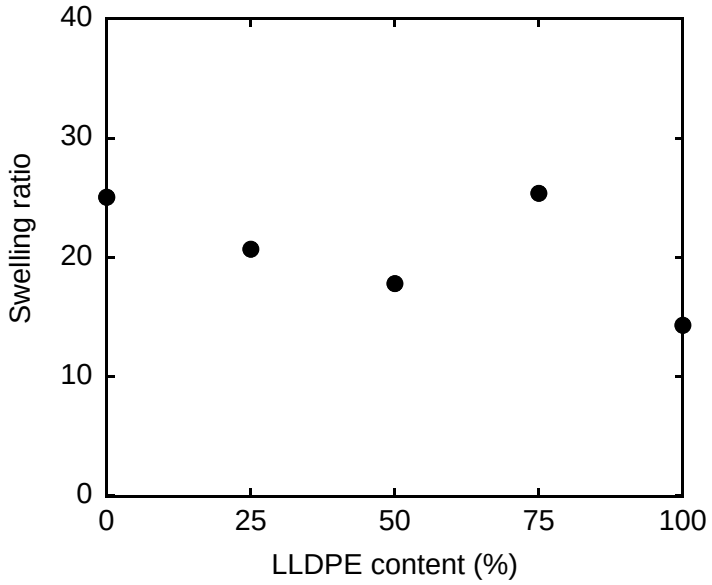

Figure 2-29. Swelling ratio of LDPE/LLDPE blends contain 0.5 wt.% of the peroxide plotted against LLDPE contents

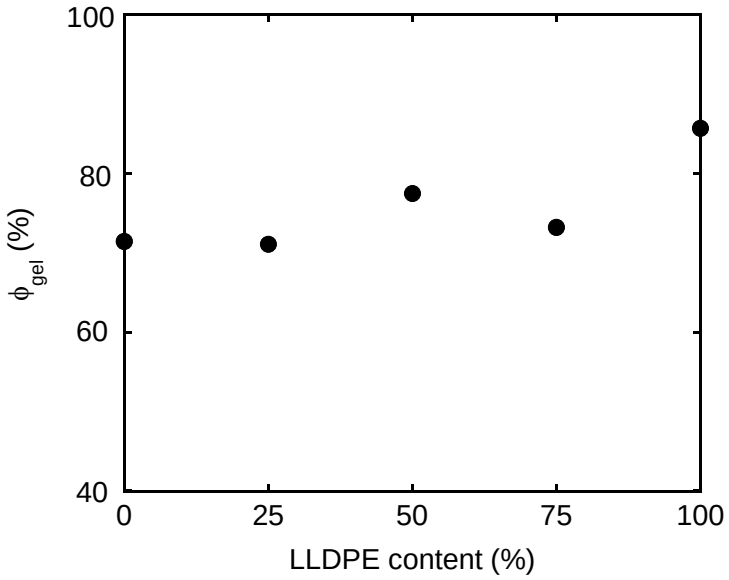

Figure 2-30. Gel fractions of of LDPE/LLDPE blends contain 0.5 wt.% of the peroxide plotted against LLDPE contents

It is found that the weak synergistic effect is observed for the blends contain 0.05 wt.% of the peroxide. Then it disappears when the peroxide content increases. It is clearly shown that the synergistic effect is depressed by a degree of cross-linking. The cross-linking reaction leads to the generation of permanent network and thus it prohibits the relaxation of polymer chains. Consequently, reptation of a branched molecule is less important. Moreover, the chain stretching occurs even without LLDPE, because it behaves like a cross-linked rubber.

2.4 Conclusions

The effects of cross-linking reaction with/without the peroxide compound on the rheological properties of LDPE/LLDPE blends, in which LLDPE has higher molecular weight than LDPE, were examined. At 280 ^{o}C, which is a typical temperature for extrusion-coating, PE without thermal stabilizer tends to be cross-linked rather than chain scission. The structural change significantly alters the rheological properties, although there are little or no changes in the molecular weight and its distributions and the numbers of double bond and short-chain branches. Furthermore, the thermally-modified LLDPE shows the following properties; (1) Time temperature superposition principle is not applicable, (2) the zero-shear viscosity greatly increases without increase in the M_w, and (3) shear modification behavior is detected. These results indicate that long-chain branches are generated in the main chains, which are responsible for the rheological changes in LLDPE. In contrast, the pronounced deviation of the drawdown force from the linear additive rule with marked strain hardening in elongational viscosity were detected for the thermally-modified blends. Correspondingly, gross melt fracture was detected even at low output rates during capillary extrusion, presumably caused by the high

elongational stress at the die entrance. The prolonged recovery of oscillatory modulus from the shear-modified state was also prominent for the blend. These results suggest that an intermolecular cross-linking reaction between LDPE and LLDPE, which provides branch chains having more than two branch points, occurs in the system during mixing.

Meanwhile, the cross-linking efficiency is greatly extended by the addition of the peroxide compound. The cross-linking reaction with the peroxide compound differently affects cross-linking behaviors in LDPE and LLDPE under flow field. It is found that the intramolecular cross-linking is predominant due to a small gyration radius of LDPE. Therefore, the cross-linking efficiency under flow field is lower than without flow field. In the case of LLDPE, however, the applied flow field leads to the intermolecular cross-linking reaction rather than intramolecular cross-linking one which gives a slightly higher cross-linking efficiency. Further, the density of cross-link points in LLDPE is higher than that in LDPE, as revealed by stress-strain curves, gel fraction and swelling ratio in a solvent. Moreover, it is found that the synergistic effect for LDPE/LLDPE blends is depressed by the generation of permanent network. It is reasonable because reptation of a branched molecule is less important.

References

1. Kuroki, T.; Sawaguchi, T.; Niikuni, S.; Ikemura, T., *Macromolecules*, **1982,** *15*, *1460.*
2. Andersson, T.; Stâlborm, B.; Wesslén, B., *J. Appl. Polym. Sci.*, **2004**, *91*, 1525.
3. Ono, K.; Yamaguchi, M., *J. Appl. Polym. Sci.*, **2009**, *113*, 1462.
4. Rangarajan, P.; Bhattacharya, D.; Grulke, E., *J. Appl. Polym. Sci.*, **1998**, 70*, 1239*.
5. Kartalis, C. N.; Papaspyrides, C. D.;Pfaendner, R. *Polym. Degrad. Stab*., **2000**, *70,* 189.
6. Dostal, J.; Kasparkova, V.; Zatloukal, M.; Muras, J.; Simek, L. *Euro. Polym. J.*, **2008**, *44,* 2652.
7. Rijke, A. M.; Mandelkern, L., *Macromolecules*, **1971**, *4*, 594.
8. Ghosh, P.; Dev, D.; Chakrabarti, A., *Polymer*, **1997**, *38*, 6175.
9. Sawatari, C.; Mastuo, M., *Polym. J.*, **1987**, *19*, 1365.
10. Stockmayer, W. H., *J. Chem. Phys.*,**1944**, *12*, 125.
11. Peacock, A. J., *Polym. Commun.*, **1987**, *28*, 259.
12. Smedberg, A.; Hjertberg, T.; Gustafsson, B., Polymer, **1997***, 38*, *4127*.
13. Rybnikar, F., *J. Polym. Sci. Polym. Symp.*, **1976**, *57*, 101.
14. Samburski, G.; Narkis, M., *J. Macromol. Sci. Phys. B*, **1996**, *35*, 843.
15. Utracki, L. A.; Schlund, B., *Polym. Eng. Sci.*, **1897**, *27*, 1512.
16. Wagner, M. H.; Kheirandish, S.; Yamaguchi, M., *Rheol. Acta* , **2004**, *44*, 198.
17. Hussein, I. H.; Williams, M. C., *Polym. Eng. Sci.*, **2004**, *44*, 660.
18. Yamaguchi, M., *Polym. Eng. Sci.*, **2006**, *46*, 1284.
19. Mieda, N.; Yamaguchi, M., *Adv. Polym. Tech.*, **2007**, *26*, 173.

20. Delgadillo-Velázquez, O.; Hatzikiriakos, S. G.; Sentmanat, M., *Rheol. Acta*, **2008**, *47*, 19.

21. Yamaguchi, M.; Takahashi, M., *Polymer*, **2001**, *42*, 8663.

22. Wagner, M. H.; Yamaguchi, M.; Takahashi, M., *J. Rheol.*, **2003**, *47*, 779.

23. Ono, K.; Yamaguchi, M., *J. Japan Soc. Polym. Process.*, **2009**, *21*, 745.

24. Yamaguchi, M.; Gogos, C. G., *Adv. Polym. Tech.*, **2001**, *20*, 261.

25. Yamaguchi, M., *J. Appl. Polym. Sci.*, **2006**, *102*, 1078.

26. Bernnat, A., *Polymer Melt Rheology and the Rheotens Test*, Ph.D. Thesis, University of Stuttgart, Stuttgart, Germany, **2001**.

27. Janzen, J.; Colby, R. H., *J. Mol. Struct.*, **1999**, *485-486*, 569.

28. Suwandam D.; Balke, S. T., *Polym. Eng. Sci.*, **1993**, *33*, 1585.

29. Yamaguchi, M.; Wagner, M. H., *Polymer*, **2006**, *47*, 3629.

30. Yamaguchi, M., *Rheological Properties of Molten Polyolefins* In *Structure and Properties of Pol Olefin Material* ; Transworld Research Network: Kerela, **2012**.

31. Kriston, I., *Some Aspects of the Degradation and Stabilization of Phillips Type Polyethylene*, Ph.D. Thesis, Budapest University of Technology and Economics, Budapest, Hungary, **2010**.

32. Keβner, U.; Münstedt, H., *Polymer*, **2010**, *50*, 507.

33. Trinkle, S.; Friedrich, C., *Rheol. Acta*, **2001**, *40*, 322.

34. Alamo, R. G.; Graessley, W. W.; Krishnamoorti, R.; Lohse, D. J.; Londono, J. D.; Mandelkern, L.; Stehling, F. C.; Wignall, G. D., *Macromolecules*, **1997**, *30*, 561.

35. Morgan, R. L.; Hill, M. J.; Barham, P. J.; Frye, C. J., *Polymer*, **1997**, *38*, 1903.

36. Doi, M., *J. Polym. Sci., Polym. Phys. Ed.*, **1983**, *21*, 667.

37. Milner, S. T.; MacLeish, T. C. B., *Phys. Rev. Lett.*, **1998**, *81*, 725.

38. Cox, W. P.; Merz, E. H., *J. Polym. Sci.*, **1958**, *28*, 619.

39. Debroth, T.; Erwin, L., *Polym. Eng. Sci.*, **1986**, *26*, 462.

40. Phillips, E. M.; McHugh, K. E.; Bradley, M. B., *J. Coat. Fabrics.*, **1990**, *19*, 155.

41. Park, C. B.; Cheung, L. K., *Polym. Eng. Sci.*, **1997**, *37*, 1.

42. Lau, H. C.; Bhattacharya, S. N.; Field, G., *J. Polym. Eng. Sci.*, **1998**, *38*, 1915.

43. Field, G. J.; Micic, P.; Bhattacharya, S. N., *Polym. Int.*, **1999**, *48*, 461.

44. Yamaguchi, M.; Suzuki, K., *J. Polym. Sci., Polym. Phys. Ed.*, **2001**, *39*, 2159.

45. Yamaguchi, M.; Suzuki, K., *J. Appl. Polym. Sci.*, **2002**, *86*, 79.

46. Kouda, S., *Polym*. *Eng. Sci.*, **2008**, *48*, 1094.

47. Ono, K.; Ogita, H.; Okamoto, K.; Yamaguchi, M., *J. Appl. Polym. Sci.*, **2009**, *113*, 3368.

48. Tordera, J., *J. Appl. Phys.*, **1963**, *7*, 215.

49. Cogswell, F. N., *Polymer Melt Rheology*; George Godwin Ltd: London, **1981**.

50. Ramamurthy, A. V., *J. Rheol.*, **1986**, *30*, 337.

51. Brochard, F.; de Gennes, P. G., *Langmuir*, **1992**, *8*, 3033.

52. Piau, J. M.; Agassant, J. F., *Rheology for Polymer Melt Processing*; Elsevier: Amsterdam, **1996**.

53. Denn, M. M., *Annu. Rev. Fluid Mech.*, **2001**, *33*, 265.

54. Fujiyama, M., *J. Appl. Polym. Sci.*, **2002**, *84*, 2120.

55. Meller, M.; Luciani, A.; Sarioglu, A.; Manson, J. E., *Polym. Eng. Sci.*, **2002**, *42*, 611.

56. Yamaguchi, M.; Miyata, H.; Tan, V.; Gogos, C. G., *Polymer*, **2002**, *43*, 5249.

57. Hatzikiriakos, S. G.; Migler, K. B., *Polymer Processing Instabilities*; Marcel Dekker: New York, **2005**.

58. Kulikov, O., *J. Vinyl. Additive Technol.*, **2005**, *11*, 127.

59. Tadmor, Z.; Gogos, C. G., *Principles of Polymer Processing*, 2nd ed.; Willy-Interscience: New York, **2006**.

60. Wang, X.; Wang, X. Y.; Wang, Z.; Hee, J., *J. Macromol. Sci. B Phys.*, **2006**, *45*, 777.

61. Allal, A.; Vergnes, B., *J. Non-Newtonian Fluid Mech.*, **2007**, *146*, 45.

62. Kulikov, O.; Hornung, K.; Wagner, H. M., *Rheol. Acta*, **2007**, *46*, 741.

63. Suzuki, M.; Amran, M. A. M.; Okamoto, K.; Taniike, T.; Terano, M.; Yamaguchi, M., *Adv. Polym. Technol.*, **2009**, *28*, 185.

64. Mieda, N.; Yamaguchi, M., *J. Non-Newtonian Fluid Mech.*, **2011**, *166*, 231.

65. Yamaguchi, M., *J. Appl. Polym. Sci.*, **2001**, *82*, 1277.

66. Koopmans, R.; Doelder, J.; Molenaar, J., *Polymer Melt Fracture*; CRC Press: Boca Raton, **2010**.

67. Cogswell, F. N., *Polymer Melt Rheology*; George Godwin: London, **1981**.

68. Kim, S.; Dealy, J. M., *Polym. Eng. Sci.*, **2002**, *42*, 482..

69. Yamaguchi, M.; Todd, D. B.; Gogos, C. G., *Adv. Polym. Tech.*, **2003**, *22*, 179.

70. Osaki, K.; Murai, A.; Bessho, N.; Kim, B. S., *J. Soc. Rheol. Jpn.*, **1976**, *4*, 166.

71. Shinohara, M., *J. Soc. Rheol. Jpn.*, **1991**, *19*, 118.

72. Loshe, D. J.; Milner, S .T.; Fetters, L. J.; Xenidou, M.; Hadjichritidis, N.; Mendelson, R. A.; Garcia-Franco, C. A.; Lyon, M. K., *Macromolecules*, **2002**, *35*, 3066.

73. Kuhn R.; Kromer H., *Colloid Polym Sci*, **1982**, *260*, 1083.

Chapter 3

Molecular Weight Segregation of Polyethylene by Annealing Procedure in Temperature Gradient

3.1 Introduction

LDPE has complicated branch structure with broad molecular weight distribution (MWD). The most pronounced molecular architecture is long-chain branch (LCB). It is well known that LDPE can be classified into two types according to the production method; one is tubular LDPE and the other is autoclave LDPE. Previous studies on the dilute solution properties have clarified the difference in molecular structure between tubular LDPE and autoclave LDPE. According to them,[1-4] autoclave LDPE has more long-chain branches than tubular LDPE. The result was also confirmed by a study using nuclear magnetic resonance.[5] Moreover, autoclave LDPE is believed to show tree-like branch structure, whereas the tubular LDPE molecules has comb-like branch structure.[6,7] It is also found from the dilution properties that high molecular weight fraction of LDPE has greater unbranched chain segment (high number of average molecular weights between long- and short-chain branching point, M_{LCB} and M_{SCB} are high) than the low molecular weight fraction. Moreover, the unbranched chain segment of tubular LDPE is higher than that of autoclave LDPE.[6,8] Further, the difference in branch structure affects the rheological properties, especially under elongational flow.[7,9] It was reported that tubular LDPE shows less strain hardening, although both types of LDPE exhibit strain hardening.

Table 3-1 LCB and SCB as a function of molecular weight (MW)[6]

MW	M_{LCB}		average number of LCB	
	autoclave	tubular	autoclave	tubular
$1x10^6$	5.5×10^3	2.1×10^4	90	23
$5x10^5$	5.2×10^3	1.8×10^4	48	13
$2x10^5$	4.9×10^3	1.3×10^4	20	7
$1x10^5$	4.7×10^3	9.0×10^3	10	5
$1x10^4$	4.0×10^3	3.1×10^3	0-1	1-2

MW	M_{SCB}		average number of SCB	
	autoclave	tubular	autoclave	tubular
$1x10^6$	9.0×10^2	1.1×10^3	1100	900
$5x10^5$	8.7×10^2	1.0×10^3	570	500
$2x10^5$	8.5×10^2	9.2×10^2	240	220
$1x10^5$	8.2×10^2	8.5×10^2	120	120
$1x10^4$	7.7×10^2	6.0×10^2	13	17

In order to clarify the relation of structure and rheological properties for LDPE in detail, fractionation is required. Therefore, various fractionation methods of molecular weight have been studied for a long time, such as size exclusion chromatography (SEC), fractional precipitation method,[10-14] and gas anti-solvent technique.[15,16] Recently, an interesting research successfully revealed that molecular weight segregation of PE blends

takes place in the molten state.[17] This type of fractionation was confirmed for poly(styrene),[18,19] styrene-acrylonitrile copolymer,[20] and poly(styreneblock-methyl methacrylate).[21] It is found that low molecular weight fraction tends to localize at a film surface, indicating that rheological properties in the surface region are different from those in the bulk. Therefore, the rheological properties of PE could be modified using the concept of fractionation methods.

In this research, a molecular weight segregation method by annealing procedure in temperature gradient is performed using autoclave and tubular LDPE in order to separate the low molecular weight fraction from the high molecular weight one to clarify the structure and rheological properties of fractionated samples. This technique can be applied to control the rheological properties at actual processing by tuning the temperature in a processing machine.

Firstly, the molecular weight segregation under temperature gradient using HDPE blends is studied as a pioneer work, because of its simple structure in HDPE. Secondly, the molecular weight segregation of LDPE having complex branch structure is investigated.

3.2 Experimental

3.2.1 Materials

All samples employed in this study were commercially available materials; two types of HDPE produced by Zieglar-Natta catalyst and three types of LDPE. The melt flow rate (MFR) at 190 ^{o}C for all samples is summarized in Table 3-2.

Table 3-2. Melt flow rate of PE used in this work

Types		Melt Flow Rate (MFR) (g/10 min)
HDPE-1	HDPE	0.3
HDPE-2	HDPE	120
t-LDPE	tubular-LDPE	1.0
a-LDPE-1	autoclave -LDPE	1.6
a-LDPE-2	autoclave -LDPE	6.5

3.2.2 Sample preparation

A binary blend of HDPE-1/HDPE-2 (50/50, w/w) was prepared by melt-mixing in a 60 cc internal batch mixer (Toyoseiki, Labo-plastmil) at 230 ºC with pentaerythritol tetrakis (3-3,5-di-tert-butyl-4-hydroxyphenyl)propionate (Ciba, Irganox1010) and tris(2,4-di-tert- butylphenyl)phosphate (Ciba, Irgafos168) as thermal stabilizers and calcium stearate as a neutralizer. The content of each additive was 5000 ppm. The total amount was 48 g. The blade rotation speed was 30 rpm, and the mixing time was 3 min. The obtained samples were compressed into a flat sheet with 1.5 and 3 mm of thickness by a compression-molding machine (Tester Sangyo, SA303IS) at 230 ºC under 10 MPa for 10 min. Then the sample was subsequently cooled down at 30 ºC. Further, the same protocol was also applied to prepare LDPE sheets.

The obtained sheets were annealed in the molten state in the compression-molding machine for various annealing times, in which the temperatures of top and bottom plates were controlled separately. The gap between the molds was controlled to be either 1.5 or

3.0 mm. After annealing treatment, the sheets were quenched at 30 ºC. Then, both surfaces of the annealed sheet were sliced in the thickness of approximately 300 μm by a knife. The sliced samples were compressed into a flat sheet by the compression-molding machine at 230 ºC of both plates and then quenched at 30 ºC.

3.2.3 Measurements

3.2.3.1 Oscillatory shear measurement

The frequency dependence of oscillatory shear modulus for two types of HDPE with different molecular weight and their blend was measured in the molten state by a cone-and-plate rheometer (TA instruments, AR2000) at various temperatures such as 160, 190, and 230 ºC under a nitrogen atmosphere. The same experiment was performed for LDPE at 130, 160 and 190 ^{o}C.

The recovery behavior of the oscillatory modulus after applied shear flow was evaluated to obtain the information on branch structure. The samples were sheared at a stress level of 24.5 kPa by the cone-and-plate rheometer at 160 °C for 30 min. After cessation of the shear flow, an oscillatory strain at 0.01 Hz was applied to the sample at 160 °C. Then, the shear storage modulus was evaluated as a function of the residence time in the rheometer. The details of this method were explained in the previous paper.[22]

3.2.3.2 Rheological response under elongational flow

Capillary extrusion was performed for LDPE by a capillary rheometer (Yasuda Seiki Seisakusyo, 140 SAS-2002) at 190 °C to evaluate the steady-state shear viscosity and the appearance of the extruded strands. The molten polymer was extruded through a die of the following dimensions: 1 mm in diameter, 10 mm in length and an entrance angle of 180°.

The drawdown force measurement was carried out at 190 °C with the capillary rheometer, equipped with a tension detector and a set of rotating wheels, as described previously.[23,24] The molten polymer was extruded through the same die used to evaluate the capillary extrusion properties. The draw ratio was 9.2. The shear rate at the die wall was 21.9 s^{-1}.

The growth curves of uniaxial elongational viscosity were evaluated at 160 °C on the rotational rheometer, equipped with a universal testing platform (Xpansion instruments, SER2-G). Flat sheet samples, 10 mm wide, 15 mm long, and 0.5 mm thick, were used.

3.3 Results and discussion

3.3.1 Molecular weight segregation of HDPE blend

Figure 3-1 shows the master curves of frequency dependence of oscillatory shear moduli such as storage modulus *G'* and loss modulus *G"* for HDPE-1, HDPE-2, and the blend. The reference temperature is 160 ºC. As well known, the time-temperature superposition principle is applicable to not only pure samples but also the blend. The apparent flow activation energy is calculated from the slope of the logarithm of the shift factors plotted against the reciprocal of absolute temperature, *i.e.,* Arrhenius plot, following the well-known Andrade equation,[25] and found to be approximately 20 kJ/mol for all samples including the blend, which is a typical value for HDPE.[1-4] The modulus of the blend is located between those of the individual pure components. Further, there is no shoulder peak ascribed to phase separation for the blend. This is reasonable because both components are HDPE, *i.e.*, a miscible blend. Moreover, it is found from the figure that the zero-shear viscosities of PE-1, PE-2 and the blend are 35000, 80, and 6300 Pa s, respectively.

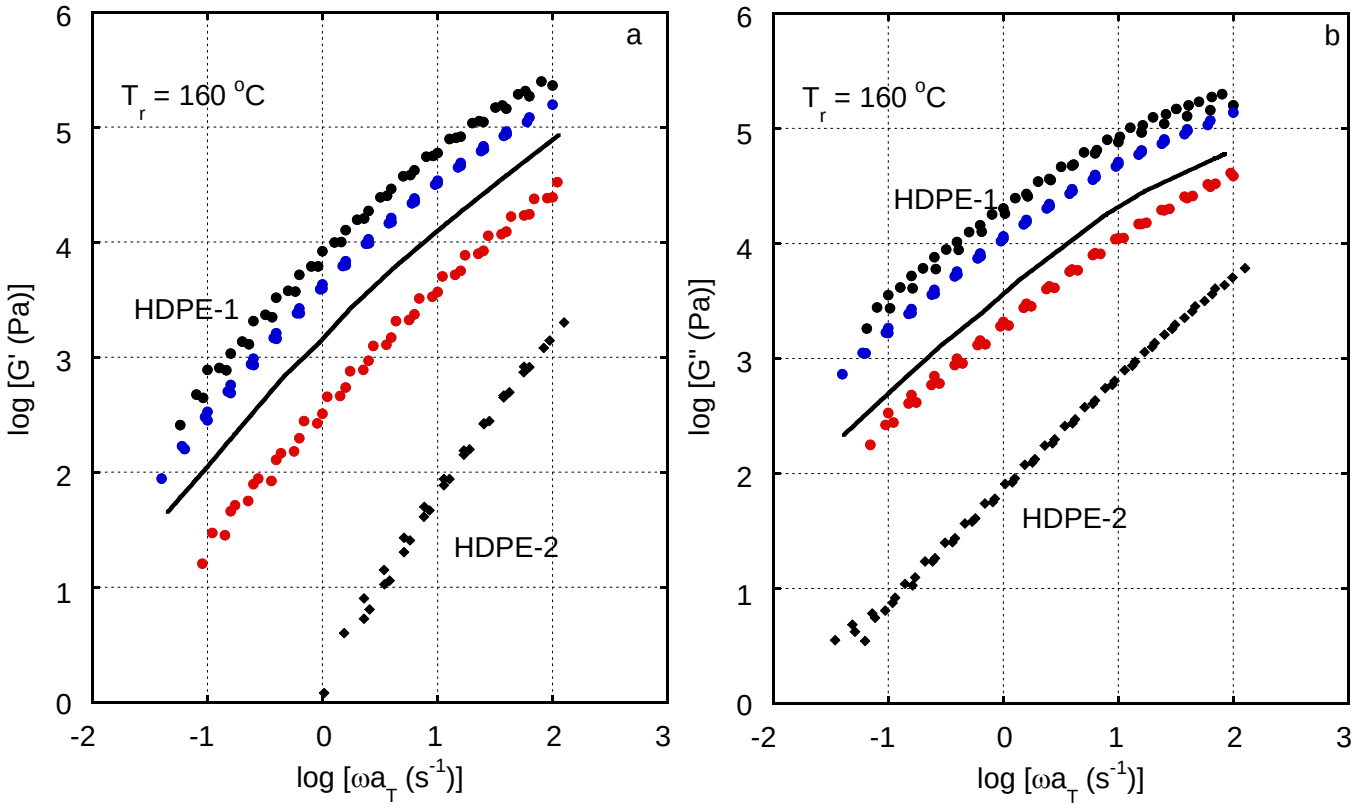

Figure 3-1 Master curves of frequency dependence of (a) shear storage modulus *G'* and (b) loss modulus *G"* at 160 ºC; (black circles) HDPE-1, (black diamonds) HDPE-2, and (solid line) the blend prior to annealing. The master curves of surface parts of the samples after annealing at the condition of (top) 300 ºC / (bottom) 150 ºC for 2hrs are also plotted; (blue circles) low temperature side and (red circles) high temperature side.

Figure 3-1 also shows the oscillatory shear moduli for the samples obtained from each surface of the sheet annealed at 300 ºC at the top and 150 ºC at the bottom for 2 hrs. As seen in the figure, both moduli for the sample collected from the top surface controlled at the high temperature are lower than those of the blend prior to annealing in the wide range of frequency, whereas the sample from the bottom surface at the low temperature exhibits higher moduli than the blend. The result suggests that low molecular

weight fraction is segregated at the high temperature side and vice versa. Further, the slopes of *G'* and *G"* for the top surface are almost similar to those for the bottom, indicating that molecular weight distribution of both samples is not so different.

The weight-average molecular weight M_w of HDPE is calculated from the zero-shear viscosity. According to Garcia-Franco, the zero-shear viscosity at 190 ºC is expressed as follows; [26]

$$\eta_0 = 4.743 \times 10^{-10} \left(\frac{M_w}{14} \right)^{3.33} \tag{3-1}$$

Following the equation, M_w of pure PE-1 (η_0 = 2.4 x 10^4 [Pa s] at 190 ºC) is calculated to be 1.8 x 10^5 and that of pure PE-2 (η_0 = 5.5 x 10^1 [Pa s]) is 2.9 x 10^4.

Figure 3-2 shows the weight-average molecular weight calculated from values of zero-shear viscosities for the surface samples annealed at various temperature conditions. It is found that a large temperature gap leads to pronounced segregation. Since the thickness of the sample sheets is a constant (1.5 mm for the experiments), it can be concluded that large temperature gradient enhances the molecular weight segregation. Further, low molecular weight fraction is segregated at the high temperature side even when the bottom plate of the compression-molding machine is controlled at higher temperature than the top. It suggests that the gravitational force has no influence on the segregation.

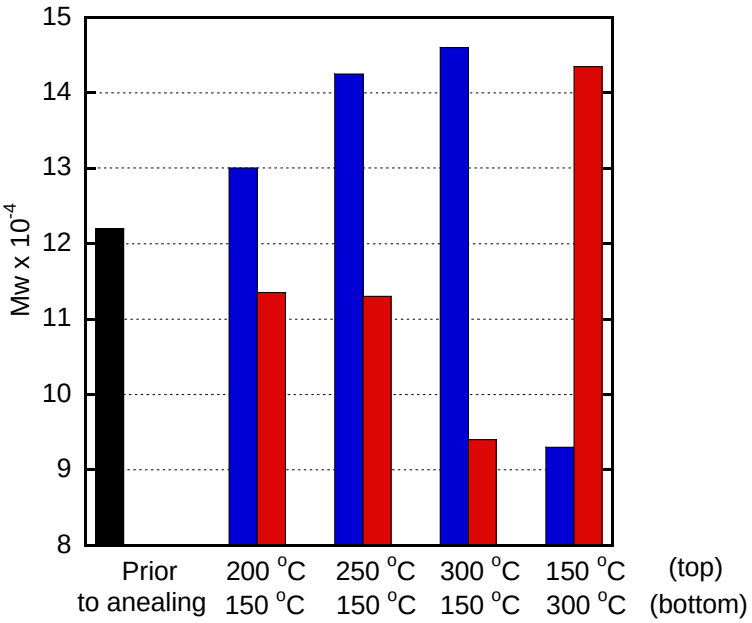

Figure 3-2 Weight-average molecular weight M_w calculated from η_0 for the blend samples annealed at various temperature conditions for 2 hrs; (black) prior to annealing, (red) surface at the bottom, and (blue) surface at the top.

Figure 3-3 shows the effect of annealing time on the segregation at the annealing condition of (top) 300 ºC and (bottom) 150 ºC. It is obvious that the molecular weight increases with the duration time of annealing for the low temperature side, and vice versa.

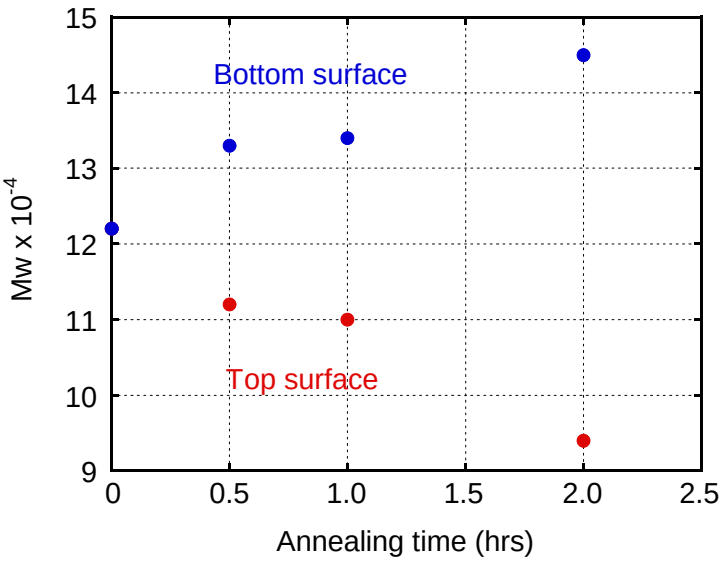

Figure 3-3 Weight-average molecular weight M_w for the surface samples after annealing for various residence times at (top) 300 ºC / (bottom) 150 ºC; (red) top surface and (blue) bottom surface.

In order to understand the effect of thermal decomposition on the segregation behavior, the sample sheet having the annealing history at 300/150 ºC for 2 hrs is kneaded again in the internal mixer at 230 ºC for 5 min and compressed into a flat sheet at 230 ºC of both plates of the compression-molding machine. The oscillatory shear modulus of the obtained sample is shown in Figure 3-4. The moduli of the re-mixed sample are completely the same as those of the original blend sample prior to annealing, demonstrating that the current experimental results shown in Figures 3-1 to 3-3 are not attributed to the thermal decomposition.

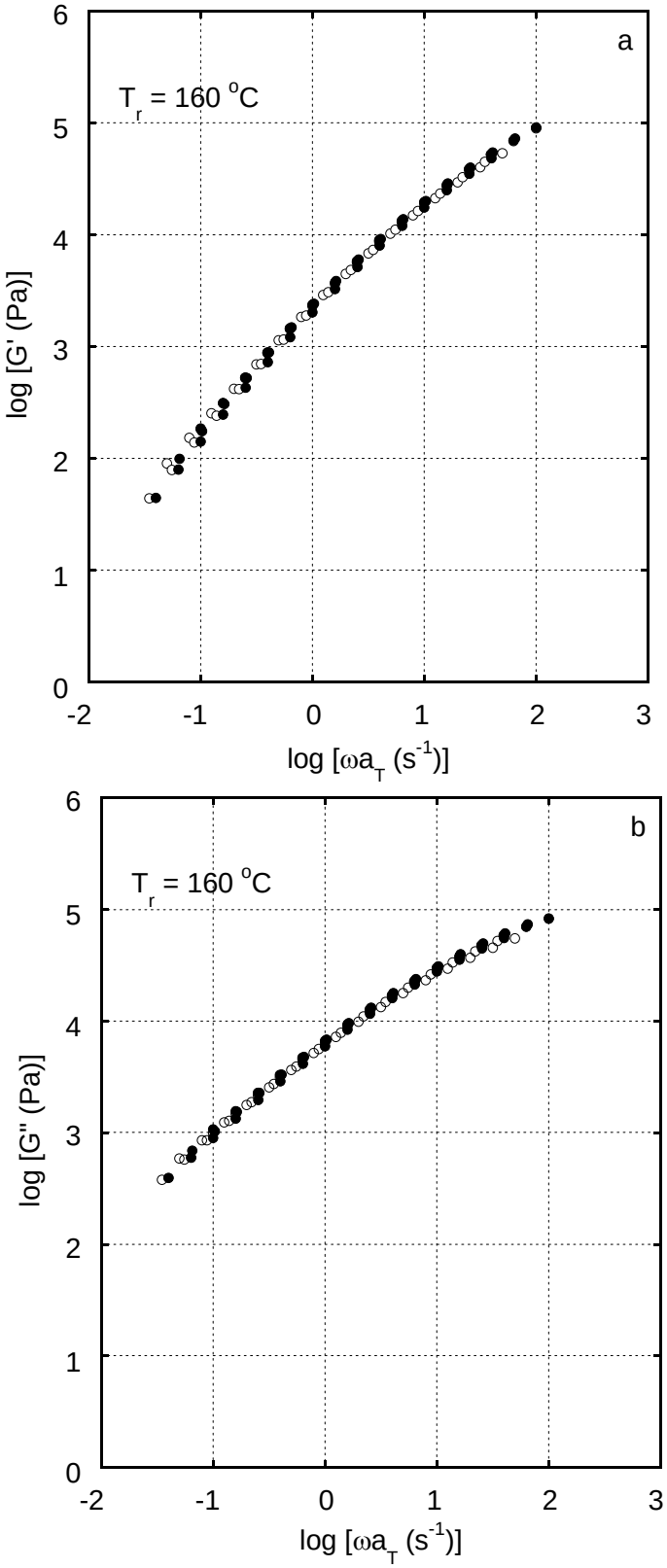

Figure 3-4 Master curves of frequency dependence of (a) shear storage modulus *G'* and (b) loss modulus *G"* for blends at 160 ºC; (closed symbols) blend sample prior to annealing and (open symbols) re-mixed sample after annealing at the condition of (top) 300 ºC / (bottom) 150 ºC for 2 hrs.

The segregation behavior is obvious at a narrow gap between both plates of the compression-molding machine. Figure 3-5 shows the loss modulus for the segregated samples annealed at (top) 200 ºC and (bottom) 150 ºC for 30 min employing two samples with different thickness. As seen in the figure, a slight difference is detected between them when the gap between the molds is 3 mm, suggesting that segregation barely occurs in the blend sample. This result indicates again that temperature gradient is important for the segregation.

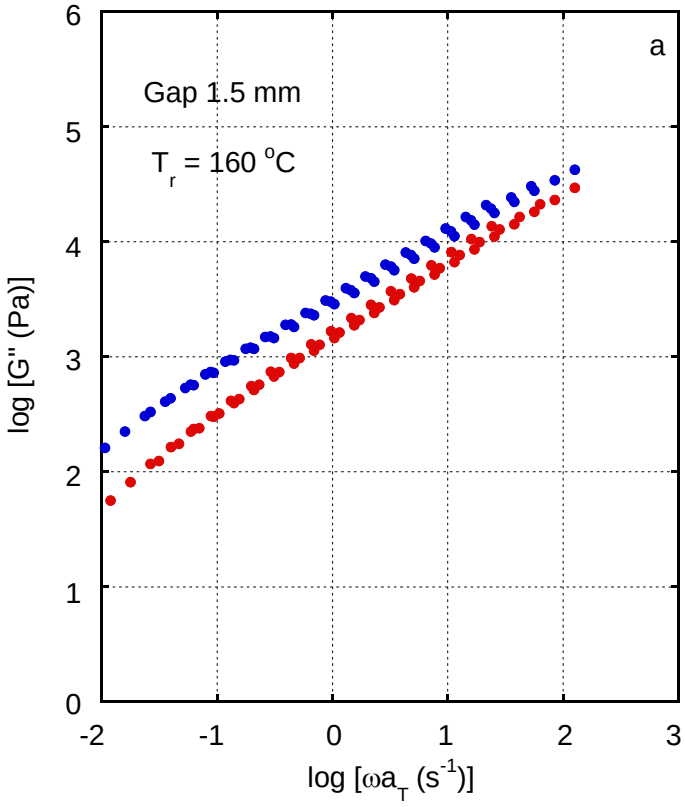

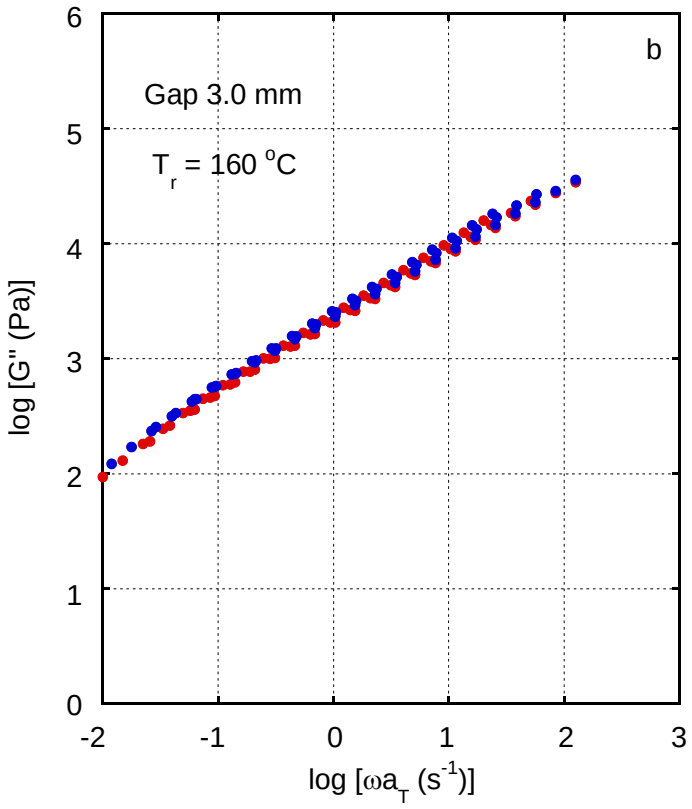

Figure 3-5. Master curves of frequency dependence of shear loss modulus *G"* for surface parts of the samples after annealing at the condition of (top) 200 ºC / (bottom) 150 ºC for 30 min. The gap between the molds was (a) 1.5 mm and (b) 3.0 mm. (blue) bottom surface and (red) top surface.

.

The experimental results presented in this study could be explained using the concept of free volume. Because the free volume fraction of a polymer melt increases with temperature, chain ends having a large free volume would prefer to a high temperature region.

The study confirms that the molecular weight fractionation of HDPE take places during annealing procedure in a temperature gradient performed by compression molding machine, in which the temperatures of top and bottom plates were controlled separately.

Further, the technique could be applied as a new fractionation method, since it does not require any solvent.

3.3.2 Molecular weight segregation of LDPE

The molecular weight segregation under temperature gradient is applied to LDPE. The gap between the top and bottom plates of the compression-molding machine was controlled to be 1.5 mm. The temperature of compression-molding machine was set to be 250 ^{o}C at the top and 150 ^{o}C at the bottom. The annealing time was 2 hrs.

Figure 3-6 shows the master curves of frequency dependence of oscillatory shear moduli for t-LDPE, a-LDPE-1 and a-LDPE-2. The reference temperature is 130 °C. The master curves in Figure 3-6 are obtained by a simple horizontal shift without a vertical one. As seen in the figure, *G"* of t-LDPE is slightly higher than that of a-LDPE-1 in the measured region of frequency, whereas a-LDPE-2 shows lower moduli. The result suggests that the molecular weights of t-LDPE and a-LDPE-1 are close to each other, whereas they are higher than that of a-LDPE-2. Yamaguchi and Takahashi[7] employed the same samples with t-LDPE and a-LDPE-1 and suggested that a-LDPE-1 has broader distribution of relaxation times from the crossover point of *G'* and *G"*. The η_0 of t-LDPE, a-LDPE-1 and a-LDPE-2 are 132000, 79600 and 20500 Pa s, respectively.

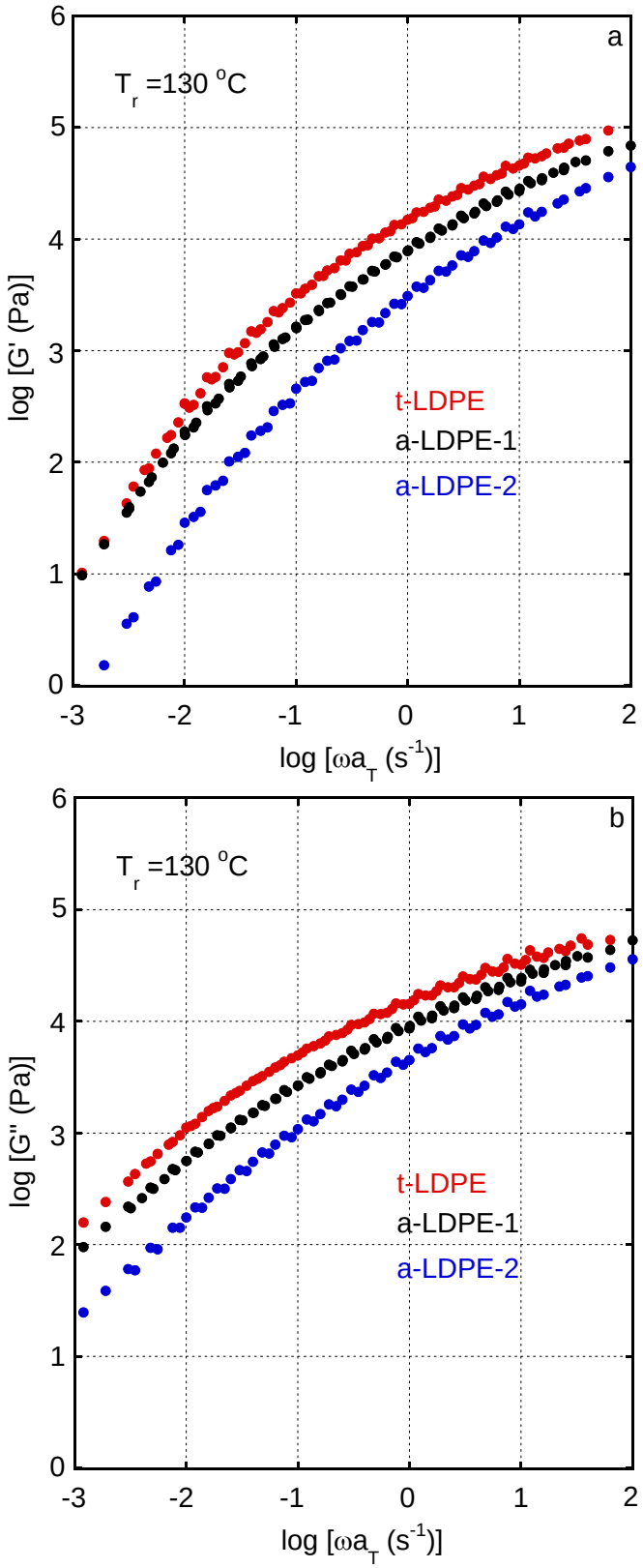

Figure 3-6. Master curves of frequency dependence of (a) shear storage modulus *G'* and (b) loss modulus *G"* at 130 ºC for the virgin sample: (red) t-LDPE, (black) a-LDPE-1 and (blue) a-LDPE-2.

Figure 3-7 shows the oscillatory shear moduli for the samples obtained from each surface of the sheet annealed at 250 °C at the top and 150 °C at the bottom for 2 hrs. As seen in the figure, both moduli for the samples collected from the top surface controlled at the high temperature are lower than those of the samples before annealing in the wide range of frequency, whereas the samples from the bottom surface at low temperature exhibit higher moduli than their references. Further, the slopes of *G'* and *G"* for the top and bottom surfaces are almost similar to those of the virgin sample, indicating that distribution of relaxation time of both samples are not so different.

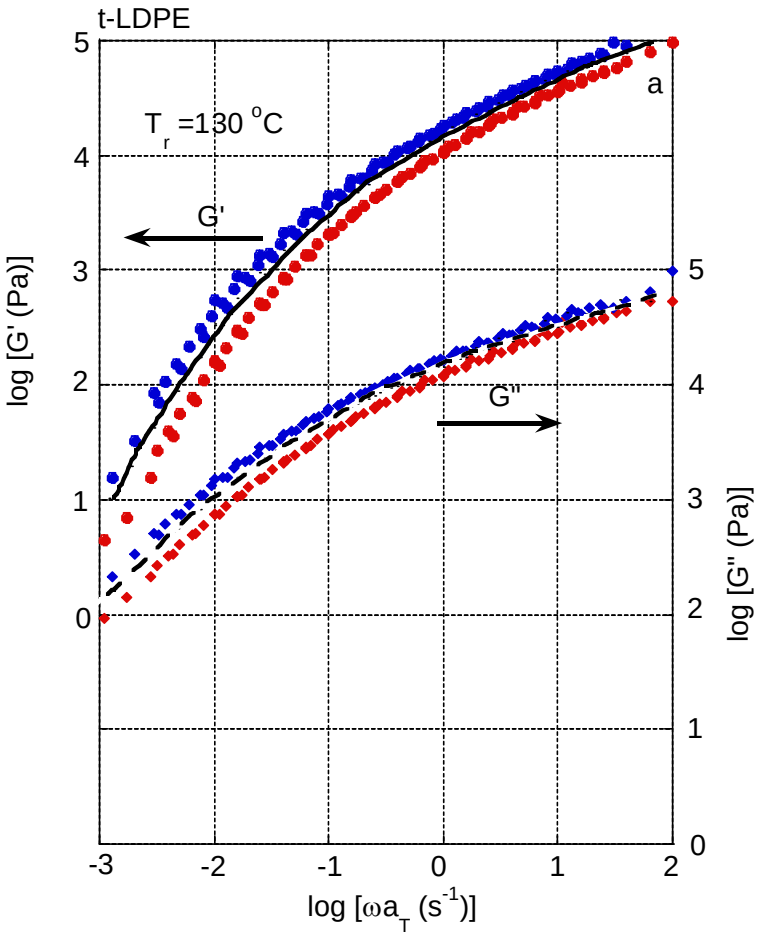

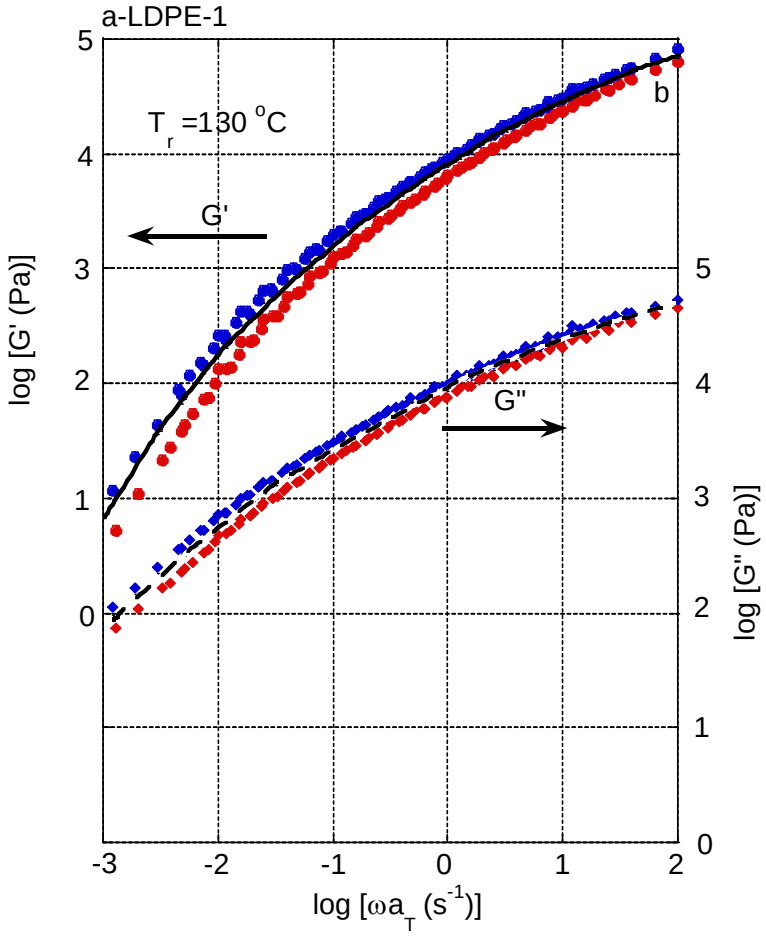
a-LDPE-1
T r =130 °C
b
G'
G"
log [G' (Pa)]
log [G" (Pa)]
log [ωa T (s-1)]
5
4
3
2
1
0
-3
-2
-1
0
1
2

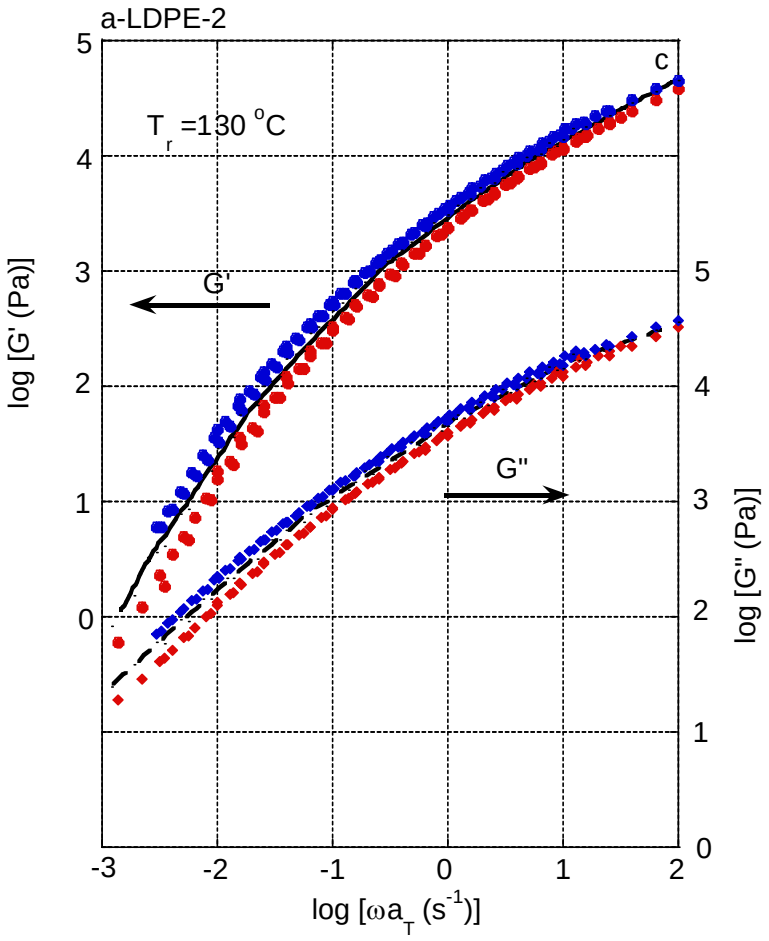

Figure 3-7. Master curves of frequency dependence of (circles) shear storage modulus *G'* and (diamonds) loss modulus *G"* at 130 ºC for (a) t-LDPE, (b) a-LDPE-1and (c) a-LDPE-2; The master curves of surface parts of the samples after annealing at the condition of (top) 250 ºC / (bottom) 150 ºC for 2 hrs are also plotted; (blue circles) low temperature side and (red circles) high temperature side. The (solid line) *G'* and (dashed line) *G"* of the virgin sample are also plotted.

The apparent flow activation energy E_a is calculated at the same level of the loss modulus *G"* using an Arrhenius-type equation, as shown in Figure 3-8. As seen in the figure, E_a increases with decreasing *G"*, demonstrating the thermo-rheologically complexity. The high value at low modulus is attributed to the high E_a of the relaxation process associated with LCB. As seen in the figure, E_a for the samples collected from the

bottom surface is higher than that of the top one for all samples. The result suggests that the branch structure of high molecular weight fraction is well-developed than the low molecular weight one.

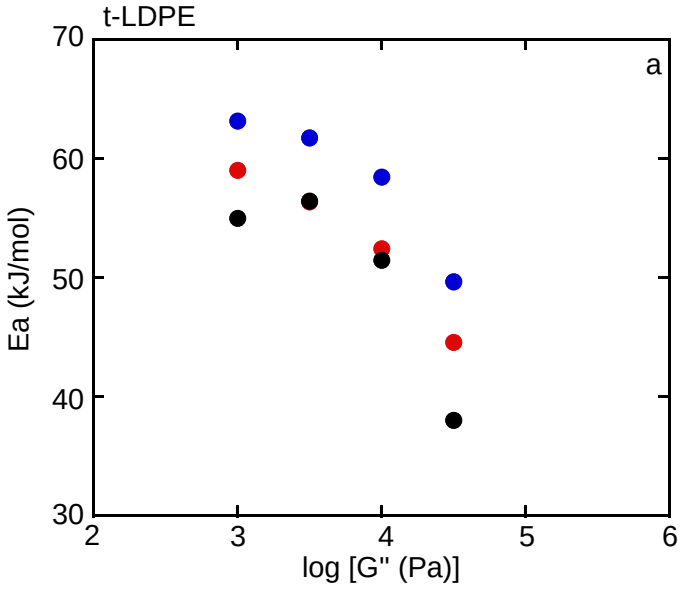

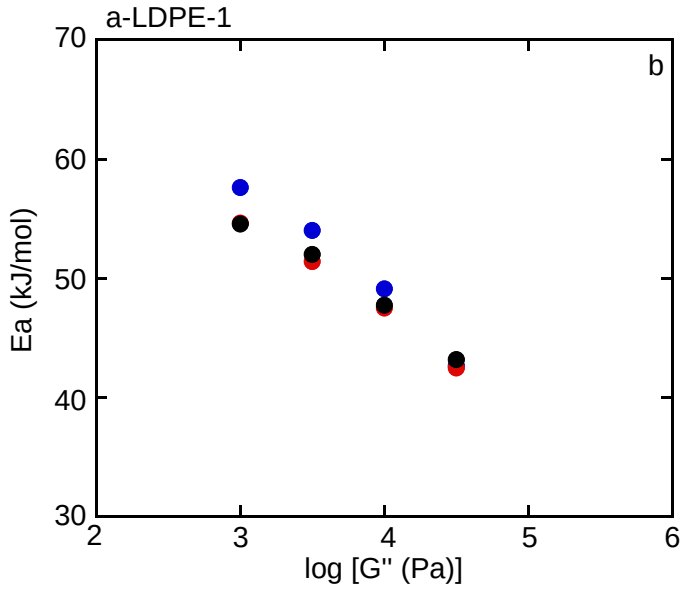

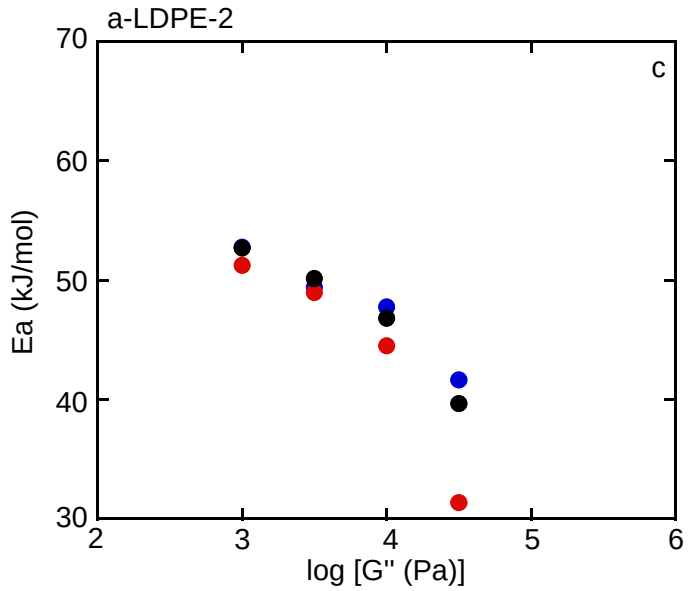

Figure 3-8 Relation between shear loss modulus *G"* and flow activation energy E_a for (a) t-LDPE, (b) a-LDPE-1 and (c) a-LDPE-2; (black circles) the sample before annealing, (blue circles) the samples collected from bottom surface and (red circles) the samples collected from top surface

In the van Gurp-Palmen plot, all data are on at the same curve. The result indicates that the relaxation time distribution is not changed by the fractionation, which corresponds to unchanged slopes of oscillatory shear modulus of the fractionated samples. Further, the lower δ values of two types of a-LDPE suggest the broader relaxation time distribution due to well-developed branch structure in autoclave LDPE.

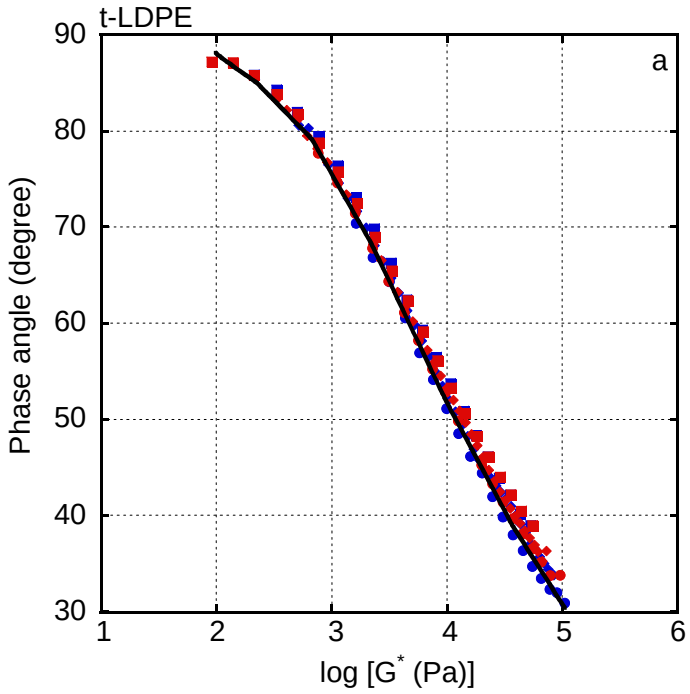
t-LDPE
a
Phase angle (degree)
log [G* (Pa)]
90
80
70
60
50
40
30
1
2
3
4
5
6

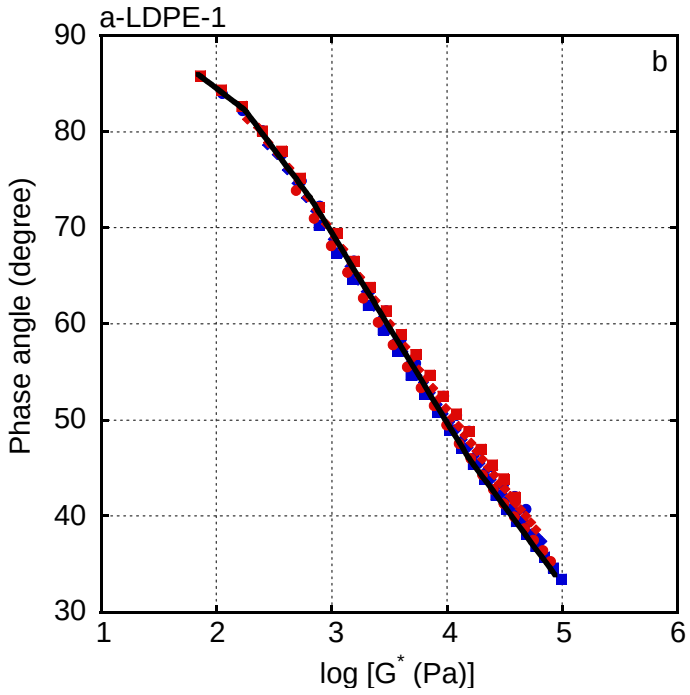
a-LDPE-1
b
Phase angle (degree)
log [G* (Pa)]
90
80
70
60
50
40
30
1
2
3
4
5
6

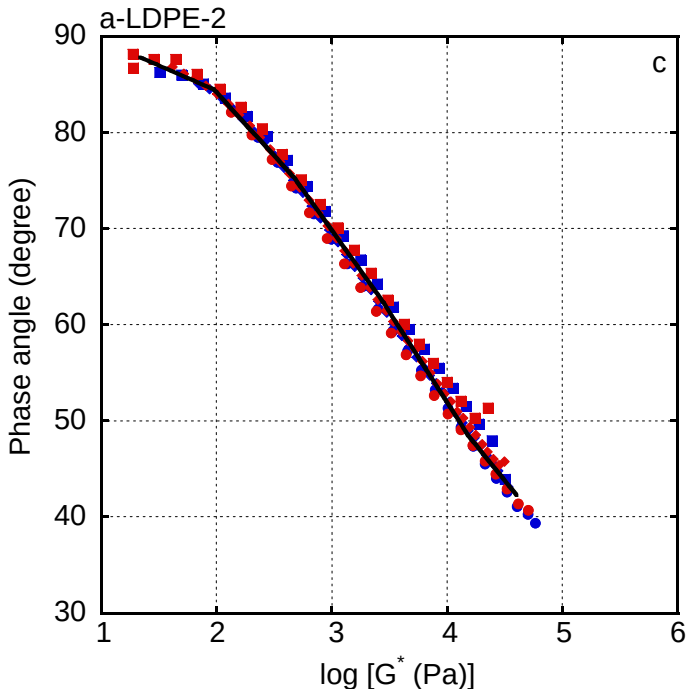

Figure 3-9 van Gurp-Palmen plots for (solid line) the samples prior to annealing, , (blue symbols) the samples collected from bottom surface and (red symbols) the samples collected from top surface at (circles)130, (diamonds) 160 and (squares) 190 °C; (a) t-LDPE, (b) a-LDPE-1 and (c) a-LDPE-2

Extrusion properties are evaluated by the capillary rheometer at 190 °C. The photographs of the extruded strands are shown in Figure 3-10. It is well known that the gross melt fracture is a flow instability occurred at die entrance, which is prominent for a polymer melt with high melt elasticity, such as LDPE.[27,28]

In the case of t-LDPE and a-LDPE-1, the onset shear rate of gross melt fracture for the samples collected from the bottom surface (138 s^{-1} for t-LDPE, 277 s^{-1} for a-LDPE-1) is lower than the samples collected from the top surface (277 s^{-1} for t-LDPE, 561 s^{-1} for a-LDPE-1) and the virgin sample (277 s^{-1} for t-LDPE, 561 s^{-1} for a-LDPE-1). The result suggests that the level of elongational stress of the samples collected from the bottom

surface is higher than that of the top and virgin ones. Moreover, the level of apparent shear stress for the samples collected from the bottom surface is the highest, whereas that of the virgin sample is between those of fractionated samples. This phenomenon corresponds to the oscillatory moduli.

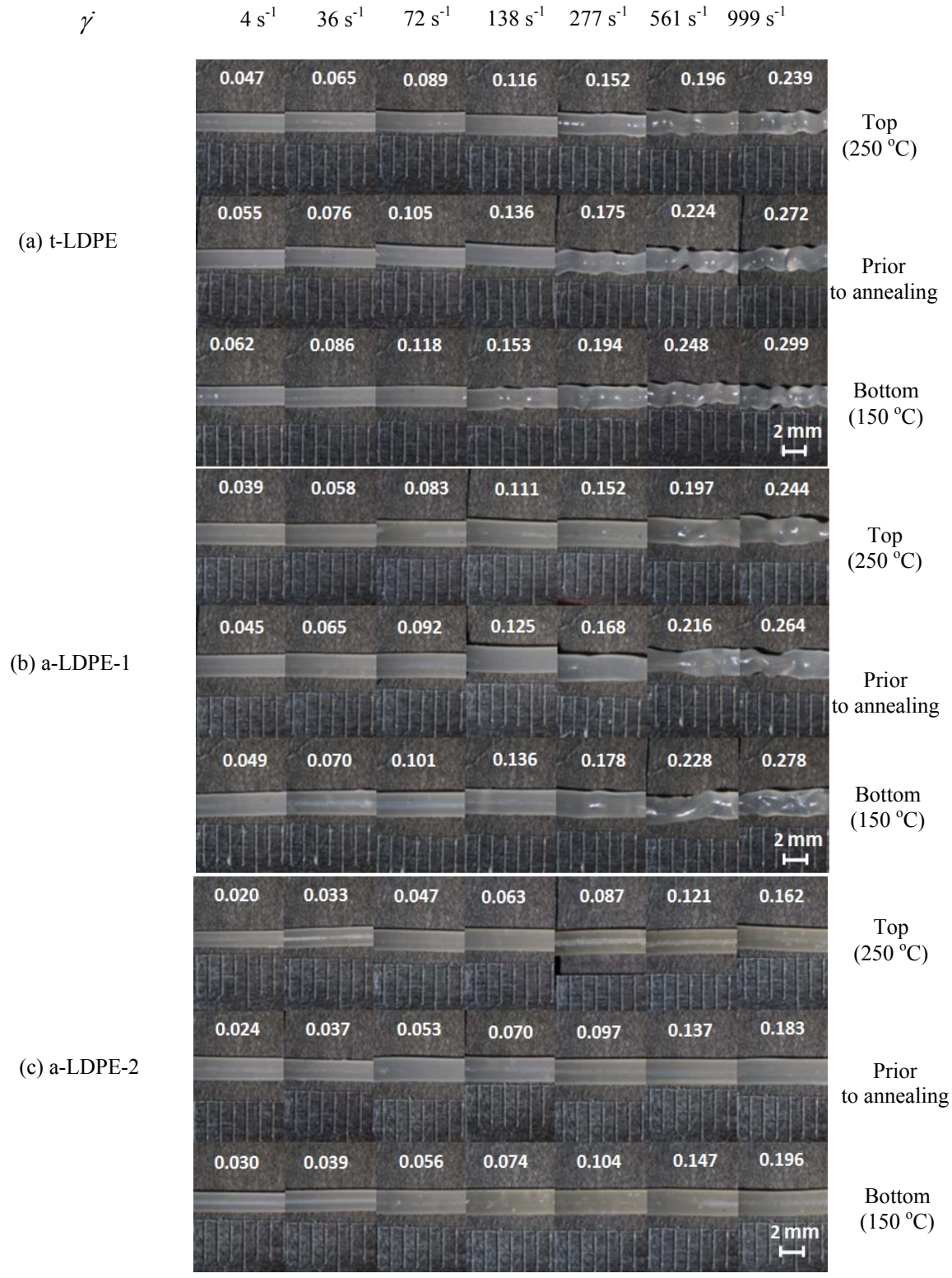

Figure 3-10. Optical photographs of extruded strands at 190 °C through a circle die with L/D = 10/1 (mm): (a) t-LDPE, (b) a-LDPE-1 and (c) a-LDPE-2. The numerals in the figure represent apparent shear stress (MPa).

The drawdown force, *i.e.*, the force required to stretch a strand,[23,29] is evaluated at draw ratio of 9.2, as shown in Figure 3-11. The drawdown force of the samples collected from the top surface is lower than that of the samples from the bottom. Further, the drawdown force of the virgin sample is between those of the fractionated samples. The result suggests that the high molecular weight fraction is localized at the bottom surface and vice versa. This result confirms that the molecular weight fractionation takes place during annealing procedure irrespective of the type of LDPE.

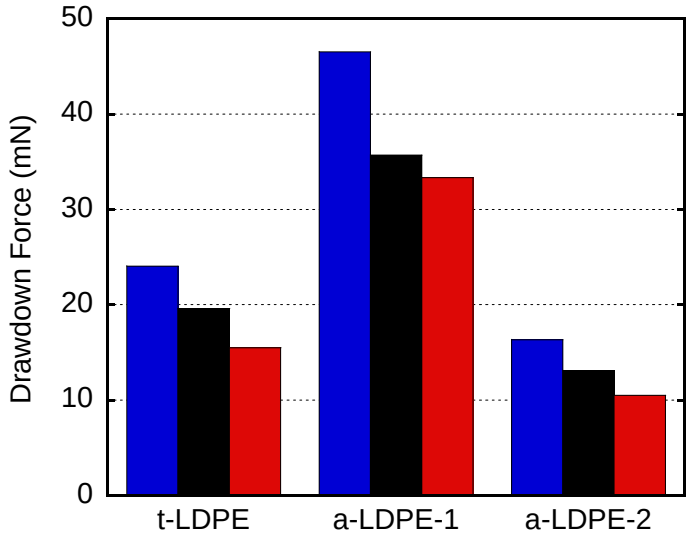

Figure 3-11. Drawdown force at 190 °C for t-LDPE, a-LDPE-1 and a-LDPE-2 annealed at temperature conditions of (top) 250 ^{o}C /(bottom) 150 ^{o}C for 2 hrs; (black) prior to annealing and annealed samples collected from (blue) bottom surface and (red) top surface. The shear rate at the die wall is 21.9 s^{-1}.

In order to characterize the branch structure in the fractionated LDPE, the elongational viscosity is measured. Figure 3-12 shows the growth curves of uniaxial elongational viscosity at 160 ^{o}C for all samples. The solid line in the figure represents

three times of the growth curve of shear viscosity in the linear region $3\eta^+$, which is calculated by the approximate equation proposed by Osaki *et al.* [30]

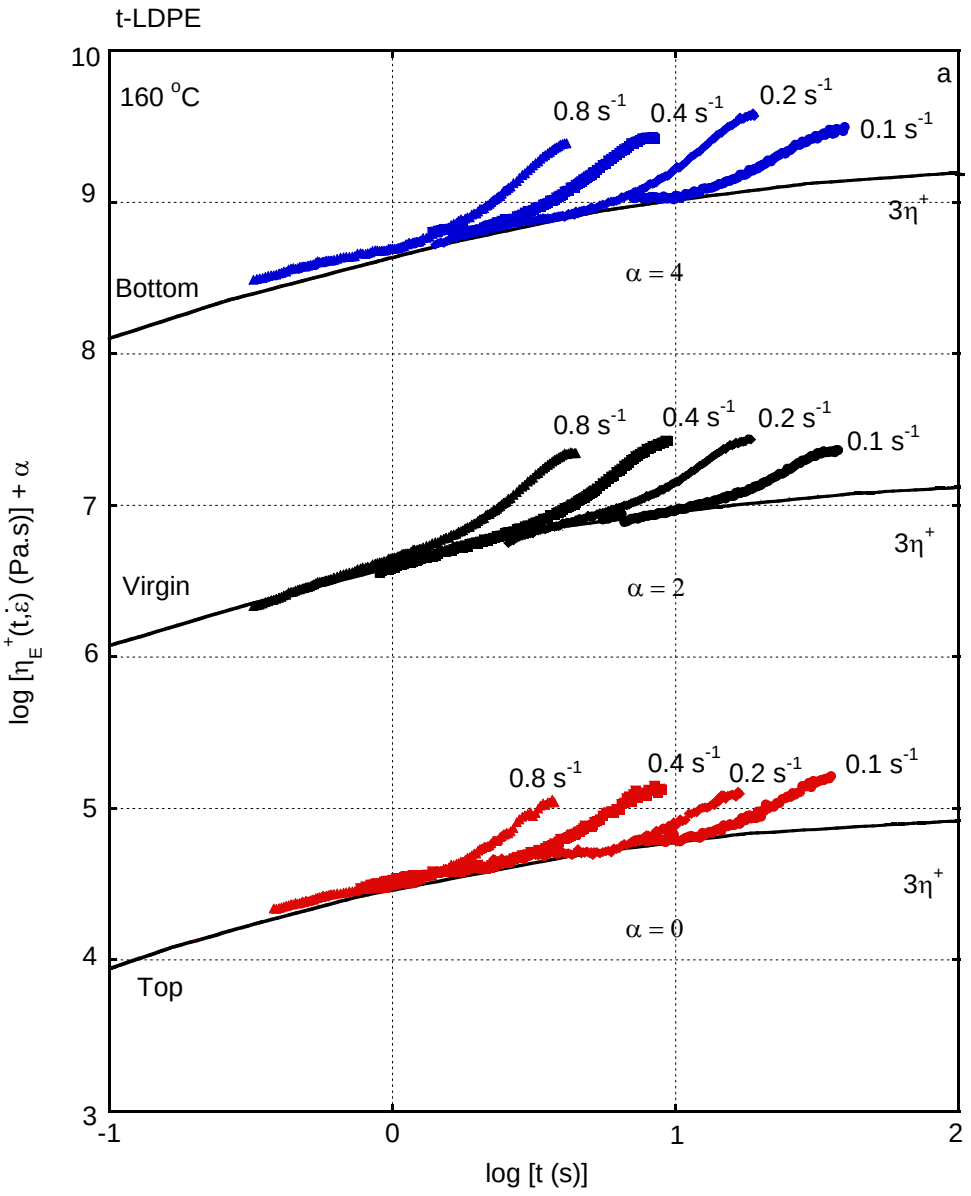

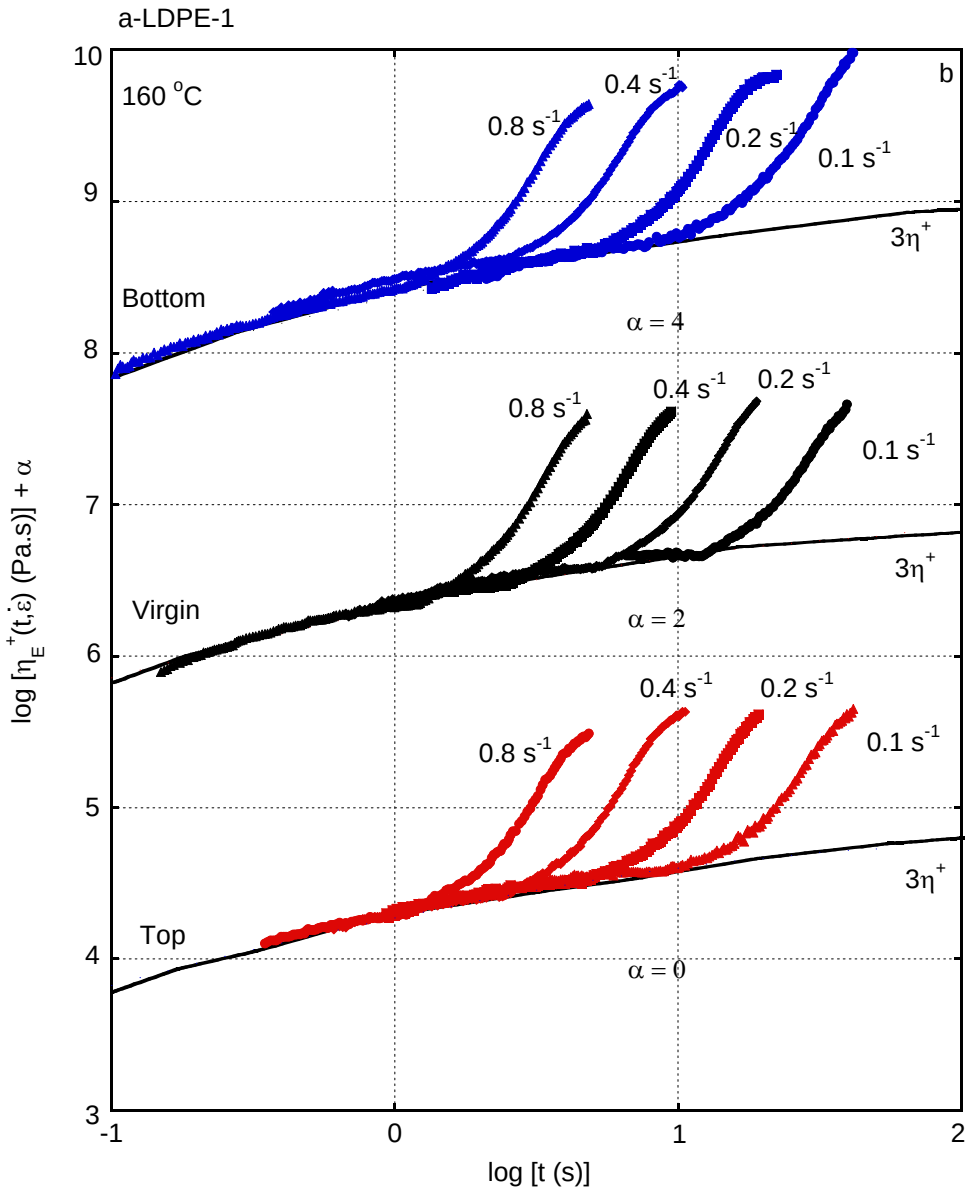
a-LDPE-1
160 °C
b
0.8 s-1
0.4 s-1
0.2 s-1
0.1 s-1
3η+
Bottom
α = 4
Virgin
α = 2
Top
α = 0
log [η+E(t,ε̇) (Pa.s)] + α
log [t (s)]
10
9
8
7
6
5
4
3
-1
0
1
2

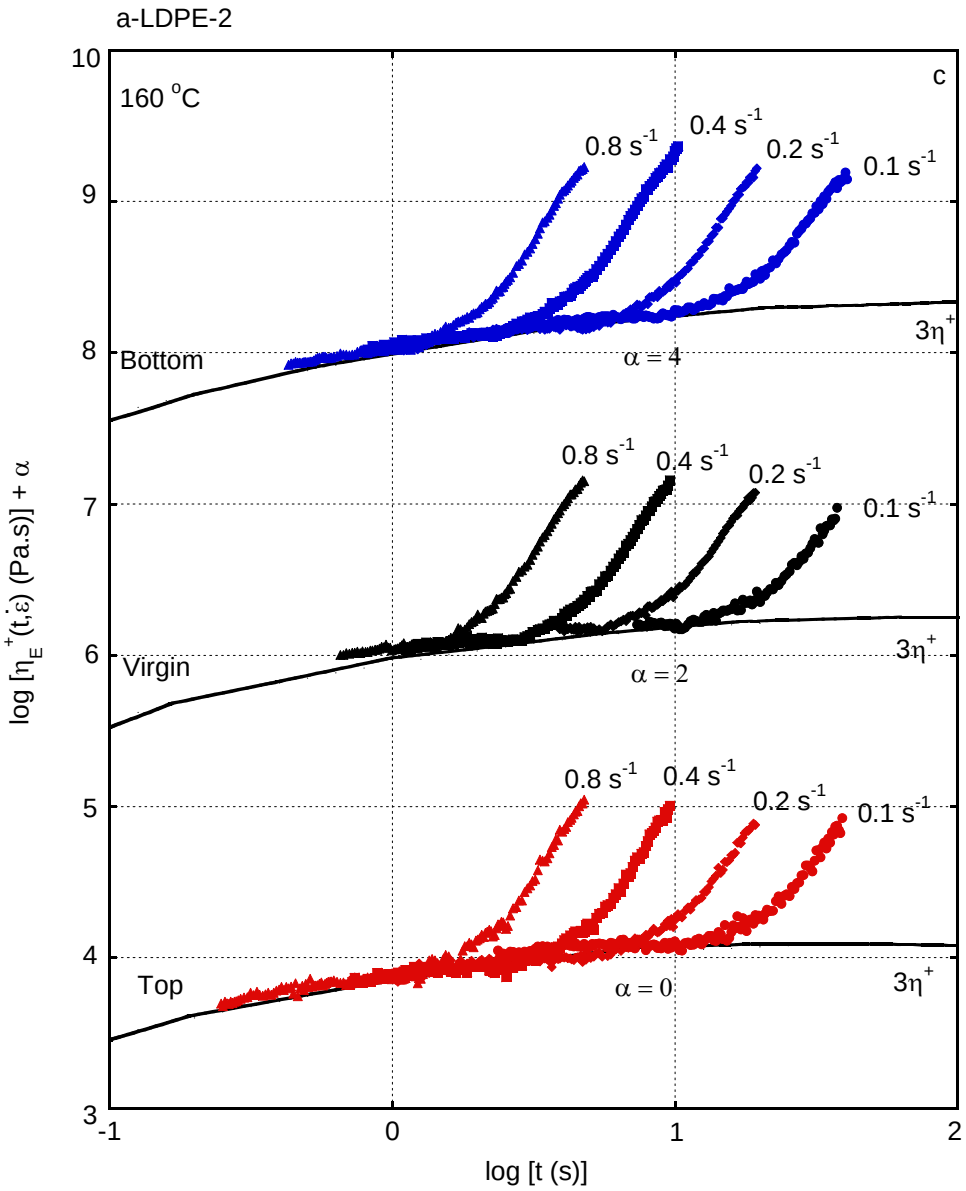

Figure 3-12. Growth curves of uniaxial elongational viscosity $\eta_E^+(t,\dot{\varepsilon})$ at 160 °C for (a) t-LDPE, (b) a-LDEP-1 and (c) a-LDPE-2; (black symbols) the virgin sample samples, (blue symbols) the samples collected from bottom surface and (red symbols) the samples collected from top surface; (circles) 0.1 s^{-1}, (squares) 0.2 s^{-1}, (diamonds) 0.4 s^{-1} and (triangles) 0.8 s^{-1}. The solid line denotes the growth curve of elongational viscosity at a low strain rate asymptote $3\eta^+(t)$.

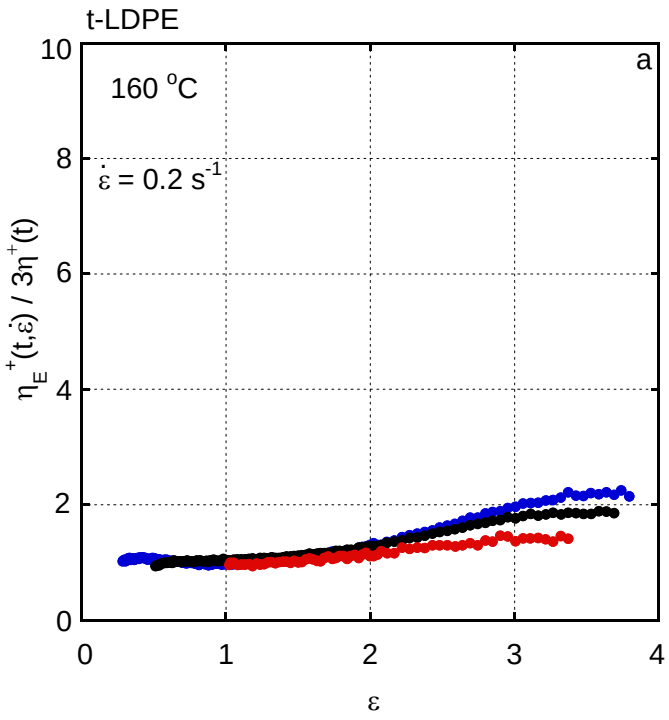
t-LDPE
a
160 °C
$\dot{\varepsilon}$ = 0.2 s^{-1}
$\eta_E^+(t,\dot{\varepsilon})$ / 3$\eta^+(t)$
ε
0
2
4
6
8
10
0
1
2
3
4

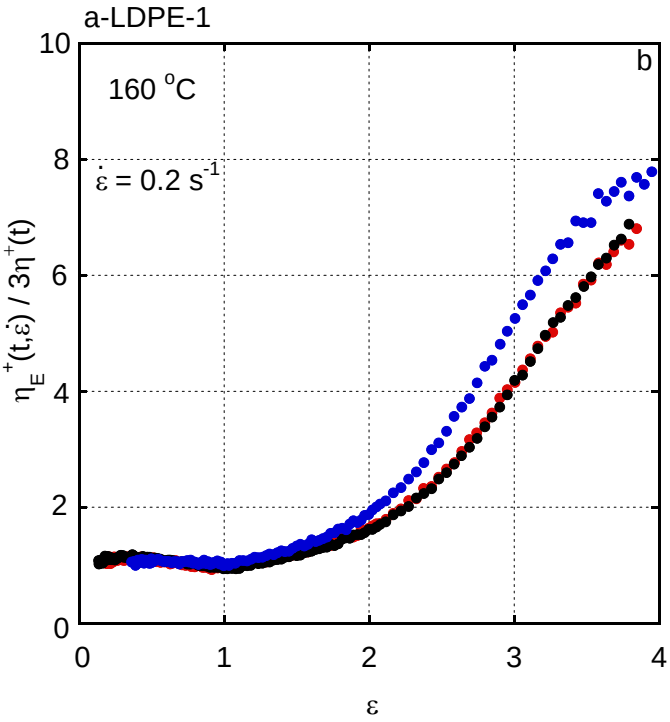
a-LDPE-1
b
160 °C
$\dot{\varepsilon}$ = 0.2 s^{-1}
$\eta_E^+(t,\dot{\varepsilon})$ / 3$\eta^+(t)$
ε
0
2
4
6
8
10
0
1
2
3
4

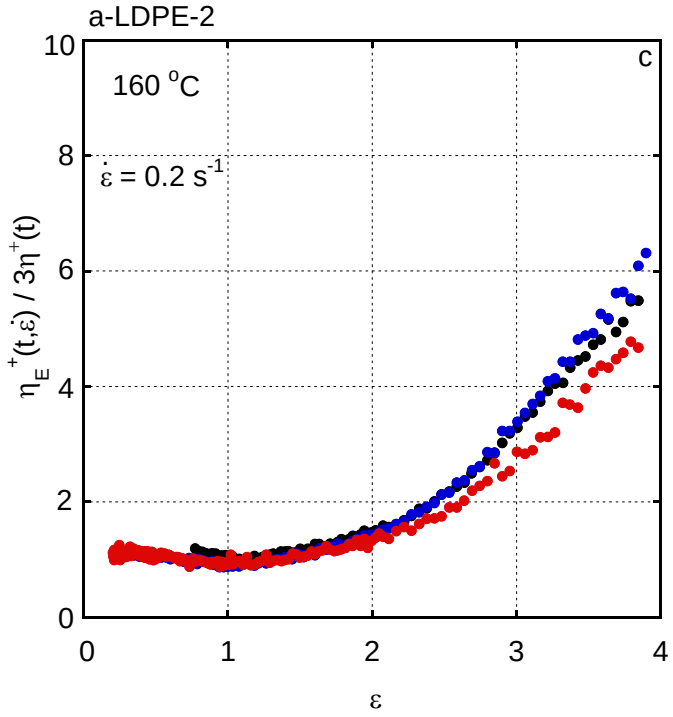

Figure 3-13 Ratio of uniaxial elongational viscosity $\eta_E^+(t,\dot{\varepsilon})$ to that at the low strain rate asymptote $3\eta^+(t)$ as a function of elongational strain ε at a strain rate $\dot{\varepsilon}$ of 0.2 s^{-1} for (a) t-LDPE, (b) a-LDEP-1 and (c) a-LDPE-2; (black) the sample prior to annealing, (blue) samples collected from the bottom surface and (red) samples collected top surface.

For the fractionated samples, the bottom one shows a steep curve of $3\eta^+$ and more pronounced strain hardening than the top one, irrespective of the type of LDPE, as seen in Figure 3-13. This feature is responsible for the large drawdown force for the bottom one. Moreover, the strain hardening behavior is also detected at smaller strains compared to that of the top one.

According to linear viscoelastic properties, high molecular weight fraction is localized at the bottom surface. Meanwhile, the elongational viscosity suggests the well-developed branch structure of the fractionated samples collected from the bottom surface,

as seen in the marked strain hardening. The result corresponds to result from the dilute solution properties of LDPE reported by Kuhn and Kromer.[6]

According to Kuhn and Kromer,[6] it is found that the ratios of average number of LCB/MW and average number of SCB/ MW, which can express the absolute amount of branched chains in each fractionated sample, decrease with MW. In another words, the amount of chain end, which is proportional to the amount of branched chains, in the low molecular weight fraction is higher as seen in Table 3-4.

It is found that the calculated ratios correspond with the results presented in this study. It is reasonable because the fractionation behavior is affected by free volume as explained in the first section. Therefore, the high molecular weight fraction having lower amount of chain end is segregated at the low temperature side and vice versa, irrespective of the type of LDPE.

Table 3-3 The ratio of average number of LCB/MW and average number of SCB/MW calculated from the results of autoclave LDPE and tubular LDPE reported by Kuhn and Kromer[6]

MW	average number of LCB/MW		average number of SCB/MW	
	autoclave	tubular	autoclave	tubular
$1x10^6$	0.000090	0.000023	0.00110	0.00090
$5x10^5$	0.000096	0.000026	0.00114	0.00100
$2x10^5$	0.000100	0.000035	0.00120	0.00110
$1x10^5$	0.000100	0.000050	0.00120	0.00120
$1x10^4$	0.000100	0.000200	0.00120	0.00170

Finally, recovery curves of the shear storage modulus from the shear-modified state were evaluated to discuss the branch structure. The details of this experiment were explained in Chapter 2.[24,29] The branch structure can be predicted from the recovery curves,[31,32] because a longer branch will need a longer recovery time to return its equilibrium state.

Figure 3-14 shows the recovery curves of *G'* and its normalized values, *i.e.*, *G'*(*t*)/*G'*(*t*=0), after removal of the shear stress at 24.5 kPa. As seen in the figure, *G'* increases with the residence time in the rheometer for all samples. The bottom samples (low temperature side) require a longer time to recover to their plateau values than the top ones. Because the recovery time is closely related to the length of long-chain branches,[31,32] the result suggests that the samples at low temperature side are composed of high molecular weight fraction with longer branches.

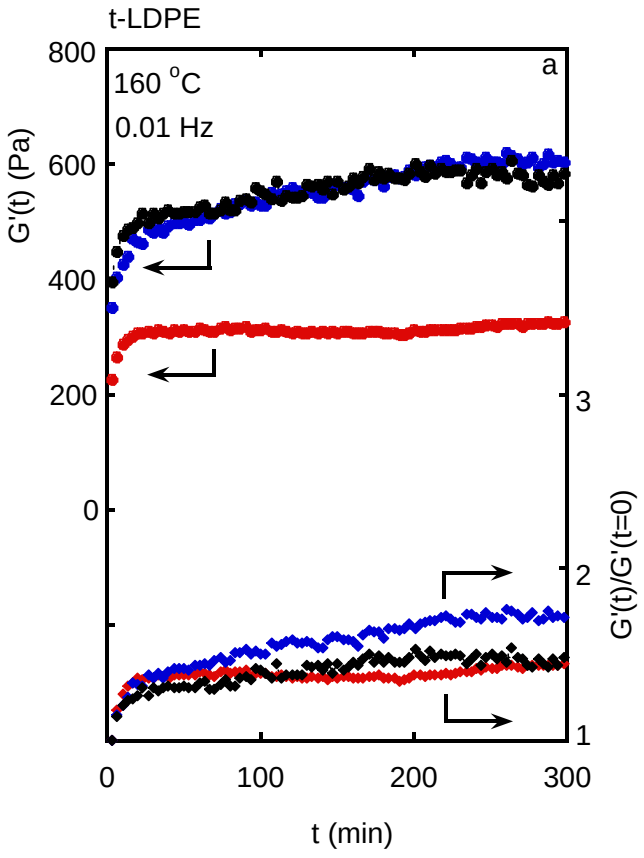

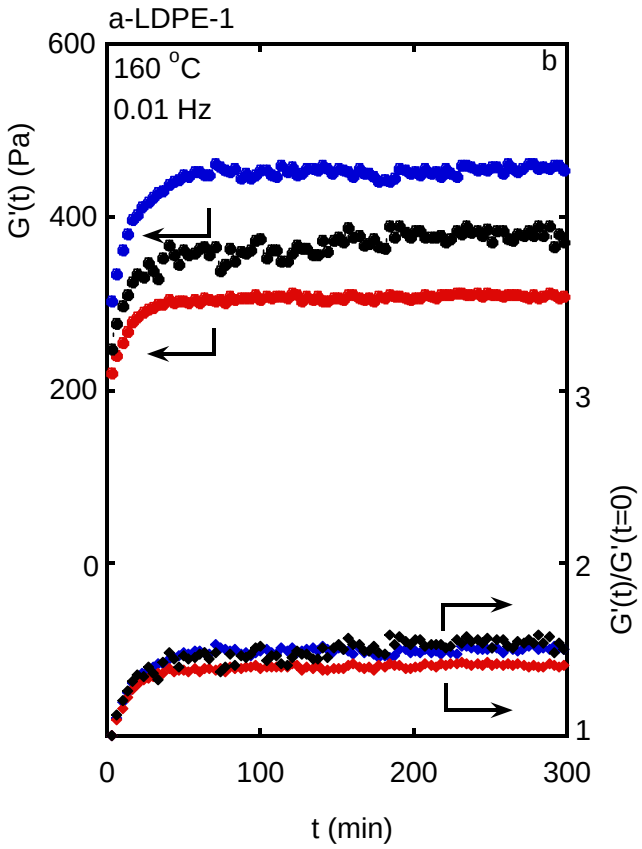
a-LDPE-1
160 °C
0.01 Hz
b
G'(t) (Pa)
G'(t)/G'(t=0)
600
400
200
0
3
2
1
0
100
200
300
t (min)

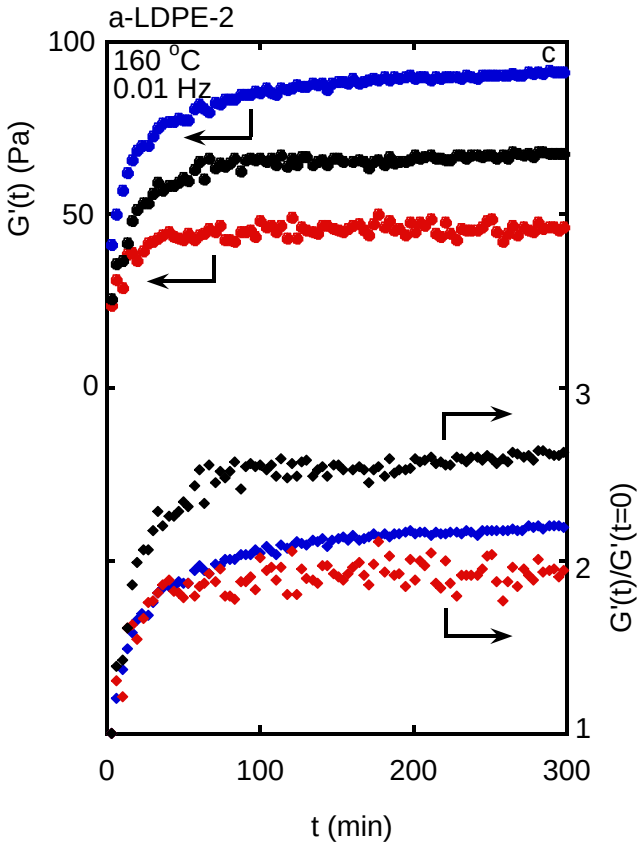

Figure 3-14 Time dependence of (circles) shear storage modulus *G'* and (diamonds) its normalized values *G'*(*t*)/*G'*(*t*=0) at 0.01 Hz after the removal of shear stress (24.5 kPa for 30 min) at 160 °C; (black symbols) the sample prior to annealing, (blue symbols) annealed samples collected from the bottom surface and (red symbols) samples collected top surface for (a) t-LDPE, (b) a-LDEP-1 and (c) a-LDPE-2

Moreover, it is found that the MWD of fractionated samples also suggests the segregation behavior. Even thought, the shape of the MWD curves for both fractionated samples are almost similar, the curve of the sample collected from the top surface is higher than that of the one collected from the bottom surface at low molecular weight region. Meanwhile, at high molecular weight region, the MWD of sample collected from the bottom surface is higher, as seen in Figure 3-15. It supports that the high molecular weight fraction is localized at surface attached to the low temperature plate of the compression molding machine.

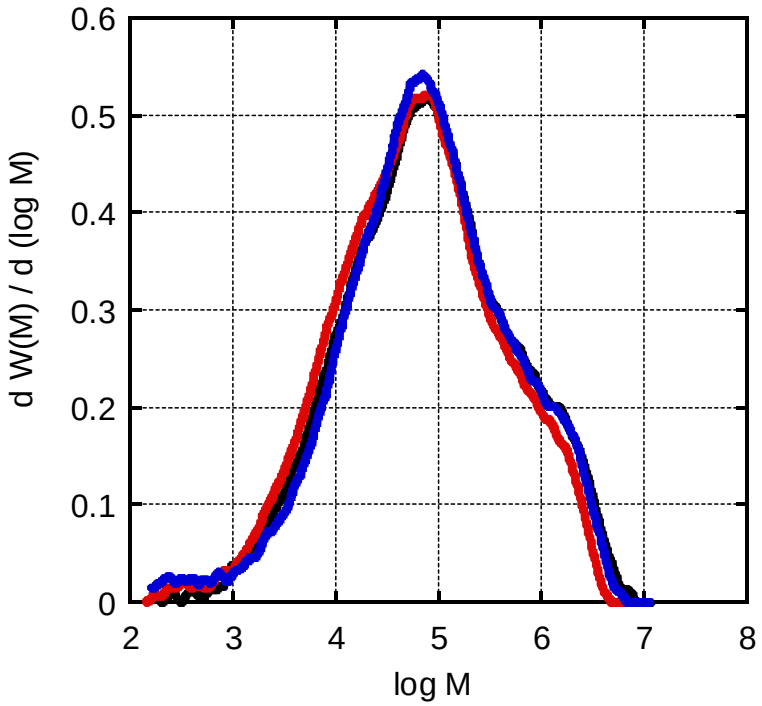

Figure 3-15. Molecular weight distribution (MWD) as a function of molecular weight for (black line) LDPE prior to annealing, and annealed LDPE collected from (blue line) the bottom surface and (red line) the top surface.

In a dilute solution, the shrinking factor *g'* is defined as the ratio of intrinsic viscosity $[\eta]$ of a branched polymer to that of a linear polymer with the same molecular weight. Similarly, another shrinking factor g is defined by the ratio of the mean square radius of gyration $\langle R^2 \rangle$ of branched and linear polymer having the same molecular weight. [33,34] Unfortunately, *g' and g"* of the samples collected from both surface of the annealed sheet are similar.

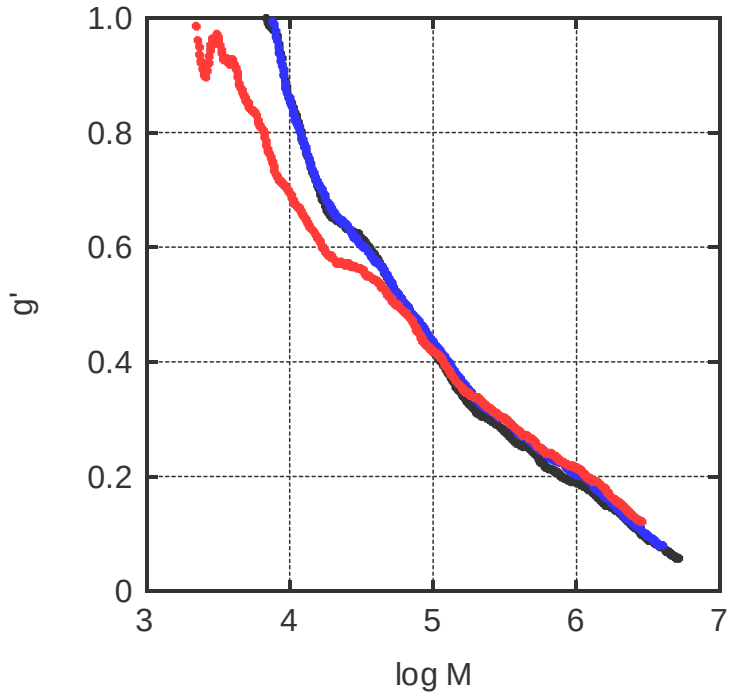

Figure 3-16. Shrinking factor *g'* as a function of molecular weight for (black line) LDPE prior to annealing, and annealed LDPE collected from (blue line) the bottom surface and (red line) the top surface.

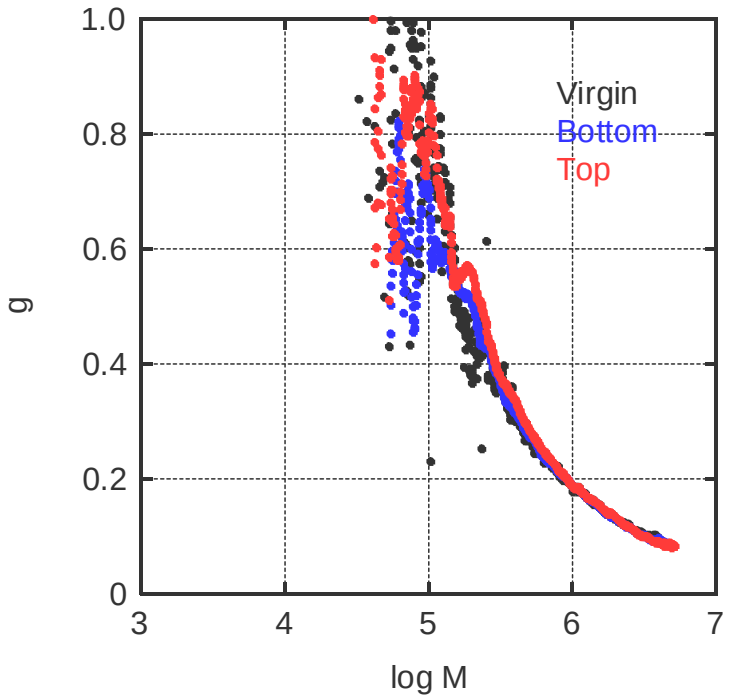

Figure 3-17. Shrinking factor *g* as a function of molecular weight for (black line) LDPE prior to annealing, and annealed LDPE collected from (blue line) the bottom surface and (red line) the top surface.

3.4 Conclusions

It is discovered that the temperature gradient induces the molecular weight segregation of PE in the molten state, which can be explained by the free volume concept which strongly depends on the amount of chain ends. The high molecular weight fraction is localized at the low temperature side and vice versa. The segregated behavior becomes obvious with the annealing time and temperature gradient. Since the method is free from toxic solvent, it could be applicable to a new fractionation method of polymers. Further, the rheological properties of PE can be modified by the molecular weight fractionation under temperature gradient.

References

1. Vega, J. F.; Santamalia, A.; Munoz-Mscalona, A.; Lafuente, P., *Macromolecules*, **1998**, *31*, 3639.
2. Stadler, F. J.; Gabriel, C.; Münstedt, H., *Macromol. Chem. Phys*., **2007**, *208*, 2449.
3. Yamaguchi, M., *Polym. Eng. Sci*., **2006**, *46*, 1284.
4. Mieda, N.; Yamaguchi, M., *Adv. Polym. Technol.*, **2008**, *26*, 173.
5. Garcia-Franco, C. A.; Harrington, B. A.; Lohse, D. J., *Macromolecules*, **2006**, *39*, 2710.
6. Kuhn, R.; Kromer H., *Colloid Polym Sci*, **1982**, *260*, 1083.
7. Yamaguchi, M.; Takahashi, M., *Polymer*, **2001**, *42*, 8663.
8. Tackx, P.; Tack, J. C. J. F., *Polym*., **1998**, *39*, 3109.
9. Wagner, M. H.; Kharendich, S.; Yamaguchi, M., *Rheol. Acta*, **2004**, *44*, 198.
10. Guzman, G. M., *Fractionation of High Polymers*, in *Progress in High Polymers*; Robb, J. C.; Peaker, F. W., Eds.; Academic Press: New York, **1961**, 113.
11. Cantow, M. J. R., *Polymer Fractionation*; Academic Press: New York, **1967**.
12. Tung, L. H., *Fractionation of Synthetic Polymers, Principles and Practices*; Marcel Dekker: New York, **1977**.
13. Billmeyer, F. W., Jr., *Textbook of Polymer Science*, 3rd ed.; John Wiley & Sons: New York, **1984**, 177.
14. McHugh, M.; Krukonis, V., *Supercritical Fluid Extraction – Principles and Practice*, 2nd Ed.; Butterworth Heinemann: Boston, **1994**.
15. Shishikura, A.; Kanamori, K.; Takahashi, H.; Kinbara, H., *J. Agric. Food Chem*., **1994**, *43*, 1993.

16. Coen, E. M.; Quinn, J. F.; Dehghani, F.; Foster, N. R.; Davis, T. P., *Polymer*, **2003**, *44*, 3477.

17. Suwa, J.; Kakiage, M.; Yamanobe, T.; Komoto T.; Uehara, H., *Langmuir*, **2007**, *23*, 5882.

18. Kim, E.; Kramer, E. J.; Garrett, P. D.; Mendelson, A. R.; Wu, W. C., *Polymer* **1995**, *36*, 2427.

19. Tanaka, K.; Takahara, A.; Kajiyama, T., *Macromolecules*, **1997**, *30*, 6626.

20. Keddie, J. L.; Jones, R. A. L.; Coury, R. A., *Europhys. Lett.*, **1994**, *27*, 59.

21. Tanaka, K.; Takahara, A.; Kajiyama, T., *Acta Polym.* **1995**, *46*, 476.

22. Yamaguchi, M.; Gogos, C. G., *Adv. Polym. Technol.*, **2001**, *20*, 261.

23. Ono, K.; Yamaguchi, M., *J. Japan Soc. Polym. Process.*, **2009**, *21*, 745.

24. Bernnat, A., *Polymer Melt Rheology and the Rheotens Test*, Ph.D. Thesis, University of Stuttgart, Stuttgart, Germany, **2001**.

25. Ferry, J. D., *Viscoelastic Properties of Polymers*; Wiley: New York, **1980**.

26. Garcia-Franco, C. A.; Harrington, B. A.; Lohse, D. J., *Macromolecules*, **2006**, *39*, 2710.

27. Cogswell, F. N., *Polymer Melt Rheology*; George Godwin: London, **1981**.

28. Kulikov, O., *J. Vinyl. Additive Technol.*, **2005**, *11*, 127.

29. Yamaguchi, M.; Todd, D. B.; Gogos, C. G., *Adv. Polym. Tech.*, **2003**, *22*, 179.

30. Osaki K.; Murai, A.; Bessho, N.; Kim, B. S., *J. Soc. Rheol. Jpn.*, **1976**, *4*, 166.

31. Yamaguchi, M., *Rheological Properties of Molten Polyolefins* In *Structure and Properties of Pol Olefin Material* ; Transworld Research Network: Kerela, **2012**.

32. Mieda, N., *Effect of long-chain branches on non-linear rheological properties for polyethylene*, Ph.D. Thesis, Japan Advanced Institute of Science and Technology, Japan, **2011**.

33. Zimm, B. H.; Stockmayer, W. H., *J. Chem. Phys.*, **1949**, *17*, 1301.

34. Zimm, B. H.; Kilb, R. W., *J. Polym. Sci.*, **1959**, *37*, 19.

Chapter 4

General Conclusions

PE is available for various polymer processing operations because of its widest variety of molecular structure, such as short- and/or long-chain branches and molecular weight distribution. The variety of chain architectures greatly affects the rheological behavior. Therefore, the study on rheological properties of PE is very impotent. Furthermore, several techniques have been proposed to control the rheological properties for PE, such as shear history, thermal history, and addition of specific processing aids. These have a strong impact on the elongational viscosity which is believed to be one of the most important rheological properties at polymer processing. In this study, several rheological modification techniques by applying thermal history were proposed to control the rheological properties of PE.

The effects of cross-linking reaction with/without the peroxide compound, *i.e.*, α,α'–di(*t*-butylperoxy)diiso-propylbenzene, on the rheological properties of LDPE/LLDPE blends were discussed in Chapter 2. Firstly, the processing history without the peroxide compound was applied at 280 ^{o}C to LDPE and LLDPE. At this temperature, cross-linking reaction occurs more frequently than chain scission. The cross-linking reaction leads to a small amount of X-type branches, which greatly affects the rheological properties. The time-temperature superposition principle is not applicable to the thermally

modified LLDPE because of the appearance of LCBs. In the case of LDPE/LLDPE blends, the upward deviation of the drawdown force from the linear additive rule is pronounced with marked strain hardening in elongational viscosity when the cross-linking reaction slightly occurs. This situation happens at high-temperature-mixing without a peroxide compound. It suggests that the intermolecular cross-linking reaction occurs between LDPE and LLDPE, which provides more than two branch points in a chain, during processing history at high temperature.

The cross-linking efficiency is greatly enhanced by the addition of the peroxide compound. Further, it is found that the addition of the peroxide compound during cross-linking reaction differently affects the cross-linking behaviors of LDPE and LLDPE under flow field. The phenomenon is explained by the ratio of intermolecular/intramolecular reactions under flow field. In the case of LDPE, the intramolecular cross-linking reaction is predominant. Once the intramolecular cross-linking occurs, the gyration radius of chain decreases. Consequently, the possibility of intramolecular cross-linking is enhanced. Meanwhile, the applied flow field leads to intermolecular cross-linking reaction rather than intramolecular cross-linking one for LLDPE. Moreover, the degree of cross-linking in LLDPE is higher than that in LDPE because of its large amount of tertiary carbon atoms. Furthermore, it is found that the synergistic effect for the LDPE/LLDPE blends becomes weak by cross-linking reaction. The cross-linking reaction with the peroxide compound leads to the generation of permanent network which restricts the simple reptation motion of whole chains. Consequently, reptation of a branched molecule is less important.

The rheological modification of PE by annealing procedure under temperature gradient was studied in Chapter 3. The applied thermal history in a compression-molding

machine, in which the temperature of one mold is higher than the other, leads to molecular weight segregation of PE in the molten state. The high-molecular-weight fraction is localized at the surface attached to the mold with low temperature and vice versa. The segregated behavior becomes obvious with the annealing time and temperature gradient. In addition, the rheological properties can be modified by the molecular weight fractionation.

In this research, several techniques were proposed to control the rheological properties by thermal history. For the first study, the elongational viscosity of LDPE/LLDPE blends is enhanced by thermal modification with/without peroxide compound. Even though, the study was not carried out at actual polymer processing, the enhanced elongational viscosity is responsible for reduction of neck-in in an extruded film at T-die extrusion process. The second study suggests that the molecular weight fractionation of PE takes place by thermal history during annealing procedure under temperature gradient. The method could be applied as fractionation and rheological modification method, although more characterization should be carried out quantitatively. In addition, the study revealed the rheological properties of fractionated LDPE. These could be used as information to understand the structure of LDPE. The study also demonstrated the potential of thermal history to the rheological properties of PE. The finding has to be reviewed quantitatively to control the rheological propertied more precisely, which will affect the processability to a great extent in actual polymer processing.

Achievements

Publications

1. **Monchai Siriprumpoonthum,** Naoya Mieda, Shogo Nobukawa, Masayuki Yamaguchi Segregation Behavior of Polyethylene with Broad Molecular Weight Distribution by Annealing Procedure in Temperature Gradient, *J. Polym. Res.*, **2011**, *18*, 2449-2453.

2. **Monchai Siriprumpoonthum**, Naoya Mieda, Vu Anh Doan, Shogo Nobukawa, Masayuki Yamaguchi
   Effect of Shear History on Flow Instability at Capillary Extrusion for Long-Chain Branched Polyethylene, *J. Appl. Polym. Sci.*, **2012**, *124*, 429-435.

3. **Monchai Siriprumpoonthum,** Shogo Nobukawa, Yasuo Satoh, Hiroko Sasaki, Masayuki Yamaguchi
   Effect of Thermal Modification on Rheological Properties of Polyethylene Blends, *J. Rheol.*, **2014**, *58*, 449-465.

4. **Monchai Siriprumpoonthum,** Shogo Nobukawa, Masayuki Yamaguchi
   Rheological Modification of Low-density Polyethylene by Segregation Behavior in Temperature Gradient (to be submitted)

Presentations

International Conferences

Reviewed

1. **Monchai Siriprumpoonthum**, Naoya Mieda, Vu Anh Doan, Shogo Nobukawa, Masayuki Yamaguchi Effect of Shear History on Flow Instability for Long-Chain Branched Polyethylene

Society of Plastics Engineers Annual Technical Conference (*ANTEC2012*), April 2-4, Orlando, Florida, United States of America (*USA*), 2012.

2. **Monchai Siriprumpoonthum**, Shogo Nobukawa, Masayuki Yamaguchi
   Effect of Thermal Modification on the Rheological Properties for Polyethylene Blends
   Eurotec 2013, July 4-5, Lyon, France, 2013.

3. **Monchai Siriprumpoonthum**, Shogo Nobukawa, Masayuki Yamaguchi
   Rheological Properties of Thermally-Modified Polyethylene Blends
   MACRO 2014 and the Chemical Society of Thailand (*CST)*, July 6-11, Chiangmai, Thailand, 2014.

Non-reviewed

1. **Monchai Siriprumpoonthum**, Naoya Mieda, Shogo Nobukawa, Masayuki Yamaguchi
   Effect of Shear History on Flow Instability at Capillary Extrusion for Long-Chain Branched Polyethylene.
   4th International Workshop on Polymer Engineering and Processing and the 5th Seminar of the Research Center for Highly Environmental and Recyclable Polymer, March 15, Ishikawa, Japan, 2012.

2. **Monchai Siriprumpoonthum**, Naoya Mieda, Vu Anh Doan, Shogo Nobukawa, Masayuki Yamaguchi
   Effect of Shear History on Flow Instability for Long-Chain Branched Polyethylene
   8th International Colloquium on Heterogeneous Ziegler-Natta Catalysts, March 28, Ishikawa, Japan, 2012.

3. **Monchai Siriprumpoonthum**, Naoya Mieda, Shogo Nobukawa, Masayuki Yamaguchi
   New Fractionation Technique of Polyethylene by Annealing in Temperature Gradient
   8th International Colloquium on Heterogeneous Ziegler-Natta Catalysts, March 28, Ishikawa, Japan, 2012.

4. **Monchai Siriprumpoonthum**, Shogo Nobukawa, Masayuki Yamaguchi
   Effect of Shear History on Flow Instability for Long-Chain Branched Polyethylene
   Asian Workshop on Polymer Processing (*AWPP2012*), August 29-31, Kyoto, Japan, 2012.

5. **Monchai Siriprumpoonthum**, Shogo Nobukawa, Masayuki Yamaguchi
   Effect of Shear History on Flow Instability for Long-Chain Branched Polyethylene
   Annual Meeting of Polymer Processing Society (*PPS28*), December 11-14, Pathaya, Thailand, 2012.

6. **Monchai Siriprumpoonthum**, Shogo Nobukawa, Masayuki Yamaguchi
   Thermal Modification of Rheological Properties for Polyethylene Blends
   International Symposium on Advanced Materials 2013, October 17-18, Japan Advanced Institute Science and Technology (*JAIST*), Nomi, Japan**,** 2013.

Domestic Conferences

Non-reviewed

1. **Monchai Siriprumpoonthum**, Shogo Nobukawa, Masayuki Yamaguchi
   Molecular Weight Fractionation in Temperature Gradient
   62nd SPSJ Annual Meeting, May 29-31, Kyoto, Japan, 2013.

2. **Monchai Siriprumpoonthum**, Shogo Nobugawa, Masayuki Yamaguchi
   Rheological Characterization of Thermally-Modified Polyethylene
   62nd Symosium on Macromolecules (*SPSJ*), September 11-13, Kanazawa, Japan, 2013.

3. **Monchai Siriprumpoonthum**, Shogo Nobugawa, Masayuki Yamaguchi
   Rheological Characterization of Thermally Modified Polyethylene
   61st Rheology symposium, September 25-27, Yamagata, Japan, 2013.

Other Publications

1. Nantanit Wanichacheva, **Monchai Siriprumpoonthum**, Anyanee Kamkaew, Kate Grudpan
   Dual Optical Detection of a Novel Selective Mercury Sensor based on 7-nitrobenzo-2-oxa-1,3-diazolyl Subunits
   Tetrahedron Lett., **2009,** *50*, 1783-1786.

Awards

1. Grant for Researchers Attending International Conferences, JAIST Research Grant for Students to present at Eurotec 2013, Lyon, France, July 2013.

2. Grant for PhD student, Graduate Research Program (GRP), (Employment-type Scholarship) from Japan Advanced Institute of Science and Technology (JAIST), October 2011- September 2014.

Effect of Heating Temperature on Flow Instability at Extrusion for Polyvinyl Chloride

1. Introduction

Polyvinyl chloride (PVC) compounds have been widely used in numerous applications because of their processability, mechanical properties, and relatively low production costs. The final properties in the solid state of the materials depend on the molecular weight of PVC. Moreover the properties of final product also depend on the species and contents of the plasticizer which is added to PVC. Therefore, PVC became an interesting material which could be used for many applications. However, they often show flow instability in extrusion, which limits productivity in processing. The origin and mechanisms of flow instability for various polymers have been discussed for a long time.[1-11] Nevertheless, it is still one of the major problems in the field of polymer processing.

Generally, the flow instabilities are classified into two groups. One is a small-amplitude and high-frequency distortion on the surface of the extrudates, which is usually called “shark skin.” This phenomenon results in the dull appearance or loss of gloss of the products. The other is characterized a scale distortion which is known as “melt fracture”. The origin of gross melt fracture is flow instability at a die entry, and is prominently found in polymers with high melt elasticity. Meller *et al.* indicated that elongational stress generated by contraction flow at the die entrance lead to the occurrence

of gross melt fracture.[12] The gross melt fracture is always detected in the case of long-chain branched polymers because they exhibit marked strain-hardening in elongational viscosity, leading to high elongational stress.

In case of shark-skin failure, two possible mechanisms have been proposed.[13-17] One is sudden large deformation at die exit due to cohesive rupture at surface of extrudates, originally proposed by Cogswell.[13] According to their work, the discontinuity in velocity at the die exit wall region, leading to elongational wall velocity acceleration and tensile stresse, is responsible for the cracks. Since the flow velocity of polymer melts on the die wall is zero, the strain rate at the die exit becomes infinity. This phenomenon eventually may appear as a "peel-off" failure.[17] Another well-known mechanism leading to shark-skin failure is slippage, *i.e.*, adhesive failure, between a polymer melt and the die wall. When the cohesive strength of the polymer melt is higher than the debonding stress between the wall and a polymer melt, the polymer slips on the wall. The detachment of a polymer melt from die surface accompanied with cracks by adhesive failure leads to surface instabilities.[18]

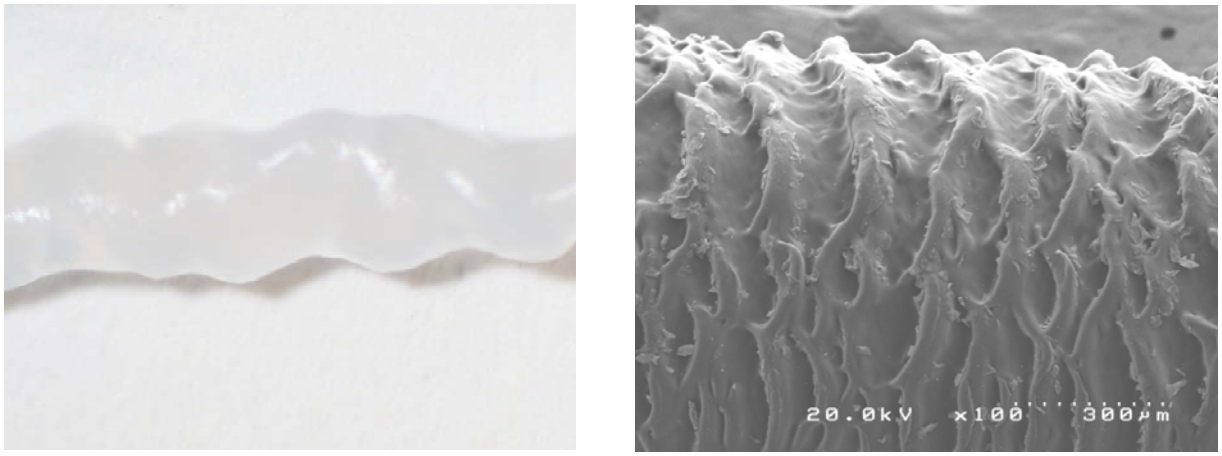

a b

Figure 1 Pictures of flow instability: a. gross melt fracture and b. shark-skin failure

According to previous researches, flow instability appears at high level of viscosity, *i.e.* elongational viscosity. Many factors affect the viscosity, such as the character of melting zone of screw inside extrusion machine, the type and content of the additive for PVC, and heating temperature. For the screw, there are more than three possible zones in a thermoplastic screw. These zones are defined as different because the terminology is not standardized in the industry. Different types of polymer will have different screw designs. However the traditional thermoplastic screws have three zones. The first zone is feed zone, sometime called solids conveying. This zone conveys the polymers into the extruder, and the channel depth is usually the same throughout the zone. Next is melting zone, also called the transition or compression zone. Most of the polymer is melted in this section, and the channel depth gets progressively smaller and depends on the melting mechanism of each material. The last zone is metering zone or melt conveying. This zone, the channel depth is again the same throughout the zone. The materials will be melted until last particles and mixed to a uniform temperature and composition. In order to get a good qualified product for PVC materials, the melting zone of screw should be designed to support the melting mechanism of PVC materials. In addition, a vented (two-stage) screw has further two zones; (1) decompression zone and (2) second metering zone. In this decompression zone will has about two-thirds down the screw. The channel suddenly gets deeper to relieve the pressure and allows any trapped gases, such as moisture or air, to be drawn out by vacuum. The second metering zone is the same as the first metering zone, but with greater channel depth, and repressurizes the melt to get it through the resistance of the screens and the die.

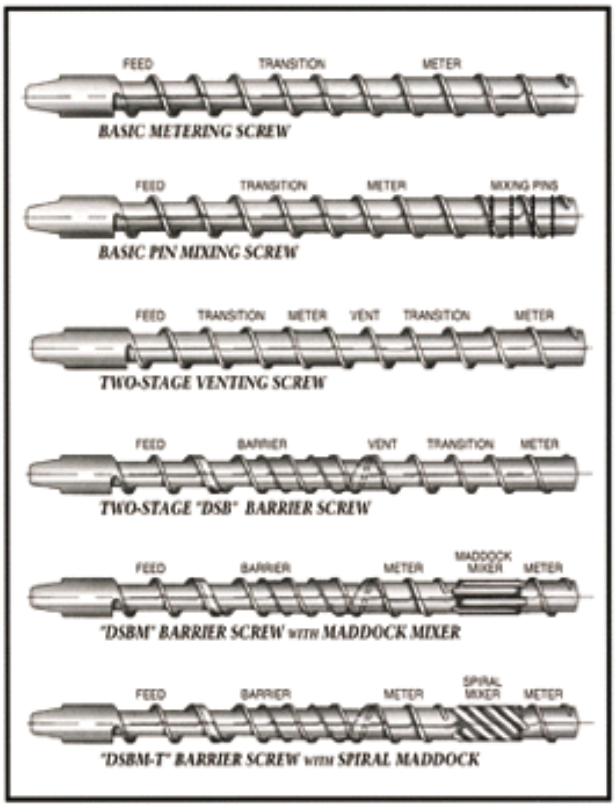

Figure 2 Screws for extrusion machine

As well known, the character of screw is very important. For the actual processing, however, the cost for chaining screw of extrusion machine is quite high. Therefore, the controlling the viscosity by heating temperature is more suitable and simple for the primary study. In this study, the viscosity of PVC material is controlled by heating temperature inside at melting zone in the screw of extrusion machine. Then the flow instability on the surface of PVC product is investigated at various conditions. This result may be useful information for improving the production speed which is usually limited by flow instability. Further, thermal degradation of product at high output need to be considered also.

2. Material and Experiments

The rigid PVC having specific density as 1.5 was used for investigation. The various type of the die, such as circular shape and specific shapes, were used. The pictures of flow instability were taken by digital camera and profile projector (AROS, SVP2010). Further the blend of acrylonitrile butadiene styrene (ABS) / polystyrene (PS) was used as a primary study. There is no characteristic data of ABS/PS because the material is a waste from production loss in a plant.

2.1 Primary study

The products were extruded through a single screw extrusion machine (Speecon, 52000-S). The controlled temperatures of six heaters are shown in the table 1. The number from low to high of heater represents the position of heater from hopper to die.

2.2 PVC study

Circular die

The products were extruded through extrusion machine (Thai Hydraulic Machinery, B-201075). The die of the following dimension; 10 mm of diameter, 100 mm in length was used. The controlled temperatures of all five heaters are shown in the table 1. The number from low to high of heater represents to the position of heater from hopper to die.

Specific dies

The samples were extruded through extrusion machine (Thai Hydraulic Machinery, A-12017). The controlled temperatures of six heaters are shown in the table 1. The geometry of die plates for sample 7 to 13 are shown in Figure 3. The cross section and tow view of samples are shown in Figure 4.

a

b

c

Figure 3. Shape of specific die: a. front plate, b. middle plate and c. final plate

a

b

Figure 4 Pictures of product shape: a. cross section view and b. top view

Table 1 Heating temperature and rotation speed conditions (rpm) for samples

Samples and condition	(rpm)	Heating temperature (°C) of each heater						Average Temp. ($T_{aver.}$,°C)
		1	2	3	4	5	6	
Primary study (ABS/PS)	Sample 1, (ABS/PS) rpm = 600 rounds/min	170	174	174	180	178	-	175
	Sample 2, (ABS/PS) rpm = 600 rounds/min	170	180	188	190	188	-	183
	Sample 3, (ABS/PS) rpm = 300 rounds/min	170	180	188	190	188	-	183
PVC study Circular die (PVC)	Sample 4, (PVC) rpm = 900 rounds/min	172	175	185	185	185	-	180.4
	Sample 5, (PVC) rpm = 900 rounds/min	183	190	195	195	195	-	191.6
	Sample 6, (PVC) rpm = 450 rounds/min	183	190	195	195	195	-	191.6
PVC study Specific die (PVC)	Sample 7, (PVC) rpm = 365 rounds/min	165	170	170	145	178	179	167.8
	Sample 8, (PVC) rpm = 385 rounds/min	165	170	170	148	178	181	168.6
	Sample 9, (PVC) rpm = 445 rounds/min	165	170	170	150	176	179	168.5
	Sample 10, (PVC) rpm = 485 rounds/min	165	170	170	151	176	180	168.6
	Sample 11, (PVC) rpm = 660 rounds/min	165	171	171	154	173	183	169.5
	Sample 12, (PVC) rpm = 750 rounds/min	165	170	170	158	174	180	169.5
	Sample 13, (PVC) rpm = 750 rounds/min	171	176	176	162	175	181	173.5

3. Results and Discussion

3.1 Flow instability of blend of acrylonitrile butadiene styrene / polystyrene (ABS/PS)

The blend of ABS/Ps was picked up as a material for primary study because it is a waste from production. Figure 5 is a picture of extruded products made from blend of ABS/PS. To confirm the effect of heating temperature, this blend was used as a primary study to investigate flow instability. It is found from the high output speed with low heating temperature of extrusion that, the extruded sample exhibits a distorted shape with rough surface (Figure 5a). The result indicates that the shape of sample is changed by flow instability. Then the shape and dimension of extruded product becomes precise when the heating temperature of extrusion machine increases (Figure 5b). Moreover, it is found that the dimension is further precise as well as smoother surface at high heating temperature and low output speed (Fig 5c). This primary study is an experimental model for next PVC experiments.

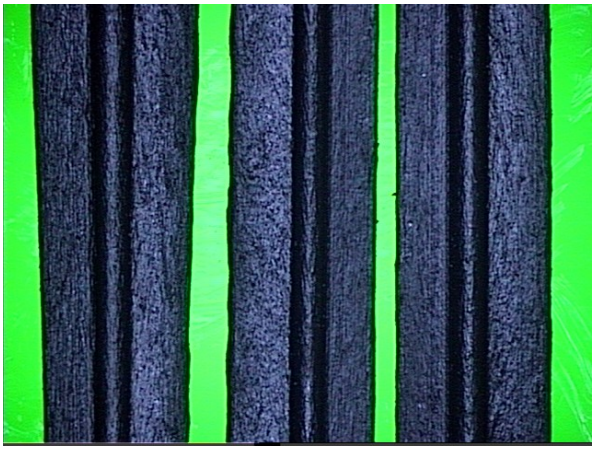

a b c

Figure 5 Pictures of surface of ABS/PS samples: a. sample 1 (ABS/PS, 600 rpm, $T_{aver.}$ = 175 ^{o}C), b. sample 2 (ABS/PS, 600 rpm, T_{aver} = 183 ^{o}C) and c. sample 3 (ABS/PS, 300 rpm, T_{aver} = 183 ^{o}C)

3.2 Flow instability of polyvinyl chloride

3.2.1 Flow instability of extruded samples using circular die

Figure 6 shows the pictures of the strand surface extruded through circular die. The shark-skin phenomenon appears at the lowest average extrusion temperature with high screw speed (Figure 6a). The level of shark-skin is reduced with increase of heating temperature. The surface of strands becomes smoother at high extrusion temperature with lower rpm of screw, as shown in Figure 6b and 6c. The results indicate the rupture of surface can be controlled by heating temperature as well as the speed of screw. It is reasonable because the flow instability, *i.e.* shark-skin behavior, on the surface of poly vinyl chloride (PVC) is reduced by reduction of viscosity. Therefore, the velocity of PVC inside extrusion machine increases and thus the shark-skin phenomenon is postponed.[13] However, in order to get a good qualified product, many parameters, such as dimension, mechanical prosperities and thermal degradation should be considered.

Figure 6 Pictures of surface of PVC samples: a. sample 4 (PVC, 900 rpm, $T_{aver.}$ = 180.4 ^{o}C), b. sample 5 (PVC, 900 rpm, T_{aver} = 191.6 ^{o}C) and c. sample 6 (PVC, 450 rpm, T_{aver} = 191.6 ^{o}C)

3.2.2 Flow instability on the surface of extruded product

As seen in the Figure 7a to7e, even the shark-skin is not observed clearly, however, the product shows the flow instability as a rough surface with slightly distorted shape at high output rate (Fig 7f). The surface becomes smoother when the heating temperature at melting zone of screw is increased, as seen in Figure 7g. The dimension of product cannot be investigated at high output rate because the amount of extruded PVC is excessive to go through the sizing part, a part for controlling the size and shape again after the materials came out through the die , of extrusion process. Therefore the experiments were carried on irrespective of dimension checking. The result indicates that the appearance of surface of final product could be controlled by heating temperature. However, the thermal degradation takes place at high heating temperature. This phenomenon can be observed by color change of extruded product. The result shows that the color of sample changes at high temperature condition, indicating the thermal degradation. Moreover, the excess

amount of material due to the very low viscosity at very high extrusion temperature leads to the dimensions loss for final product.

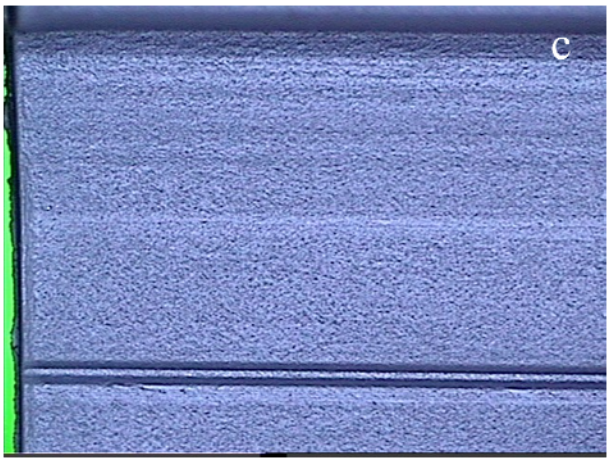

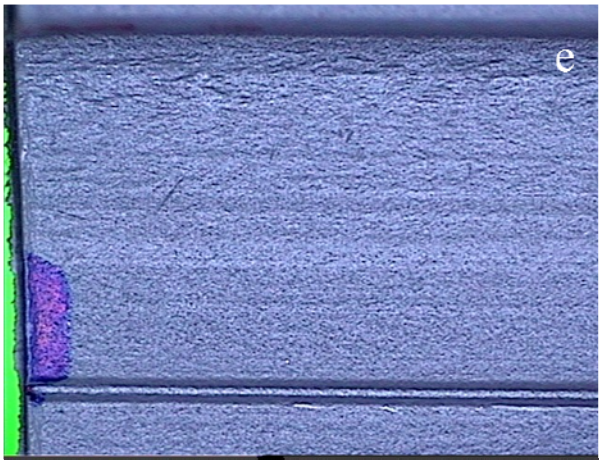

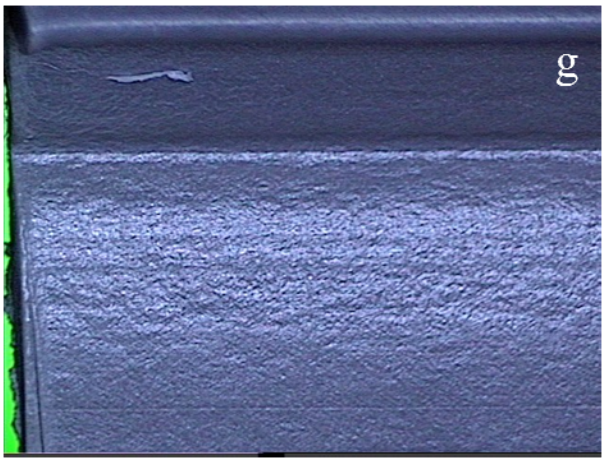

Figure 7 Pictures of surface of PVC samples: a. sample 7 (PVC, 385 rpm, $T_{aver.}$ = 167.8 ^{o}C), b. sample 8 (PVC, 385 rpm, T_{aver} = 168.6 ^{o}C) c. sample 9 (PVC, 445 rpm, T_{aver} = 168.5 ^{o}C), d. sample 10 (PVC, 485 rpm, $T_{aver.}$ = 168.6 ^{o}C), e. sample 11 (PVC, 660 rpm, T_{aver} = 169.5 ^{o}C) g. sample 12 (PVC, 750 rpm, T_{aver} = 169.5 ^{o}C) and c. sample 13 (PVC, 750 rpm, T_{aver} = 175.5 ^{o}C)

4. Conclusion

The flow instability of polymer at high output rate is controlled by heating temperature and the speed of screw inside the extrusion machine. This study is useful for improving the production speed. In the case of extrusion process, however, more parameters have to be controlled also, such as draw ability, cooling temperature and residence time inside the extrusion machine and cooling time for material. All of these parameters should be investigated and developed simultaneously. Because of the enhancement of extrusion temperature leads to reduction of viscosity of PVC, it is more difficult to control the shape of final product. Therefore, the knowledge of die design is necessary. Moreover, the cooling behavior of material is also important because the contents of amorphous and crystalline which determine the mechanical properties of final product are depended on the cooling temperature and cooling time. Another problem at high production speed is an excess amount of extruded material at very high extrusion temperature. Because of excess amount, the material could not go through sizing part. The draw resonance and thermal degradation should be considered also for actual polymer processing.

References

1. Tordera, J. P., *J. Appl. Phys.*, **1963**, *7* , 215.
2. Pearson, J. R. A., *Mechanical Principles of Polymer Melt Processing*; Pergamon: Oxford, **1966**.
3. Ballenger, T. F.; Chen, I. J.; Crowder, J. W.; Hagler, G. E.; Bogue, D. C.; White, J. L., *Trans. Soc. Rheol.*, **1971**, *15*, 195.
4. Cogswell, F. N., *J. Non-Newton Fluid Mech.*, **1977**, *2*, 37.
5. Tu, C. F., *J. Vinyl Technol.*, **1980**, *2*, 240.
6. Riley, D. W., *Encyclopedia of Poly Vinyl Chloride*; Nass, L. I., Eds.; Marcel Dekker: New York, **1986**.
7. Kalika, D. S.; Denn, M. M., *J. Rheol.*, **1987**, *31*, 815.
8. Brochard, F.; de Gennes, P. G., *Langmuir*, **1992**, *8*, 3033.
9. Wang, S. Q.; Drda**,** P. A., *J. Rheol.*, **1996**, *40*, 875.
10. Deeprasertkul, C.; Rosenblatt, C.; Wang, S. Q., *Macromol. Chem. Phys.*, **1998**, *199*, 2113.
11. Mhetar, V.; Archer, L. A., *Macromolecules*, **1998**, *31*, 8607.
12. Meller, M.; Luciani, A.; Sarioglu, A.; Manson, J. E., *Polym. Eng. Sci.*, **2002**, *42*, 611.
13. Cogswell, F. N., *Polymer Melt Rheology*; George Godwin Ltd.: London, **1981**.
14. Dealy, J. M.; Wissbrun, K. F., *Melt Rheology and Its Role in Plastics Processing*; Van Nostrand Reinhold: New York, **1989**.
15. Piau, J. M.; Agassant, J. F., *Rheology for Polymer Melt Processing*; Elsevier: Amsterdam, **1996**.

16. Hatzikiriakos, S. G.; Migler, K. B., *Polymer Processing Instabilities*; Marcel Dekker: New York, **2005**.

17. Tadmor, Z.; Gogos, C. G., *Principles of Polymer Processing*, 2nd Ed.; Willy-Interscience: New York, **2006**.

18. Siriprumpoonthum, M.; Mieda, N.; Doan, V. A.; Nobukawa, S.; Yamaguchi, M., *J. Appl. Polym. Sci*., **2012**, *124*, 429.

Acknowledgements

Firstly and foremost I would like to express the deepest gratitude to my supervisor, Prof. Masayuki Yamaguchi for supporting, educating, supervision, and give me motivation throughout the completion of my doctoral study even during tough times in my Ph.D. life. I am extremely grateful for his teaching and advice, not only the research methodologies but also many other methodologies in life. Only the words written in here are still not enough to express my feeling. It is a great honor for me to be a member and graduate from Yamaguchi's laboratory. I appreciate all his contributions of time, ideas, and funding to make my Ph.D. experience productive and stimulating. Without his supports, I would not have achieved this far and this thesis would not have been completed.

Secondly, I would like to express my appreciation to Professor Minoru Terano and Assistant Professor Shogo Nobukawa, who provided me a lot of valuable support. I also deeply appreciate the members of my committee: Associate Professor Dr. Kazuaki Matsumura, Associate Professor Tatsuo Kaneko, and Associate Professor Toshiaki Taniike of JAIST, and Professor Dr. Shuichi Tanoue of University of Fukui for their helpful comments. I am profoundly grateful to Associate Professor Yuki Nagao for his generous hospitality and support throughout my sub-theme research. Further I would like to thank JAIST and Graduate Research Program Scholarships (GRP scholarships) for financial support during my doctoral study. Without these facilities and sponsorship, I would not have been able to achieve and complete my study. Furthermore, I would to

thank Prime Polymer Co. Ltd. for their supporting the samples used in this study and their discussions.

I would like to express my appreciation to all of my teachers during I was a bachelor and master student in Silpakorn University, especially to Ajarn Nantanit Wanichachewa for giving me a chance to come to JAIST in 2009.

I am indebted to my close friend, Tong Huang, who supported and encouraged me. Without him, my life in here would not be easy. My special thanks are extended to all present and former members of Yamaguchi Laboratory. Moreover, thank you all Thai members in JAIST especially to Kultida Songsurang, Jiraporn Seemork, Chavakorn Samthong and everyone else for their warm love, emotional support and take part in a one of good memory in my life.

Finally, I would like to extend my deepest gratitude to my beloved family, Siripurmpulthum's family, for their unconditional loves. Without their love, assistance, and encouragement, it is impossible to finish my Ph. D degree.

Monchai Siriprumpoonthum (Monchai Siripurmpulthum)

August, 2014

Ishikawa, Japan